DOE/ID/12833--1
(DE95004212)
Distribution Category UC-1400

OXYGEN ENRICHED COMBUSTION SYSTEM PERFORMANCE STUDY

Phase II Final Report
100 Percent Oxygen Enriched Combustion
in Regenerative Glass Melters

by

Geoffrey B. Tuson
Hisashi Kobayashi
M. J. Campbell

August, 1994

Work Performed Under Contract No. DE-FCO7-88ID12833

Prepared for
U.S Department of Energy
Idaho Operations Office, Idaho Falls, Idaho
Sponsored by the Office of the Assistant Secretary for
Energy Efficiency and Renewable Energy
Office of Industrial Technology
Washington, DC

Prepared by
Praxair Incorporated
Old Saw Mill River Road
Tarrytown, NY 10591

DISCLAIMER

This report was prepared as an account of work sponsored by an agency of the United States Government. Neither the United States Government nor any agency thereof, nor any of their employees, make any warranty, express or implied, or assumes any legal liability or responsibility for the accuracy, completeness, or usefulness of any information, apparatus, product, or process disclosed, or represents that its use would not infringe privately owned rights. Reference herein to any specific commercial product, process, or service by trade name, trademark, manufacturer, or otherwise does not necessarily constitute or imply its endorsement, recommendation, or favoring by the United States Government or any agency thereof. The views and opinions of authors expressed herein do not necessarily state or reflect those of the United States Government or any agency thereof.

DISCLAIMER

Portions of this document may be illegible in electronic image products. Images are produced from the best available original document.

TABLE OF CONTENTS

	Page
List of Tables	
List of Figures	
1.0 EXECUTIVE SUMMARY	4
2.0 INTRODUCTION	7
3.0 HOST MELTER CHARACTERISTICS	10
3.1 End-Port Melter	10
3.2 Side-Port Melter	14
4.0 END-PORT MELTER CONVERSION AT CARR-LOWREY GLASS COMPANY	15
4.1 Measurement and Data Collection Methods	15
4.2 Installation and Start Up of Oxy-Fuel Combustion System	18
4.3 Comparative Performance - Air-Fuel and Oxy-Fuel Melting	23
4.3.1 General Observations	23
4.3.2 Glass Quality	25
4.3.3 Energy Performance	27
4.3.3.1 Method of Energy Performance Comparison	27
4.3.3.2 Baseline Energy Performance	29
4.3.3.3 100% OEC Energy Performance and Energy Savings	30
4.3.4 Stack Emissions	36
4.3.4.1 NO_x Emissions	37
4.3.4.2 Particulate Emissions	39
4.3.4.3 Carbon Monoxide Emissions	42
4.4 Burner Performance	42
5.0 SIDE-PORT MELTER CONVERSION AT GALLO GLASS COMPANY	44
5.1 Measurement and Data Collection Methods	44
5.2 Installation and Start Up of Oxy-Fuel Combustion System	45
5.3 Comparative Performance - Air-Fuel and Oxy-Fuel Melting	46
5.3.1 Energy Performance	46
5.3.2 Stack Emissions	51
5.3.2.1 NO_x Emissions	52
5.3.2.2 Particulate Emissions	54
5.3.2.3 Carbon Monoxide and SO_2 Emissions	55
5.4 Burner Performance	57

Page

5.5 VPSA Oxygen Supply System 57
5.5.1 Process Description and Plant Design 57
5.5.2 Installation and Start-up 62
5.5.3 VPSA Plant Performance 64

6.0 ENERGY IMPLICATIONS AND ECONOMICS OF REGENERATIVE MELTER CONVERSION TO 100% O.E.C. 70
6.1 Energy Implications 70
6.2 Economics of Melter Conversion 73

7.0 COMBUSTION SPACE MODELLING 82

8.0 REFERENCES 84

1.0 EXECUTIVE SUMMARY

Glass melting with 100% Oxygen Enriched Combustion (100% OEC) is gaining acceptance within the U.S. glass industry as an economical way of reducing melter energy consumption and stack emissions, and reducing the capital costs of melter construction or rebuild. The two successful glass melter conversions described in this report, conducted with supporting funds provided by the U.S. Department of Energy, have reinforced this growing industry interest in and acceptance of 100% OEC melting. The melter conversions constituted the second phase of a cooperative project between the Department of Energy and Praxair, Inc. Phase I of the project involved market and technical feasibility assessments of oxygen enriched combustion for a range of high temperature industrial heating applications, along with performance evaluation of a pilot scale Pressure Swing Adsorption (PSA) oxygen plant. The results of the Phase I studies were previously published by the Department of Energy (1,2,3).

Goals of the Phase II evaluation project were to:

1. Demonstrate that energy savings are achievable with 100% OEC compared to regenerative preheated air combustion.
2. Verify that an advanced Pressure Swing Adsorption oxygen production system can reliably supply oxygen for industrial heating applications at an energy consumption rate of less than 350 kWh/ton of equivalent pure oxygen produced.
3. Demonstrate reduction in NO_x emissions by 90% compared with regenerative combustion systems.

4. Achieve reductions in emissions of particulates and other pollutants.

Two regenerative container glass melters were converted to 100% OEC operation for the Phase II study. The first was a 75 tpd end-fired melter at Carr-Lowrey Glass Company in Baltimore, Maryland. This was a temporary conversion conducted for purposes of the evaluation project. The melter operated for five weeks with 100% OEC, with oxygen delivered to the plant as a liquid.

The second melter conversion took place in a 350 tpd container glass melter owned by Gallo Glass Company in Modesto, California. This was a permanent conversion to 100% OEC operation, and its success has since led Gallo to convert additional melters to 100% OEC. An on-site Pressure Swing Adsorption oxygen supply system was installed at Gallo to supply oxygen for 100% OEC melting. PSA oxygen plants were identified during Phase I as offering the most economical combination of capital and energy costs for the range of oxygen demands typical at many glass melting, as well as many other industrial heating facilities (4).

Major conclusions derived from the glass melter conversions conducted at Carr-Lowrey and Gallo are summarized as follows:

- Glass melter energy consumption is reduced by conversion to 100% OEC, even when baseline operation involves regenerators that are highly efficient at transferring heat from furnace exhaust gases to combustion air. Natural gas savings of 10 to 20 percent, along with similar percentage reductions in electric boost, are achievable. These savings are attributable to the high combustion energy availability achieved with 100% OEC, and to reduced radiative heat

losses from the furnace due to greatly reduced exhaust port area.

- It was verified that a commercial scale advanced PSA oxygen plant can reliably supply oxygen at an energy consumption rate well below 350 kWh per ton of equivalent pure oxygen. The particular PSA plant design used at Gallo achieves maximum efficiency by cycling the adsorbent beds between pressurized and evacuated states, and is referred to as a Vacuum/Pressure Swing Adsorption (VPSA) plant. The plant at Gallo supplied 90 to 91% purity oxygen at 20 to 25 psig to Gallo's header at an electrical demand of 320 to 325 kWh per ton of oxygen. Without plant silencers, which were required at this location, power consumption would have been 310 kWh per ton. VPSA plants delivering oxygen at lower pressure, and using the latest technology advances, can produce oxygen at 250 kWh per ton.
- Even with the high oxygen production efficiency of VPSA technology, a "back to the power plant" analysis indicates that the overall energy impact of 100% OEC conversion of regenerative melters is roughly a break even proposition in cases where electric boost energy input is unchanged. A net energy savings results in cases where electric boost energy input is significantly reduced and replaced with oxy-fuel input. Utilization of exhaust gas waste energy to preheat melter charge materials, which has not yet been demonstrated on an oxy-fuel melter, would move this technology to a clear net energy savings.
- Large NO_x emissions reduction are achieved by conversion to 100% OEC operation. Both conversions resulted in NO_x emissions reductions of about

90%. In the case of the Gallo melter, where no batch nitrates were used, NO_x emissions below 1.0 lb per ton of glass were achieved, both with a high purity oxygen supply, and when the oxidant stream had a nitrogen concentration of 3 percent.

- Where direct comparison between baseline and 100% OEC operation at equal pull was possible, particulate emissions were reduced by 25 percent following 100% OEC conversion. Carbon monoxide emissions were also reduced, while SO_2 emissions increased slightly over baseline levels.
- Economic analysis of various melting options shows the net present value (NPV) of the combined capital and operating costs of 100% OEC melting is higher than that of conventional regenerative operation with no flue gas treatment. However, 100% OEC is the most economical means of achieving NO_x emissions well below the best levels achievable with conventional regenerative firing.

2.0 INTRODUCTION

The field test project described in this report was conducted to evaluate the energy and environmental performance of 100% oxygen enriched combustion (100% OEC) in regenerative glass melters. Additional objectives were to determine other impacts of 100% OEC on melter operation and glass quality, and to verify on a commercial scale that an on-site Pressure Swing Adsorption oxygen plant can reliably supply oxygen for glass melting with low electrical power consumption. The tests constituted Phase II of a cooperative project between the United States Department of Energy, and Praxair, Inc. Phase I of the project

involved market and technical feasibility assessments of oxygen enriched combustion for a range of high temperature industrial heating applications. An assessment of oxygen supply options for these applications was also performed during Phase I, which included performance evaluation of a pilot scale 1 ton per day PSA oxygen plant (4).

Two regenerative container glass melters were converted to 100% OEC operation and served as host sites for Phase II. A 75 ton per day end-fired melter at Carr-Lowrey Glass Company in Baltimore, Maryland, was temporarily converted to 100% OEC in mid-1990. A 350 tpd cross-fired melter at Gallo Glass Company in Modesto, California was rebuilt for permanent commercial operation with 100% OEC in mid-1991. Initially, both of these melters were supplied with oxygen from liquid storage. Subsequently, in late 1992, a Pressure Swing Adsorption oxygen plant was installed at Gallo to supply oxygen for 100% OEC glass melting. The particular PSA plant design used at Gallo achieves maximum efficiency by cycling the adsorbent beds between pressurized and evacuated states, and is therefore referred to as a Vacuum/Pressure Swing Adsorption (VPSA) plant.

Low level oxygen enrichment, oxygen lancing, and auxiliary oxy-fuel burners have been used in glass melting since the 1940's, primarily to increase glass melter production rates. Beginning in the mid 1980's, some glass manufacturers began conversion of numerous day tanks and unit melters to 100% OEC using specially designed oxy-fuel burners (5,6). Pre-conversion operation of these smaller melters typically involved little or no heat recovery, making it possible in many cases to justify 100% OEC by energy savings alone. Other reported advantages of 100% OEC in these conversions included reduced NO_x and particulate emissions, and improved glass quality.

While smaller melters with limited heat recovery have proven to be economical candidates for 100% OEC, about 90 percent of glass tonnage is produced in large melters equipped with regenerators to transfer heat from exhaust gases to combustion air. In these melters, the energy savings in percentage terms achievable with 100% OEC is not as great as in melters with little or no heat recovery. However, Phase I analysis indicated significant energy savings could still be expected following conversion to 100% OEC, due to reduction in energy carried away by stack gases, and to reduced furnace radiation heat losses because of greatly reduced exhaust port area (2). This energy savings potential, combined with reduced capital requirements for furnace rebuild, and with the potential for reduced stack emissions without resorting to flue gas treatment, has resulted in great interest in 100% OEC by a glass industry facing increasing regulatory pressure to reduce emissions. This is evidenced by Figure 1 which estimates, based on data compiled from a variety of sources, the volume of oxygen consumed for OEC glass melting in the U.S. in recent years.

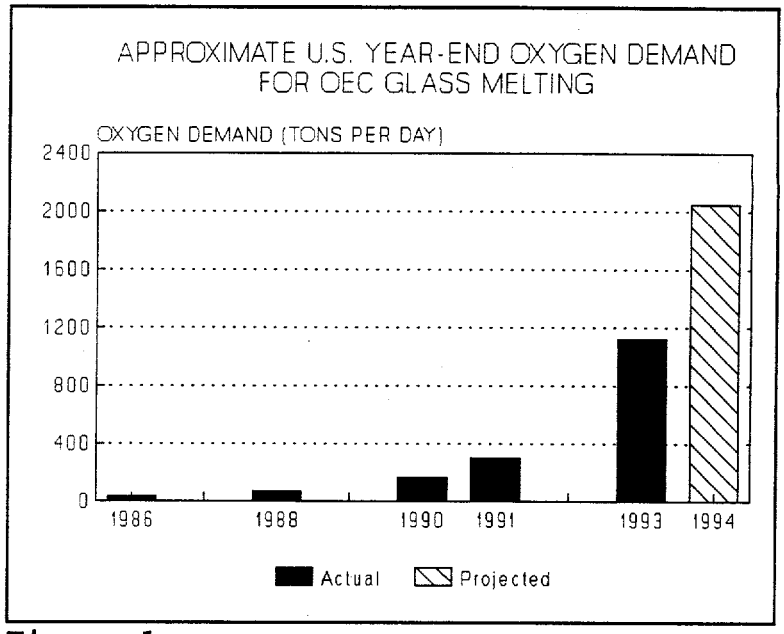

Figure 1

3.0 HOST MELTER CHARACTERISTICS

Evaluation project field work was carried out at two locations: Carr-Lowrey Glass Company, in Baltimore, Maryland, and Gallo Glass Company in Modesto, California. Descriptive features of the host melters at these location are summarized in Table I. Gallo Glass originally agreed to serve as host site for the entire project, and plans were made to convert a melter to 100% OEC just prior to the end of its regenerative campaign. However, because of a change in Gallo's furnace rebuild schedule, an alternate location was sought in order to get the project under way. Carr-Lowrey Glass Company agreed to host an initial evaluation of 100% OEC, which was conducted during a temporary melter conversion during the summer and fall of 1990.

As test work at Carr-Lowrey was being completed, Gallo's rebuild schedule, along with their decision to evaluate oxy-fuel firing, became firmer. Gallo agreed to be the host for continued 100% OEC testing work, beginning in the summer of 1992. In particular, the greater pull and oxygen demand of Gallo's melter made Gallo a good location for evaluating performance issues related to on-site VPSA oxygen supply.

3.1 End-Port Melter

Melter #7 at Carr-Lowrey Glass Company, is a 75 ton per day, end-fired melter producing flint glass for cosmetics bottle manufacture. Carr-Lowrey's primary interest was to test the use of auxiliary oxy-fuel burners to reduce particulate emissions. Carr-Lowrey agreed to a temporary test of 100% OEC prior to this more limited use of oxygen. A melter rebuild was scheduled for December, 1989, which presented an opportunity to install burner blocks and make other preparations. Tests of 100% OEC were conducted at Carr-Lowrey

TABLE I. HOST MELTER FEATURES AND BASELINE OPERATION

	CARR-LOWREY MELTER #7	GALLO GLASS MELTER #1
TYPE	END-FIRED	CROSS-FIRED
GLASS TYPE	CONTAINER	CONTAINER
HEARTH AREA	300 SQ.FT.	1248 SQ.FT.
PRESSURE CONTROL SYSTEM	NATURAL DRAFT STACK W/DAMPER	MORGAN ISELY EJECTOR
MELTER EXHAUST TEMPERATURE	2650 F	2800 F. (est)
AIR PREHEAT TEMPERATURE	2130 F	2300 F
FUEL CONSUMPTION (MMBTU/TON)		
EARLY CAMPAIGN	4.73	
LATE CAMPAIGN		4.1
ELECTRIC BOOST (MMBTU/TON)	0.68	0.55
TOTAL ENERGY CONS. (MMBTU/TON)		
EARLY CAMPAIGN	5.4	
LATE CAMPAIGN		4.65

for three weeks in July, and two weeks during October, 1990, with combustion equipment supplied by Praxair. Auxiliary oxy-fuel burners were then operated for an additional six months, to collect data on burner maintenance requirements and durability.

A cross-sectional view of Carr-Lowrey's melter #7 is shown in Figure 2. The melter is 25 feet long by 12 feet wide (300 square foot hearth area). Normally, it is fired with natural gas through injectors located beneath the combustion air ports. Fuel oil is used as a back up fuel during natural gas curtailments. The combustion system is supplemented by five pairs of boosting electrodes spaced along the length of the melter.

Combustion products leave the charge end of the melter through inclined ports into a two pass regenerator, and then exhaust through a natural draft stack. Melter pressure is controlled by stack damper adjustment. Combustion air is drawn into a blower from the melt shop floor, and forced through the regenerators into the melter. Reversal of exhaust and combustion air flow through the regenerators occurs every twenty minutes.

Glass exits the melter through a submerged throat into an attached refiner, from which glass is distributed to four forehearths. The refiner is fired with natural gas burners with no air preheat. Refiner combustion products are usually exhausted over the top of a shadow wall into the melter, although they can be exhausted separately through ports in the refiner crown.

Melter #7 supplies glass to a manufacturing operation producing bottles for an assortment of specialized orders. Consequently, pull from the melter, and melter operating conditions, change frequently in response to job changes on the production floor. Figure 3 plots daily pull during 2 months covering part of the baseline data collection period and the

FIGURE 2. PLAN SECTION - CARR-LOWREY MELTER #7

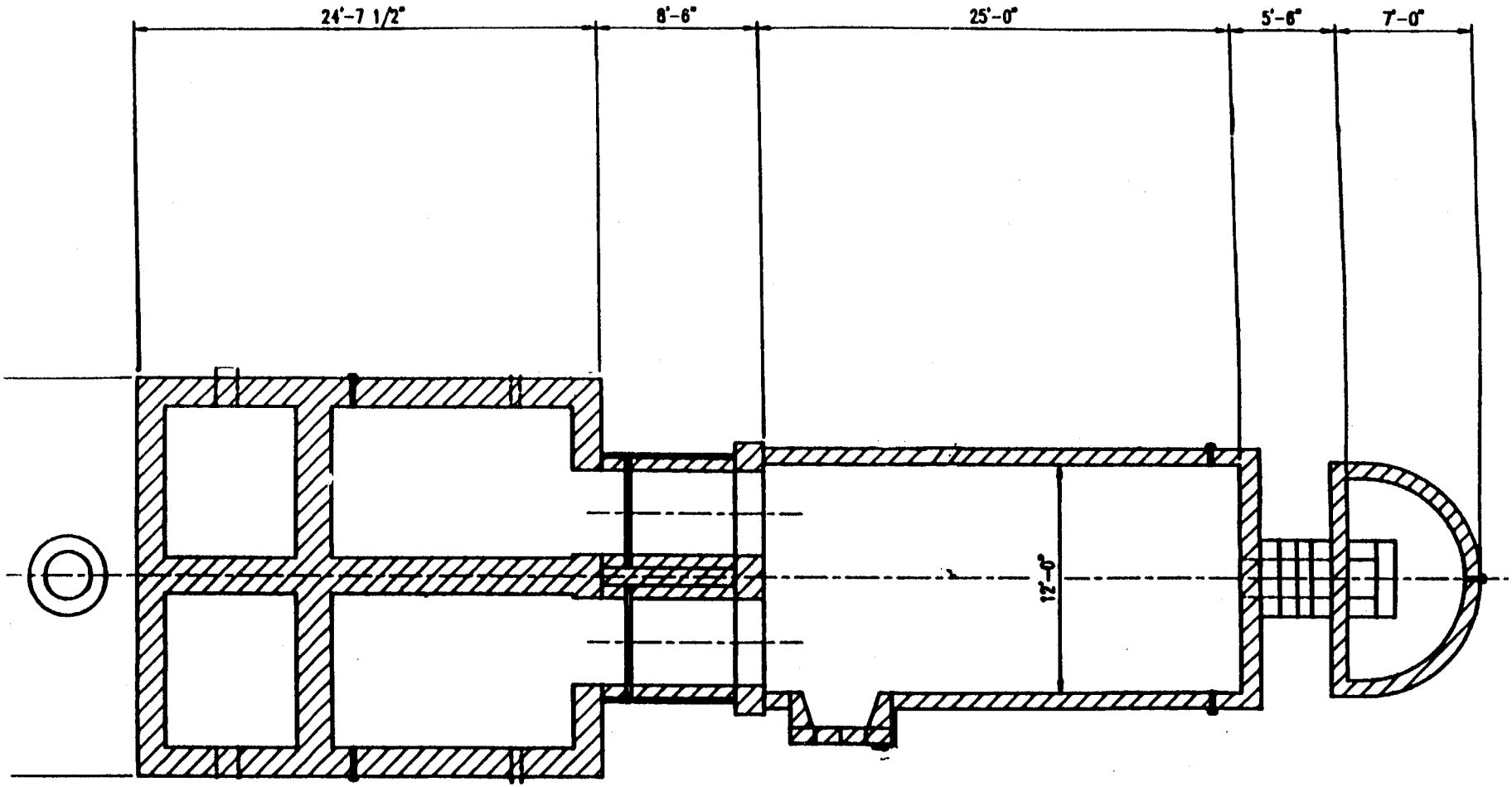

first period of 100% OEC testing. As indicated, pull from melter #7 ranged from 37 to 78 tons per day during this period.

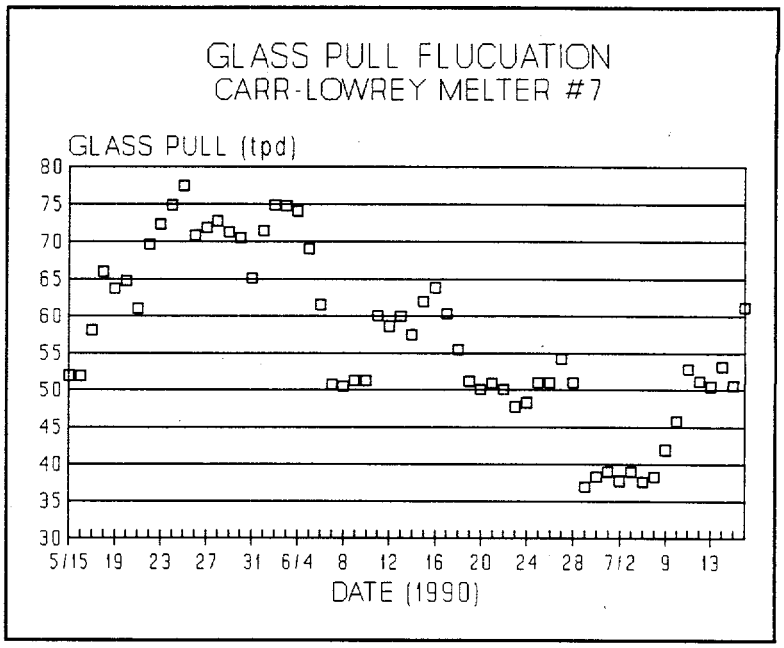

FIGURE 3

As glass pull fluctuates, the melter operators monitor batch line position and the temperature of glass approaching the throat of the melter. Firing rate and electric boost are adjusted in order to keep unmelted batch from advancing beyond the hot spot near the midpoint of the melter, and to keep the temperature of glass approaching the throat within a desired range. In making these adjustments, the operators maintain a preset ratio between the use of top firing and electric boost.

3.2 Side-port Melter

Gallo Glass Company's melter #1 produces flint soda-lime glass for wine bottle manufacture. Melter hearth area is 1248 square feet, and typical glass pull is 330 to 350 tpd. Large pull fluctuations like those at Carr-Lowrey occur rarely at Gallo, making this a more typical container operation. Prior to conversion to 100% OEC the melter was fired from five natural gas combustion ports in each melter breastwall. The melter is equipped with boost electrodes to supplement combustion heat input.

Gallo's primary objective in converting melter #1 to 100% OEC was to reduce NO_x

emissions (7). The melter was rebuilt in the spring of 1991, and the regenerators were removed. An oxy-fuel combustion system designed and built by Corning, Incorporated was installed for permanent commercial operation. Start up of the melter with 100% OEC occurred in late July, 1991. The melter operated for over a year supplied by liquid oxygen delivered by truck to the plant. Late in 1992, Praxair started up an on-site VPSA oxygen plant at Gallo to supply oxygen for glass melting.

4.0 END-PORT MELTER CONVERSION AT CARR-LOWREYGLASS COMPANY

A total of five weeks of 100% OEC testing was conducted at Carr-Lowrey, broken into two periods separated by about 3 months. Following these tests, two oxy-fuel burners were operated in the melter for six months in an auxiliary firing mode to evaluate longer term burner maintenance and reliability issues.

4.1 Measurement and Data Collection Methods

Carr-Lowrey's melter #7 was operated with air-gas firing for the first six months following its rebuild during early winter, 1989. The baseline melter operating conditions listed in Table I were measured during this period. The same parameters, with some additions, were also measured during 100% OEC operation. The data collection methods used, summarized in Table II, included the following:

1. Fuel and power consumption, glass and refractory temperatures, furnace pressure, and refiner firing rate were recorded on hourly log sheets. In addition, during 100% OEC operation, oxygen and fuel consumption data from the oxygen combustion system control panel was recorded. During oxy-fuel operations, the natural gas meter used for baseline measurements operated in series with the calibrated meter on the fuel skid of the oxygen

TABLE II. DATA COLLECTION METHODS

TYPE OF DATA	COLLECTION METHOD
BASELINE FUEL CONSUMPTION	TURBINE METER
FUEL/OXYGEN CONSUMPTION	VORTEX FLOW METERS
REFINER FUEL CONSUMPTION	ORIFICE METERS
EXHAUST & AIR PREHEAT TEMPERATURES	SUCTION PYROMETER
MELTER AND REGENERATOR REFRACTORY TEMPERATURES	OPTICAL PYROMETER AND THERMOCOUPLES
MELTER GAS COMPOSITION	ELECTROCHEMICAL NOx INFRARED CO2 ELECTROCHEMICAL O2
STACK EMISSIONS	STANDARD EPA METHODS BY MONARCH LABS
GLASS QUALITY	SEED COUNT

combustion system. This made possible a direct comparison of meter readings, and indicated that the baseline fuel measurements understated actual fuel usage. As a result, a correction factor was determined and applied to the baseline data. Oxygen and fuel flow across orifice runs at the individual oxy-fuel burners were recorded periodically during 100% OEC operation. This provided data on firing rate distribution, and served as a check on the flow control skid meters.

2. A water cooled sample probe and portable gas analyzers were used to determine CO_2, O_2, and NO concentrations in the exhaust ports and at various locations in the melter. This information was used to estimate air infiltration rates, and to determine the effect of operating adjustments on NO_x emissions.

3. A suction pyrometer was used to measure exhaust and air preheat temperatures at varying pulls and firing rates.

4. Thermocouples were inserted between the rider tiles several inches above the rider arches on both sides of the regenerator. This was done in response to concerns raised about possible rider arch overheating during 100% OEC operation.

5. Gauges were installed at orifice runs for air-gas burners firing the attached refiner. This was necessary for closing the melter energy balance, and to detect any shift of load between the melter and refiner.

6. Carr-Lowrey personnel conducted seed counts on a daily basis, and otherwise monitored glass quality.

In addition to the above, Monarch Analytical Laboratories, Inc. was contracted to conduct stack emissions tests during the baseline and 100% OEC operation. NO_x, SO_2, CO, and particulate emissions were measured using standard E.P.A. methods.

4.2 Installation and Start Up of Oxy-Fuel Combustion System

Preparations for 100% OEC operation were made during the melter rebuild at Carr-Lowrey, with assistance from KTG Glassworks Technology, Inc. Burner blocks for five oxy-fuel burners were installed in the melter breastwalls, at the locations shown in Figure 4. The blocks were arranged so the burners would be installed horizontally, with centerlines about 20 inches above the glass surface. KTG also prepared slots in the port necks for insertion of baffles during 100% OEC operation to reduce radiation from the melter to the regenerator.

The oxygen supply and combustion system installed in melter #7 consisted of the following major components:

1) A liquid oxygen supply tank located outside the melt shop building. Oxygen from the tank passed through atmospheric vaporizers, a main pressure regulator, and the main oxygen supply shutoff valve before entering the building piping.

2) Main fuel and oxygen flow control skids, for measuring and controlling the flow of natural gas and oxygen to the melter.

3) Auxiliary orifice assemblies for fuel and oxygen at each burner to measure and control the flow of natural gas and oxygen to each burner.

4) A main control console housing programmable controllers and hard-wired interlocks for safe, automatic control of the combustion system.

5) Five water-cooled Praxair "A" burners installed in burner blocks in the melter breast walls. Two of these burners were replaced with non-water cooled burners during the second period of 100% OEC testing.

Figure 4

OXY-FUEL BURNER LOCATIONS
END-FIRED MELTER

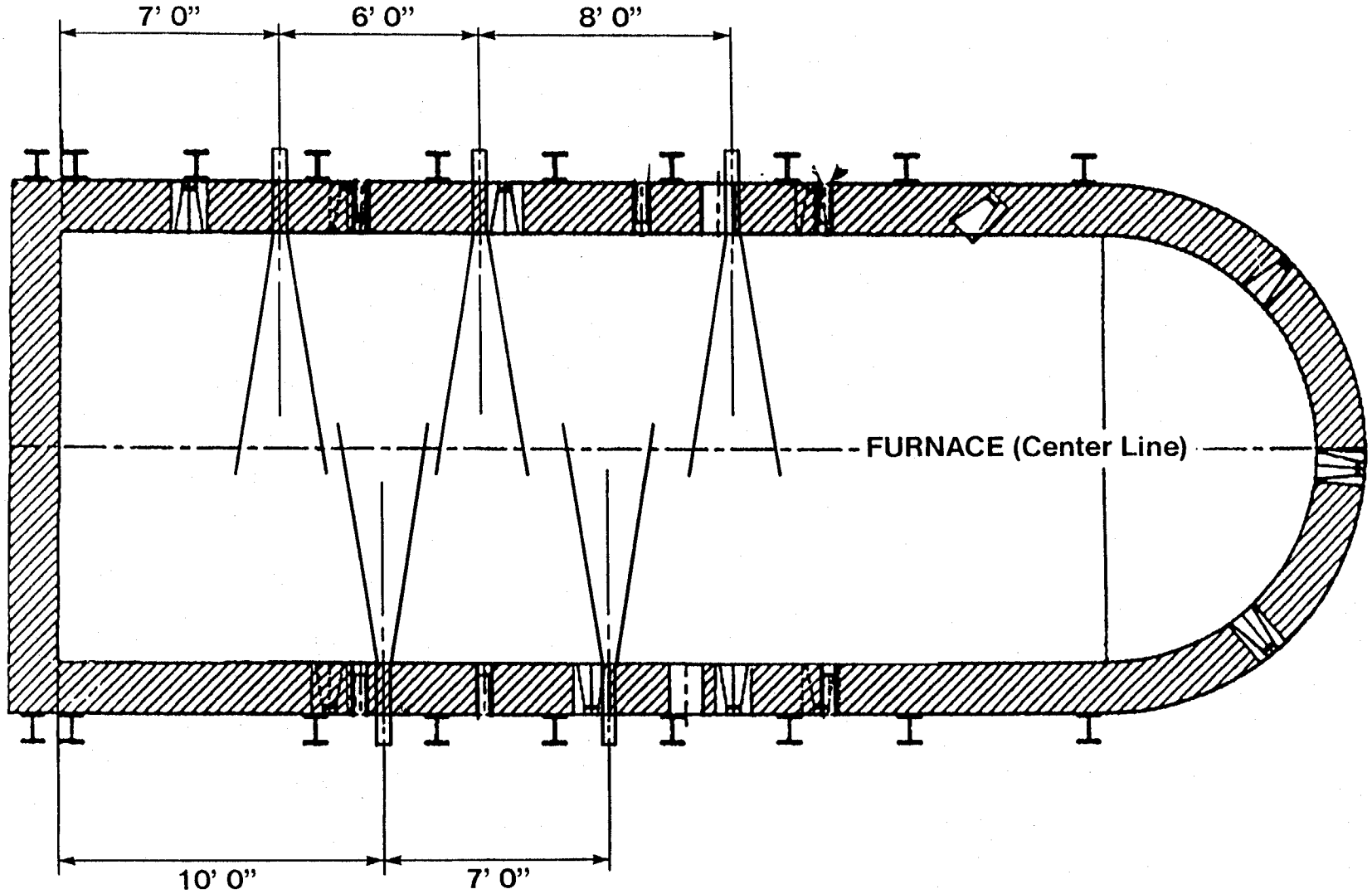

Praxair "A" burners were selected for the test because of their low NO_x emissions characteristics. "A" burners are characterized by a central fuel tube surrounded by a ring of oxygen nozzles. Oxygen from these nozzles is injected into the furnace at sufficiently high velocity to entrain a large volume of furnace gases prior to mixing with the fuel. The result is low concentration mixing of oxygen and fuel, relatively low flame temperature, and a reduced rate of NO_x formation. A detailed discussion of "A" burner NO_x emissions measured under laboratory conditions, and a comparison to emissions achieved with other burners, was reported as part of the earlier DOE funded Phase I study (3). Figure 5 plots NO_x emissions measured during that study from various burners operated at different levels of oxygen enrichment.

Installation of oxygen and gas piping to and around the melter, and site preparation for the liquid oxygen supply system, commenced during the second half of May, 1990. All mechanical and electrical installation work other than burner mounting was complete by June 22nd. The burners were installed, and final control system checks were made, on June 25th. Start up of the oxygen combustion system took place on June 26th.

Once installation and final checks were complete, changeover from air-fuel operation to 100% OEC took less than an hour. The "A" burners were started up at low fire with the air-fuel system still operating. After determining that ignition was established and the oxygen combustion system was operating normally, the firing rate of the "A" burners was gradually increased to a level sufficient to meet the furnace heat load. Simultaneously, the air-fuel system was turned down and then shut off, and the reversing damper was locked at mid-position. Adjustments were made at the auxiliary orifice assemblies to distribute fuel

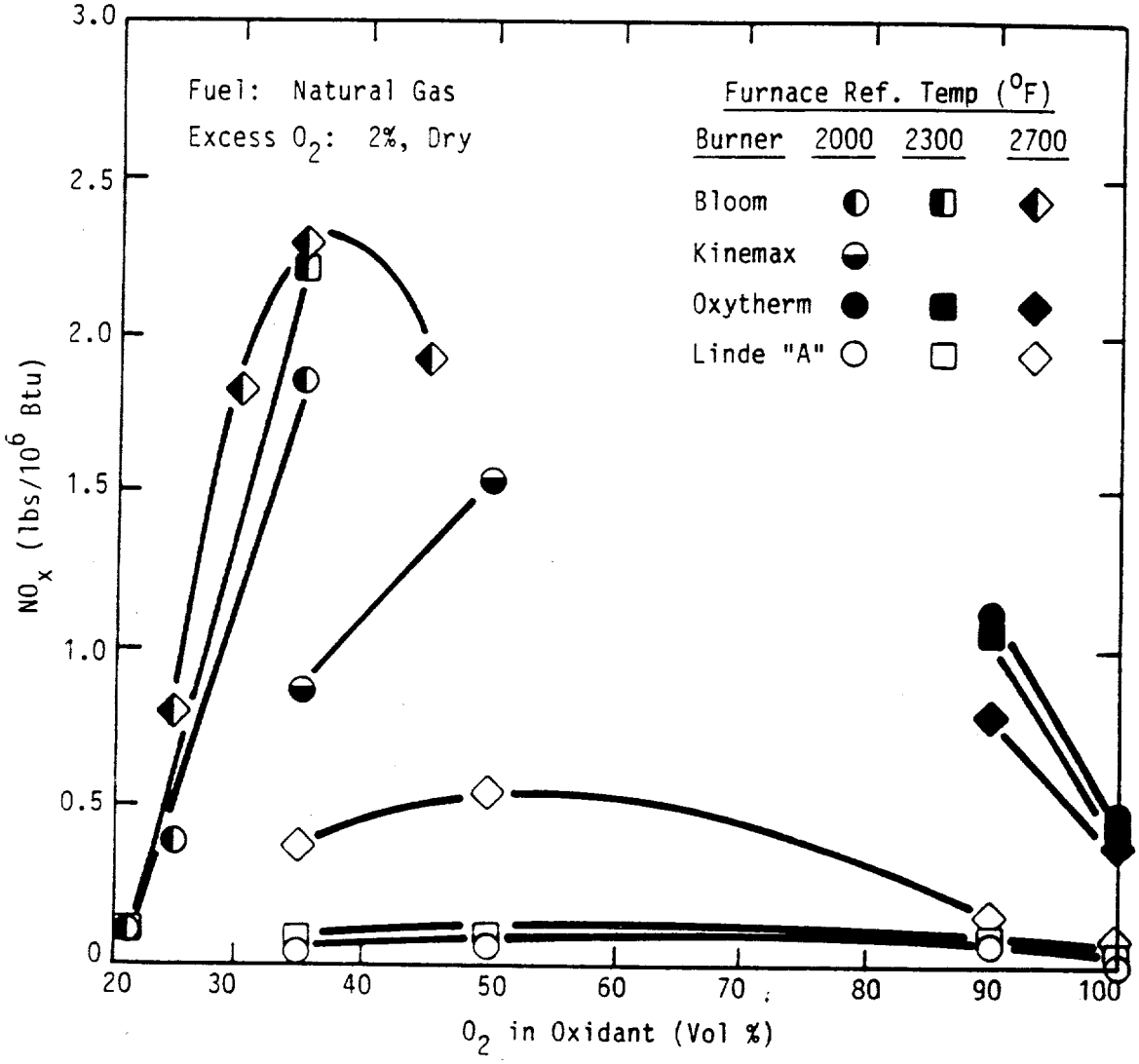

Figure 5 . Summary of NO_x emissions for pilot scale burners fired with natural gas.

and oxygen flows through the individual burners, while overall oxygen to fuel ratio was held constant by the automatic control system. Finally, bricks were removed from the port neck slots prepared earlier by KTG, and baffles constructed of ceramic fiber boards were inserted to reduce radiation losses from the melter. Inserting these baffles as deeply as planned proved difficult, and only about a 60 percent port area reduction was achieved. In a permanent conversion, port area can be reduced by about 90 percent, based on the exhaust gas volume reduction achieved with 100% OEC.

During the period of the start up when both combustion systems were operating, fuel supply valves were set so the oxygen combustion system's fuel flow control skid was piped in parallel with fuel piping supplying the air-fuel system. Once the air-fuel system was turned off, valves were reset so the fuel skid operated in series with melter #7's natural gas meter. This was done to allow Carr-Lowrey's fuel meter readings to be compared directly to those of the calibrated meter on the oxygen combustion system fuel skid.

One additional step taken prior to the first period of 100% OEC operation was the installation of temporary blowers and ductwork so cooling air could be introduced at the top of the regenerators in the event of rider arch overheating. Readings from thermocouples installed between the rider tiles indicated this was unnecessary, and blowers were not installed during the second period of 100% OEC testing.

4.3 Comparative Performance - Air-Fuel and Oxy-Fuel Melting

4.3.1 General Observations

Several observations were made by Carr-Lowrey and Praxair personnel comparing melter operation with air-fuel and oxy-fuel firing. These observations related to issues such as ease of melter control, glass surface appearance, and air infiltration rate.

Carr-Lowrey's melter operators stated that the cross firing arrangement of the oxy-fuel burners, and the ability to redistribute fuel input among burners, allowed improved melter control relative to end-port regenerative firing. They observed that batch line location responded more quickly to firing rate changes, and that melter temperature profile was more easily adjusted.

At the initial start up of the oxygen combustion system, fuel input was distributed about evenly among the five burners in the melter breastwalls, with some bias toward higher firing rates in burners 3 and 4. As the test period progressed, heat input was gradually transferred from the burners closest to the melter end walls (burners 1 and 5), to burners 2, 3 and 4. This arrangement provided a steeper temperature profile and a more clearly defined hot spot at about midway up the melter. Carr-Lowrey's operators felt this contributed to the improved control of the batch line.

Refractory temperatures from side to side of melter were relatively uniform during oxy-fuel operation. No refractory hot spots were observed during the 100% OEC tests, either on the crown, the burner blocks, or on the breastwalls opposite the burners. There was no increase in stones that would evidence any localized refractory overheating.

Melter operators adjusted total firing rate in order to maintain a preset relationship

between bridgewall temperature to pull. When adherence to this relationship caused bottom temperatures to deviate from target levels, electric boost adjustments were made. Electric boost and fuel energy consumption for air-fuel and oxy-fuel operation are compared and discussed in detail in section 4.3.3

There was a large amount of air infiltration into the melter, despite maintenance of positive furnace pressure. The extent to which excess air came from the combustion system, as opposed to infiltration, was difficult to determine during baseline operation due to uncertainty about combustion air metering accuracy. However, at similar operating pressures during 100% OEC operation, the air infiltration rate was determined to be about 25,000 scfh, based on measurements of CO_2 and O_2 concentrations in the combustion space atmosphere.

A major source of air infiltration was the side wall cooling system, which directs air at the flux line blocks and other areas requiring cooling. Temporarily shutting off this system while monitoring oxygen and CO_2 concentrations in the melter indicated that it was responsible for about 50 percent on total air infiltration. Air-fuel combustion products also likely passed over the shadow wall between the refiner and melter, even when the refiner exhaust ports were open. After packing around the burners and sealing obvious openings, the overall oxygen to fuel ratio to the burners was reduced to compensate for remaining infiltration. The ratio was eventually reduced to about 1.65:1, in order to hold exhaust oxygen concentration below 2 percent (dry basis).

Foaming behavior of the glass melt was affected by conversion to oxy-fuel firing. During air-fuel operation at Carr-Lowrey, a thin layer of foam sometimes covered portions of the glass surface between the batch line and the front wall. The amount of foam is

influenced in part by the condition of the combustion atmosphere, as evidenced by the fact that foam at times disappears and reappears along with changes in the direction of melter firing. The thickness of the foam layer, and the extent of the glass area covered, increased noticeably during the first period of 100% OEC operation. The foam presented a barrier to heat transfer from the combustion space to the glass, and as detailed later, electric boost levels had to be raised during the first period of testing to compensate for this.

Opinions of consultant glass chemistry experts were solicited on how foam formation could be reduced during a planned second round of 100% OEC testing. There was general agreement that the likely source of the foam was SO_2 bubbles released from the melt. A more oxidizing atmosphere lowers glass surface tension, which can allow these bubbles to form a stable foam (8). The increased oxidizing potential of the melter atmosphere, due to high water vapor concentration during 100% OEC operation, was therefore a likely cause of the increased foaming. Remedies suggested were to more closely control the oxygen to fuel ratio to lower oxygen concentration in the combustion space, and to adjust the batch formulation to slightly reduce the oxidation state of the glass. These solutions were tried in combination during the second round of 100% OEC testing. The dry basis oxygen concentration in the melter was maintained at 1 to 2 percent, and the carbocite content of the batch was increased. The result of these adjustments was that the area of glass surface covered with foam was greatly reduced. This permitted electric boost usage to be reduced levels below normal baseline usage.

4.3.2 Glass Quality

There was no disruption of the forming operation during any of the changeovers to

or from 100% OEC. Glass quality, as measured by seed count, workability, and stones, was generally unaffected by the conversions. One exception to this was the development of a thermal cord in one of four forehearths supplied by the melter during part of the first period of 100% OEC operation. Temperature gradients caused by increased foam on the glass surface during this period may have been the cause. There was no recurrence of the cord problem during the second test period, when the surface foam problem was largely corrected.

4.3.3 Energy Performance

4.3.3.1 Method of Energy Performance Comparison

The approach used to collect and compare data on melter energy consumption during baseline and 100% O.E.C. operation at Carr-Lowrey is outlined as follows, with details in the sections that follow:

1. To determine baseline energy consumption, the change in Carr-Lowrey's natural gas flow totalizer was recorded for each 24 hour period, and six electric boost power readings per 24 hour period were averaged. Average pull for each 24 hours was determined from hourly pull records on melter log sheets.
2. A correction factor was applied to baseline fuel consumption to adjust for metering inaccuracy. This inaccuracy was detected during 100% OEC operation, when Carr-Lowrey's fuel meter was piped in series with the fuel meter on the oxygen combustion system fuel skid. The accuracy of the oxygen combustion system fuel meter was checked prior to shipment to Carr-Lowrey, and its readings agreed well with flow totals from orifice meters serving the individual burners, and with a CO_2 mass balance using data collected during stack emissions tests.
3. Energy consumption and glass pull data during oxy-fuel firing was collected in the same manner as baseline data, with the exception that the totalized fuel consumption values were taken from the oxygen combustion system fuel flow meter.

4. A linear regression was performed to determine the relationship between electric boost power consumption and pull during baseline operation. Fuel and electric boost data from the 100% OEC test period were then adjusted to allow fuel consumption for 100% OEC and baseline operation to be compared at equal levels of electric boost.

Additionally, the firing rate of the attached refiner was routinely recorded so that any shift of heating load from the melter to the refiner could be detected. As indicated by Figure 6, the relationship between refiner firing rate and pull was essentially the same for baseline and 100% OEC operation. This was consistent with the fact that the melter operators kept the temperature of glass approaching the throat in a narrow range throughout the tests. Recording refiner firing rate data also allowed the heating of refiner combustion products as they passed through the melter to be factored into the melter energy. Finally, cullet ratio was monitored throughout the baseline and 100% OEC operating periods. Cullet ratio was constant at 35% throughout the entire test, and therefore did not affect the energy performance comparison.

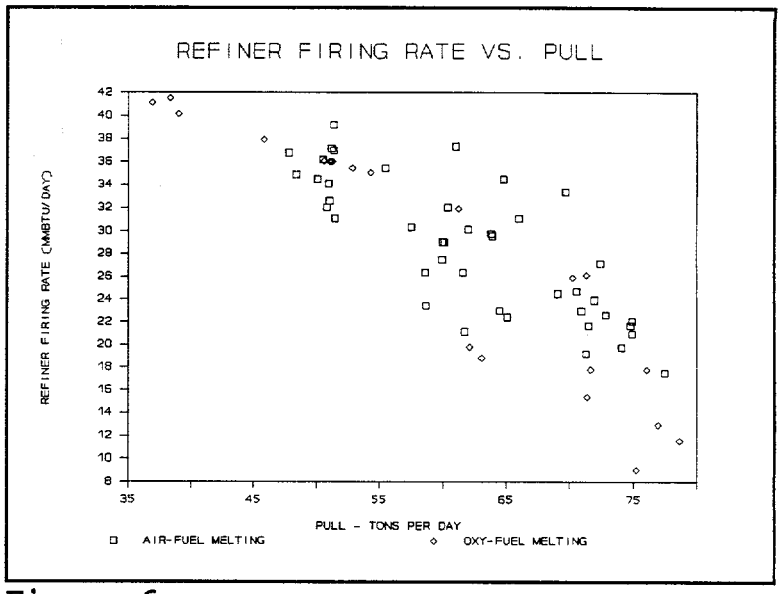

Figure 6

4.3.3.2 Baseline Energy Performance

Figure 7 plots fuel and electric boost energy consumption against glass pull during the baseline operating period. Electric boost supplied an almost constant 12 percent of total energy input during the baseline period. (Stated differently, electrical energy input equalled between 13 to 14 percent of fuel energy input).

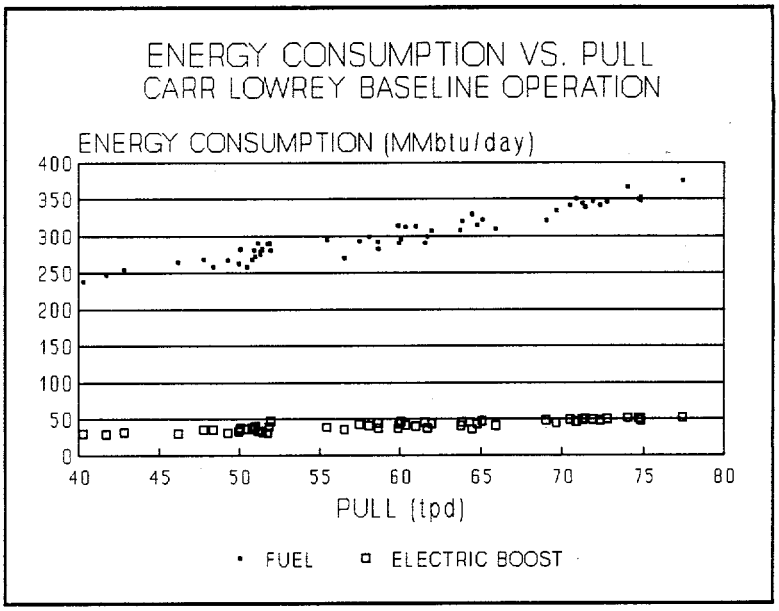

FIGURE 7

The nearly constant fuel to electric boost ratio, along with the linearity of the energy consumption versus pull data in Figure 7, suggests that the available energy from combustion (fuel energy input, less energy content of combustion products exiting the regenerator) changed little during baseline operation, despite pull fluctuations. This is

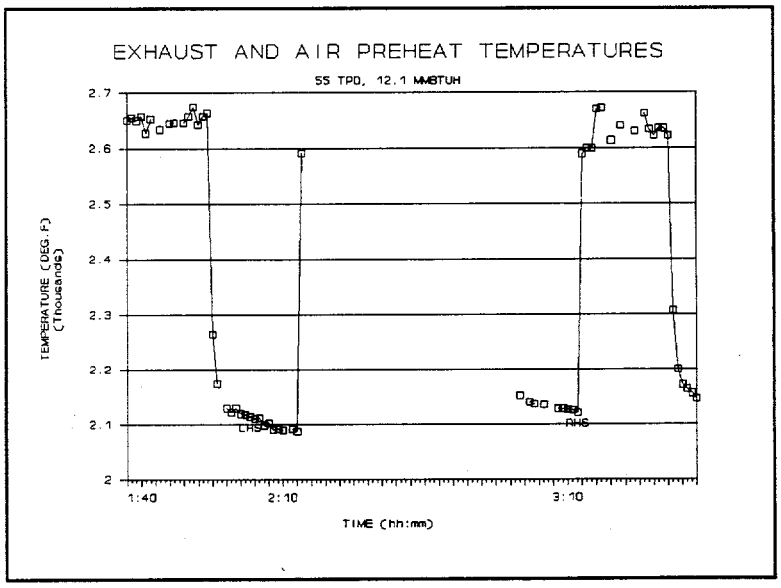

Figure 8

consistent with the fact that the difference between exhaust gas temperature and air preheat temperature was relatively constant, as illustrated by Figures 8 and 9. These figures plot baseline exhaust and air preheat temperatures in the port necks at 55 tpd pull/12.1 MMbtuh firing rate, and 67 tpd pull/12.8 MMbtuh firing rate, respectively. Comparison of the two figures indicates that baseline exhaust temperature varied little with changing pull, and that to the extent it did, air preheat temperature varied similarly.

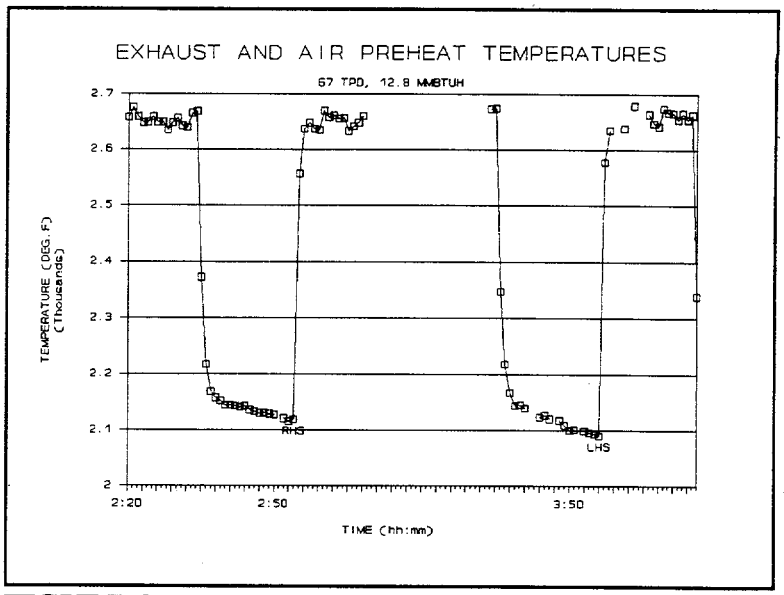

FIGURE 9

The insensitivity of baseline exhaust temperature to pull can be explained by the relative locations of the batch charger and exhaust ports. Exhaust gases approaching the exhaust port pass over relatively cool unmelted batch which absorbs heat and cools the charge end refractories and exhaust gases by radiation. As the firing rate increases with increasing pull, the mass flow of cold batch into the melter also increases, helping to hold temperatures relatively constant.

4.3.3.3 100% OEC Energy Performance and Energy Savings

The first step in comparing melter energy performance during oxy-fuel and baseline operation was a comparison of electric boost power consumption. Figure 10 replots the baseline electric boost data from Figure 7 on a different scale, along with a least squares

linear fit to the data. Figure 11 plots electric boost usage during 100% OEC testing, and shows that it differed from the "standard" level of boost defined by the linearization of the baseline data. The higher use of electric boost at low pull during 100% OEC operation than during baseline operation is attributed to increased glass surface foam during the first oxy-fuel test period, when most of the low pull data was collected. This foam inhibited heat transfer to the glass from combustion space gases and refractory, requiring that more electric boost be used to maintain targeted temperature in glass approaching the throat of the melter. The 100% OEC data at higher pulls was collected after the problem of increased surface foam was largely corrected by batch and firing

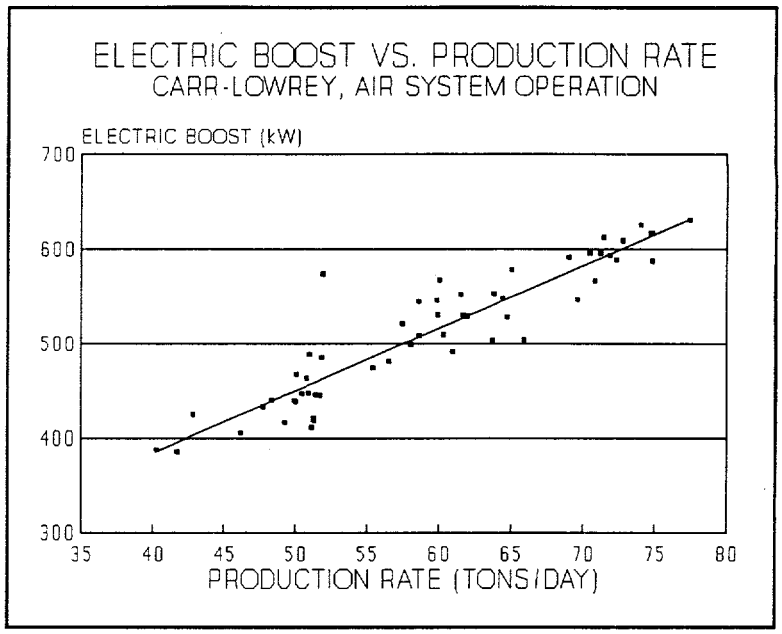

FIGURE 10

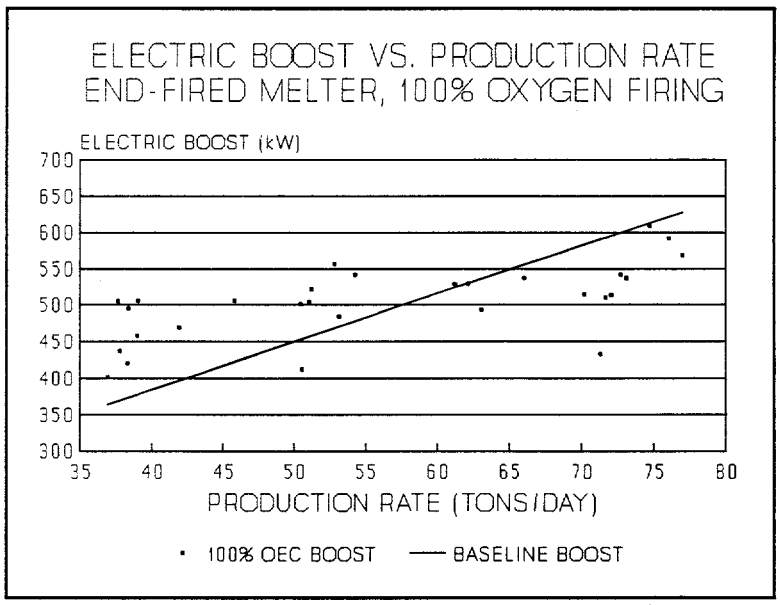

FIGURE 11

adjustments. These data indicate electric boost usage averaged about 10 percent less than baseline usage.

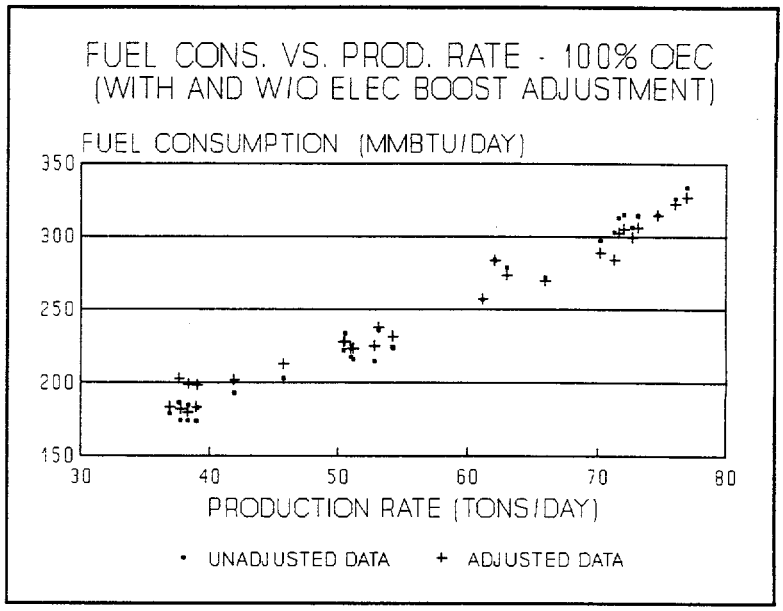

FIGURE 12

Baseline and 100% OEC energy performance are most easily compared by adjusting fuel consumption data for differences in electric boost. This was done for each 24 hour period of 100% OEC operation, by calculating the expected change in fuel consumption that would have resulted if a "standard" amount of electric boost, defined by the linearization shown on Figure 10, had been used. At the exhaust conditions measured during 100% OEC operation, 1.47 btu of natural gas input would be needed to replace 1 btu of electrical input. This corresponds to an increase (decrease) of 0.12 MMbtu per day of fuel input per 1.0 kW decrease (increase) required to adjust electric boost to the "standard" level. The impact of this correction on the 100% OEC fuel consumption data was small, as shown in Figure 12.

The adjusted fuel consumption data from Figure 12 is replotted on Figure 13, along with baseline fuel data from Figure 7. Linear regressions of the two sets of data are also plotted. Comparison of these linearizations indicates that natural gas savings achieved at Carr-Lowrey, after adjustment for electric boost differences, averaged about 15 percent. Savings ranged from about 20 percent at 40 tpd pull to 12 percent at 75 tpd pull. Specific

fuel consumption and total specific energy consumption at 75 tpd pull decreased from 4.7 to 4.1 MMbtu per ton, and from 5.35 to 4.75 MMbtu per ton, respectively.

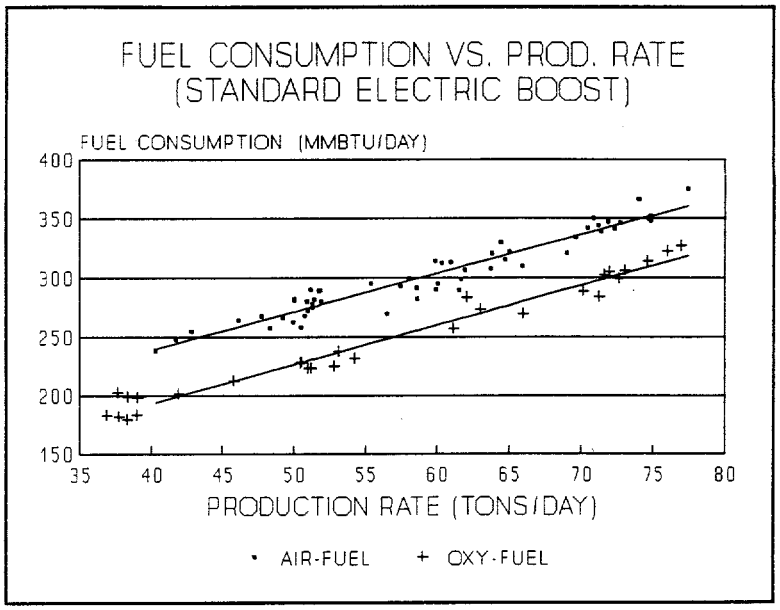

Figure 13

The fuel savings achieved with 100% OEC can be attributed to two main factors: higher fuel energy availability with 100% OEC than with preheated air-fuel combustion, and reduced net radiative heat flux from the melter to the regenerator ports. The first of these factors is illustrated by Figure 14, which plots the energy input needed to deliver 1 btu of useful energy for 100% OEC and air-fuel firing with methane, at a dry basis exhaust oxygen concentration of 3 percent. The figure indicates that, for a given temperature of furnace gases entering the exhaust ports, regenerators must preheat

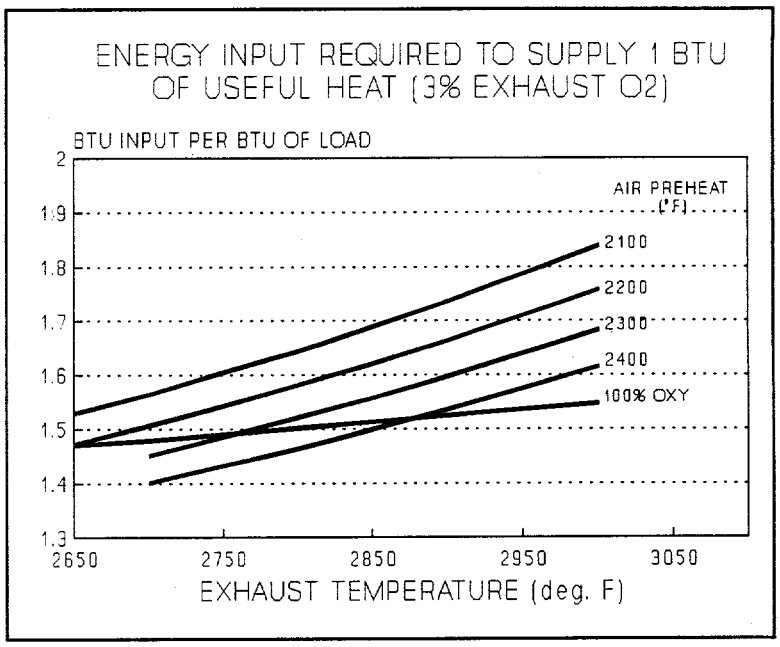

Figure 14

combustion air to within about 450°F of that temperature in order to achieve the same energy availability as with 100% OEC.

As indicated earlier by Figures 8 and 9, typical baseline exhaust and air preheat temperatures measured at Carr-Lowrey, averaged over a reversal cycle, were 2650°F and 2130°F, respectively, and the estimated air:fuel ratio at the burner would have resulted in a dry basis exhaust oxygen concentration of 3.5% in the absence of air infiltration. Exhaust temperatures measured during 100% OEC operation also averaged about 2650°F. Under these conditions, about 3.5% percent less fuel energy was needed to satisfy a given load with 100% OEC than with air-fuel firing.

The second major contributor to fuel savings at Carr-Lowrey was reduced radiation from the melter to the regenerator. As indicated by the melter energy balances presented in Table III, this load was reduced by about two-thirds, based on a thermal radiation model using as inputs the port areas, view factors, and temperatures involved. The control boundary for the energy balance passes vertically through the charge end wall, and through the shadow wall separating the melter from the refiner. Therefore, net radiation from the melter to the regenerator ports is treated as an output, and the heat content of gases entering the melter from the refiner is treated as an input.

A permanent melter conversion to 100% OEC at Carr-Lowrey would have allowed a greater reduction in exhaust/combustion port area than achieved during the test project. Modelling indicates that a 90 percent reduction in port area would have reduced total specific energy consumption to 4.65 MMbtu/ton, and increased fuel savings at 75 tpd to about 15 percent. It should also be noted that this and other specific energy numbers

TABLE III. ENERGY BALANCE COMPARISON: END-FIRED MELTER

OPERATING CONDITIONS	AIR	OXYGEN	OXYGEN-ADD'L PORT REDUCTION
GLASS PRODUCTION (TPD)	75	75	75
NATURAL GAS CONSUMPTION (MMBTUH)	14.7	12.9	12.5
ELECTRICITY CONSUMPTION (kW)	590	590	590
TOTAL SPECIFIC ENERGY CONS. (MMBTU/TON)	5.35	4.77	4.64
A/F OR O2/F RATIO AT BURNERS	11.2	1.65	1.65
OXYGEN CONSUMPTION (TPD)		21.5	20.9
COLD AIR INFILTRATION (SCFH)	25000	25000	25000
MELTER EXHAUST TEMP (deg.F)	2650	2650	2650
PREHEAT TEMP (deg.F)	2130	80	80
ENERGY BALANCE			
INPUTS (MMBTU/DAY)			
FUEL	352	310	301
ELECTRIC POWER	48	48	48
REFINER COMB. PRODUCTS	13	13	0
AIR PREHEAT	164	0	0
TOTAL INPUT:	577	371	349
OUTPUTS (MMBTU/DAY)			
TO GLASS (including batch CO2)	184	184	184
RADIATION TO REGENERATOR	21	7	2
STRUCTURE HEAT LOSS	42	42	42
EXHAUST GAS (excluding batch CO2)	331	138	121
TOTAL OUTPUT:	577	371	349
FUEL SAVINGS MMBTU/DAY		42	51
PERCENT		11.9	14.5
MMBTU/TON O2		1.95	2.44

presented so far were achieved with a high rate of air infiltration. Specific energy consumption with 100% OEC would have been reduced additionally, to about 4.3 MMbtu/ton, if the estimated air infiltration rate had been reduced by 80 percent, assuming compensating adjustments were made to fuel input rather than electric boost.

The energy savings analysis presented above compares 100% OEC energy performance to energy performance early in a baseline campaign. Data from the end of the previous baseline campaign showed specific fuel, electric, and total energy consumptions of 4.8, 1.58, and 6.38 MMbtu/ton, respectively, at 65 tpd pull. A precise comparison of 100% OEC data to this late baseline campaign data is difficult due to much heavier use of electric boost during the previous campaign, and to uncertainty about fuel metering accuracy prior to the rebuild. However, taken at face value, the data indicates a reduction in total specific energy consumption with 100% OEC of about 25 percent compared to late baseline campaign operation, despite heavier use of electric boost at that time. Some deterioration in energy performance is also to be expected during a campaign with 100% OEC, due to refractory wear resulting in increasing wall heat loss. However the performance deterioration should be less than during baseline operation, where increased energy use is related primarily to regenerator fouling, with wall heat loss increases playing a secondary role (9).

4.3.4 Stack Emissions

Stack emissions tests at Carr-Lowrey were conducted by Monarch Analytical Laboratories, Inc. Baseline tests were conducted on two consecutive days in June, 1991, with three one-hour sampling runs conducted each day. One day of stack tests was conducted

during each of the two 100% OEC test periods in July and October, 1991. Standard EPA methods were followed to determine flue gas volume and composition, and the rate of emissions of nitrogen oxides, particulates, and carbon monoxide.

4.3.4.1 NO_x Emissions

Table IV summarizes NO_x emissions data collected during baseline and oxy-fuel operation at Carr-Lowrey, including approximate composition of the combustion space atmosphere at the time of the measurements. Baseline NO_x emissions averaged over 20 lbs per ton of glass; near the high end of the range generally reported for regenerative container melters. Most of this baseline NO_x emission can be assumed to be thermal NO_x resulting from the combustion process. A small portion (roughly 2 pounds per ton of glass) probably came from the breakdown of niter contained in the batch. The batch used in melter #7

NOx EMISSIONS - CARR-LOWREY MELTER #7

	AIR	OXYGEN	OXYGEN
PULL (TPD)	62.7	46.8	75.8
BRDGWALL TEMP (F)	2676	2672	2766
FUEL (MMBTU/HR)	13.6	8.9	13.7
FLUE GAS (SCFH)	200,000	53,000	66,000
FURNACE ATMOSPHERE			
N_2 (%WET)	72	38	30
H_2O (%WET)	14	36	43
CO_2 (%WET)	9	22	26
O_2 (%WET)	5	4	1
NOx (LB/HR)	56.4	5.75	6.5
(LB/MMBTU)	4.28	0.68	0.5
(LB/TON)	21.6	2.9	2.1
NOx FROM NITER (@ 100% CONVERSION)			
(LB/HR)	7.0	5.2	8.5
(LB/TON)	2.7	2.7	2.7

TABLE IV

contains about 5.0 pounds of niter (NaNO3) per ton on glass produced. Complete conversion of the nitrogen content of this niter to NO_2 would yield 2.7 pounds of NO_2 per ton of glass.

An 85 to 90 percent reduction in NO_x emissions on a pounds per ton of glass basis was achieved by conversion to 100% OEC, despite nitrogen concentrations of over 30 percent in the combustion space due to the high rate of air infiltration discussed earlier. NO_x emissions averaged 2.9 and 2.1 lbs. per ton of glass during the first and second periods of 100% OEC operation, respectively. On a pounds per MMbtu basis, the corresponding numbers are 0.68 and 0.5 pounds per MMBtu, respectively. The lower NO_x emissions during the second round of 100% OEC testing than the first, despite higher pull and combustion space temperatures, is probably attributable to the lower oxygen and nitrogen concentrations maintained in the melter during the second period.

While NO_x emissions were greatly reduced by conversion to 100% OEC, they were significantly higher than the level predicted for thermal NO_x emissions alone based on laboratory tests. In tests conducted as part of Phase I, NO_x emissions of 0.03 pounds per MMbtu were measured during 100% OEC operation of a Praxair "A" burner fired into a 2700°F lab furnace with low nitrogen concentration (3). Results consistent with these have been found in "A" burner tests in a 2800°F furnace with varying nitrogen concentrations at Praxair's Tarrytown, NY Technical Center. In these tests NO_x emissions have varied in proportion to furnace nitrogen concentration, and were below 0.5 pounds per MMbtu even during simulation of auxiliary firing into an air-fuel fired furnace with a nitrogen concentration of 70%.

Figure 15 compares typical NO_x data from a 2800°F lab furnace fired with an "A" burner to actual NO_x emissions measured during 100% OEC operation at Carr-Lowrey. As indicated by the figure, the actual NO_x emissions measured were two to three times higher than predicted by the lab data.

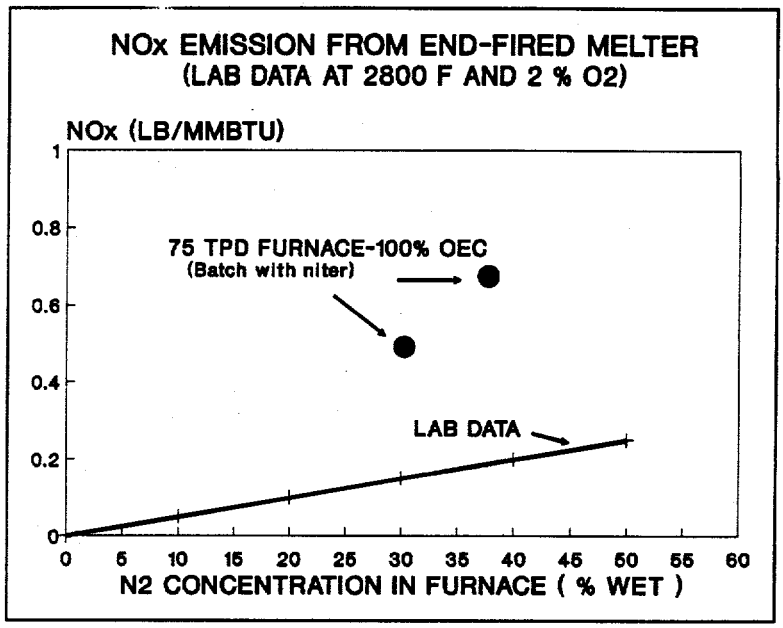

FIGURE 15

The most likely explanation for this difference is the presence of niter in Carr-Lowrey's batch. As stated earlier, complete conversion of the nitrogen contained in Carr-Lowrey's batch niter to NO_2 would yield 2.7 pounds of NO_x (as NO_2) per ton of glass. Assuming that a majority of this nitrogen was converted to NO_x, as predicted by thermochemical data, the NO_x remaining to attribute to combustion agrees more closely with the laboratory data.

4.3.4.2 Particulate Emissions

Particulate emissions from soda-lime glass melters are predominantly the result of volatilization of NaOH from the glass melt, which subsequently reacts with SO_2 in the flue system to form submicron sized Na_2SO_4 particulate (10). Modelling studies conducted for Praxair predict reduced volatilization of NaOH for a given glass surface temperature following conversion from regenerative to oxy-fuel firing (11). The extent of reduction depends in part on the degree to which gas velocity at the glass surface is reduced by

converting to 100% OEC. The model predicts that a particulate emissions reduction of approximately 50% should be typical.

Particle size analysis of the particulate captured during both baseline and 100% OEC operation at Carr-Lowrey confirmed the expectation that emissions resulted primarily from the condensation of volatiles, as opposed to physical entrainment of batch materials. The mass median diameter of the particulate captured was 0.4 microns during baseline operation, and 0.2 microns during 100% OEC operation. In contrast, batch particle fines typically range in size up to about 20 microns (12).

Figures 16 and 17 plot baseline and 100% OEC particulate emissions data from Carr-Lowrey against pull and bridgewall temperature, respectively. The baseline data shown at the lowest pulls (47 and 54 tpd, 2710 bridgewall temperature) is probably not representative, because pull was reduced just prior to these measurements, and the melter operation was not at a steady state.

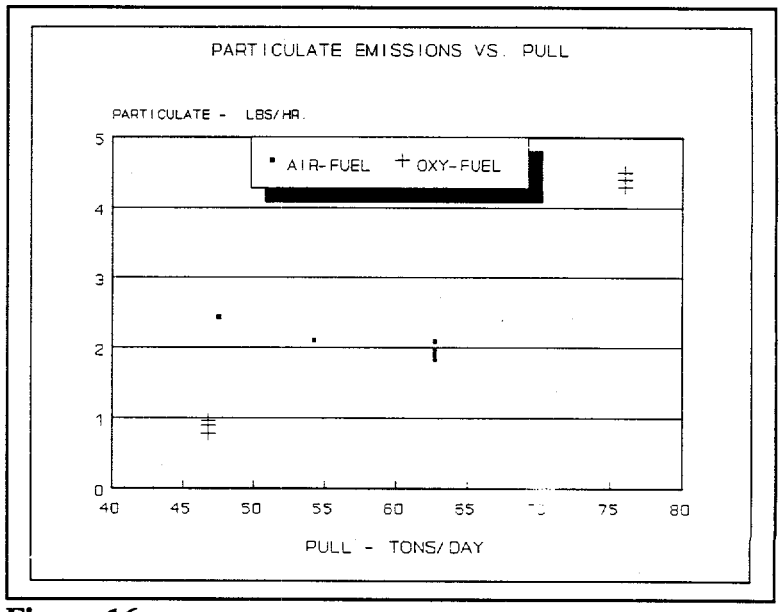

Figure 16

Changes in pull from measurement to measurement make drawing conclusions about the impact of conversion to 100% OEC on particulate emissions difficult. However, the changing emissions levels measured can be compared to behavior reported elsewhere. An

empirical equation developed by Ryder et al. for particulate emissions from container melters predicts a 19% increase in particulate emissions with each 25°F increase in bridgewall temperature. The equation also predicts that particulate emissions will vary directly with pull, if all other variables are held constant (10). Taking these factors into consideration, and using baseline particulate data at 63 tpd as a starting point, the approximate doubling of particulate emissions during 100% OEC operation at 76 tpd and 90°F higher temperature is in line with predicted behavior for regenerative firing, which suggests no reduction from expected levels was caused by conversion to oxy-fuel firing. In contrast, the reduction in particulate emissions relative to baseline operation that occurred with 100% OEC at 47 tpd, is greater than predicted for changes in pull and bridgewall temperature alone.

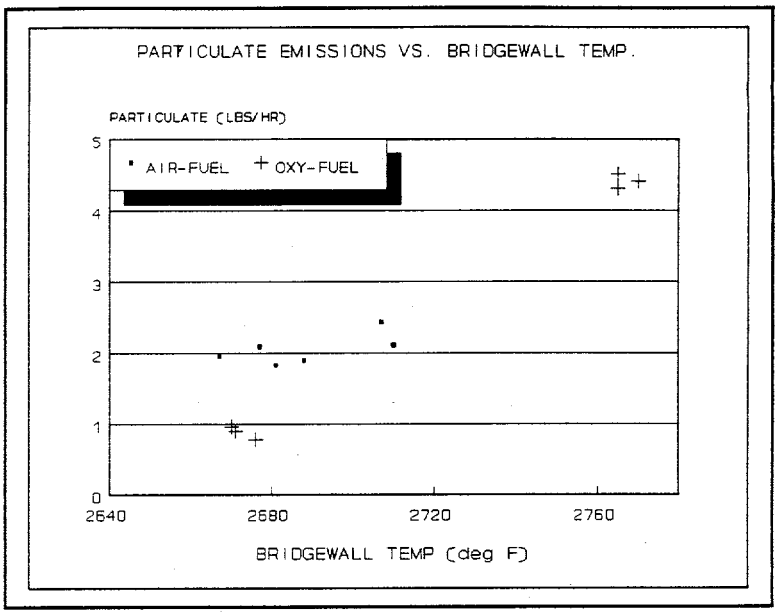

Figure 17

A possible explanation for this discrepancy in results is presented in Figure 18, which shows the temperatures measured between the rider tiles prior to and during the stack emissions test with 100% OEC at 76 tpd. As the stack tests were being conducted, the temperature of the right hand side of the regenerator was leveling off at a level well above the usual temperature at the end of a baseline exhaust cycle. This excursion to higher than normal temperatures likely caused release of previously condensed Na_2SO_4 from the regenerator during the stack test period.

Stack opacity during high pull operation at Carr-Lowrey increased from baseline readings in the high teens, to readings in the low 20's after conversion to 100% OEC. Reduced gas volume at the stack exit was the likely cause of this increase. Measured stack gas volume flow at the sampling point during 100% OEC operation at 76 tpd was only 75 percent of the volume measured during baseline operation at 63 tpd.

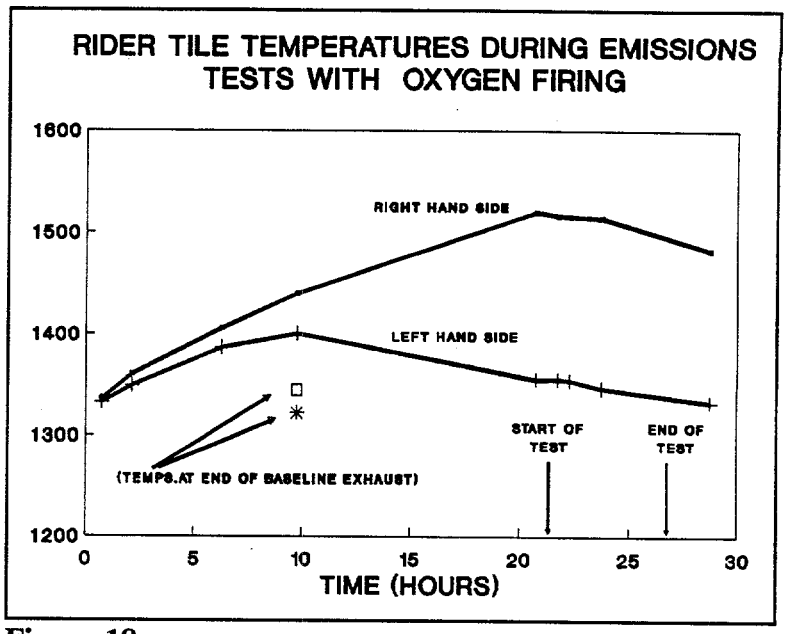

Figure 18

4.3.4.3 Carbon Monoxide Emissions

Carbon monoxide emissions measured during the baseline and 100% OEC test periods at Carr-Lowrey are summarized in Table V. Carbon monoxide emissions were negligible during the first 100% OEC test period, with concentrations at the sampling point consistently below 1 ppm. During the second 100% OEC test period, when excess oxygen in the melter was more tightly controlled, CO emissions ranged from 1 to 6 ppm, which was similar to the baseline emissions range.

4.4 Burner Performance

The water cooled "A" burners used during the first round of tests frequently became fouled by condensibles from the furnace atmosphere. These burners had to be retracted

Table V

CARBON MONOXIDE EMISSIONS - CARR-LOWREY MELTER #7			
	AIR-FUEL	OXY FUEL	
		PERIOD 1	PERIOD 2
CARBON MONOXIDE			
ppm	1.8 - 4.5	0.4-0.7	1.0 - 5.7
LB/HR	0.04 - 0.11	<.01	0.02 - 0.10
LB/TON	0.02 - 0.04	<.01	0.01 - 0.03

from the melter and cleaned every 36 to 48 hours in order to prevent plugging of the oxygen nozzles. Non-water cooled burners were used to replace two of the "A" burners during the second 100% OEC test period. These burners operated the two weeks of the second test period without requiring any cleaning. This led to a decision to use non-water cooled burners for previously planned extended burner testing.

The "extended burner test" commenced in January, 1991. The purpose was to evaluate long term oxy-gas burner performance in a glass melting environment. For this purpose, one auxiliary oxy-gas burner was installed in each melter breastwall, to supplement the heat input of the regenerative air-fuel system. These burners alternately cycled on and off as the air-fuel system reversed, so that only the burner on the exhausting side of the melter was firing. The firing rates of the auxiliary burners ranged from two to three MMbtuh. As was the case during second period of 100% OEC testing, no significant fouling of the non-water cooled burners occurred during the extended burner test. A cursory

cleaning of the burners was done every four to six weeks when they were pulled out for inspection.

5.0 SIDE-PORT MELTER CONVERSION AT GALLO GLASS COMPANY

The main objectives of continuing the 100% OEC Evaluation Project at Gallo Glass were to demonstrate the compatibility of VPSA oxygen supply with good glass melting performance and low stack emissions, and to evaluate VPSA plant energy performance. Gallo also agreed to collection of melter energy performance data with 100% OEC, and comparison of this data to historical energy performance data.

Testing at Gallo was conducted in a series of steps over a two year period. Baseline emissions data on Gallo's melter #1 was collected in January, 1991 as the melter neared the end of its regenerative melting campaign. The melter was rebuilt during the following spring, with modifications for 100% OEC operation. Oxy-fuel melting of glass commenced in August, 1991. Energy performance and stack emissions data were collected during the first two months of 100% OEC operation. A final set of emissions measurements, and energy performance measurements of the melter and VPSA oxygen plant, were conducted in February 1993.

5.1 Measurement and Data Collection Methods

Annubar meters on the oxygen combustion system flow control skids supplied by Corning were used to measure fuel and oxygen consumption during 100% OEC operation at Gallo. This data, along with electric boost power consumption and other continuously measured operating parameters, was recorded automatically by Gallo's control room computers. The fuel and electric boost data, in combination with Gallo's pull and cullet

ratio records, were used to determine the energy performance of the melter with 100% OEC. This was compared to historical baseline energy performance data based on fuel and combustion air measurements from orifice flow meters.

Portable CO_2, O_2 and NO_x analyzers like those used at Carr-Lowrey were used to gather data on gas composition in the melter and melter exhaust during 100% OEC operation. This data was collected prior to and during each of the 100% OEC stack emissions tests, and provided a basis for estimating air infiltration rates and nitrogen concentration in the melter. It supplied useful feedback on the effectiveness of steps taken to seal the melter, and the impact of various firing adjustments on NO_x emissions.

Stack emissions tests using standard EPA methods were conducted by Monarch Analytical Laboratories at Gallo prior to the melter rebuild, seven weeks following start up of the melter with 100% OEC, and a third time after start up of the on-site VPSA oxygen plant.

The measurement methods used to evaluate VPSA plant performance are covered in section 5.4.3.

5.2 Installation and Start Up of Oxy-Fuel Combustion System

Gallo Glass Company and Corning Incorporated worked together in preparing melter #1 for oxy-fuel firing. During the melter rebuild, all but one port on each side of the 1248 square foot furnace was removed. The two remaining ports served as exhaust outlets to direct furnace gases to a Morgan-Isley ejector system (7). Corning designed and supplied the oxy-fuel burners and combustion control system. A total of ten non-water cooled oxy-fuel burners were installed in an opposed arrangement in burner blocks in the melter

breastwalls. While the melter was being rebuilt, Praxair installed liquid oxygen supply tanks, vaporizers, and pressure regulating equipment to meet the melter's projected oxygen demand and combustion control system pressure requirements.

Heat up and fill of the glass melter proceeded smoothly, and more quickly than typical of the regenerative air-fuel melters at Gallo. Temporary heat up burners were used to raise melter temperature sufficiently to permit auto-ignition of the oxy-fuel burners. Once oxy-fuel firing commenced, melter fill with cullet, and then batch, proceeded quickly and without interruption. The high available heat from the oxy-fuel combustion resulted in a steady rise in furnace temperature during the fill process. In contrast Gallo's experience in filling conventional melters is that filling often has to be stopped in order to allow furnace temperature to recover (7).

Within one week of fill, all forming machines supplied by the melter were operating at full production. Glass quality following conversion to oxy-fuel melting, as measured by seed and blister levels, was equivalent to pre-conversion quality (7).

5.3 Comparative Performance - Air-Fuel and Oxy-Fuel Melting

5.3.1 Energy Performance

Specific energy consumption of Gallo's melter #1 prior to and following conversion to 100% OEC operation are presented in Table VI. The energy figures are averages from multiple 24-hour operating periods with melter pull ranging from 335 to 345 tpd, and at a cullet ratio of 25 percent.

Table VI

SPECIFIC ENERGY CONSUMPTION COMPARISON
GALLO GLASS MELTER #1

	LATE CAMPAIGN AIR-FUEL	TYPICAL AIR-FUEL	OXY-FUEL
GLASS PULL (tpd)	340	340	340
CULLET RATIO (%)	25%	25%	25%
ENERGY (MMbtu/ton)			
Natural Gas:	3.95	3.75	3.35
Electric Boost:	0.58	0.52	0.43
Total:	4.53	4.27	3.78

Specific fuel consumption following conversion to oxy-fuel firing was reduced by 15% relative to operation late in the baseline campaign, and by about 11% relative to more typical baseline operation earlier in the campaign. Electric boost usage was reduced by 26% relative to usage late in the baseline campaign, and by about 17% relative to typical baseline operation.

Energy balances for baseline and 100% OEC operation are presented in Table VII. As at Carr-Lowrey, the energy savings achieved with 100% OEC is attributable to higher combustion energy availability following conversion to 100% OEC, and to reduced thermal radiation from the melter to the exhaust ports due to the large reduction in port area. This last factor was enhanced by the location of the exhaust ports near the charge end of the melter, and profiling the melter to keep temperatures relatively low in this zone. This resulted in lower exhaust gas temperature than the average exhaust temperature achieved with regenerative firing.

TABLE VII. GLASS FURNACE ENERGY BALANCE
MELTER #1 - GALLO GLASS CO., MODESTO, CA

FURNACE OPERATING CONDITIONS	AIR BASE CASE	OXY-FUEL (LIQUID SUPPLY)	OXY-FUEL (VPSA SUPPLY)
PRODUCTION RATE (TPD)	340	340	340
FEED CHARACTERISTICS			
BATCH MOISTURE(% OF WET BATCH)	3	3	3
IGNITION LOSS (% OF DRY BATCH)	15.0	15.0	15.0
CULLET RATIO (% OF WET CHARGE)	25.0	25.0	25.0
CULLET MOISTURE (% OF WET CLT)	4	4	4
GROSS CHARGE RATE (TPD)	396.10	396.10	396.10
WET BATCH CHARGE (TPD)	297.07	297.07	297.07
WET CULLET CHARGE (TPD)	99.02	99.02	99.02
H2O IN BATCH (TPD)	8.91	8.91	8.91
H2O IN CULLET (TPD)	3.96	3.96	3.96
ELECTRIC BOOSTING (KW)	2,160	1,785	1,785
BURNER OPERATING CONDITIONS			
NAT. GAS FLOW RATE (SCFH)	52,400	46,800	47,000
(HHV MMBTU/HR)	53.16	47.48	47.68
(LHV MMBTU/HR)	47.95	42.82	43.00
OXIDANT COMPOSITION			
O2 (%)	20.9	100.0	90.0
N2 (%)	79.1	0.0	5.0
Ar (%)		0.0	5.0
OXIDANT PREHEAT TEMP (F)	2300	77	77
COMBUSTION STOICH. RATIO (%)	115.0	100.0	100.0
OXIDANT CONSUMPTION (SCFH)	577,227	93,694	104,549
CONTAINED OXYGEN (SCFH)	120,641	93,694	94,094
(TPD)	122.0	94.8	95.2
FLUE GAS FLOW RATE (SCFH)	630,256	141,055	152,113

TABLE VII. GLASS FURNACE ENERGY BALANCE
MELTER #1 - GALLO GLASS CO., MODESTO, CA

	AIR BASE CASE	OXY-FUEL (LIQUID SUPPLY)	OXY-FUEL (VPSA SUPPLY)
FLUE GAS FLOW RATE BY SOURCE			
H2O FROM CHARGE (SCFH)	22,623	22,623	22,623
CO2 FROM CHARGE (SCFH)	31,076	31,076	31,076
FLUE GAS FROM COMBUSTION(SCFH)	630,256	141,055	152,113
AIR INFILTRATION (SCFH)	20,000	20,000	20,000
TOTAL FLUE GAS (SCFH)	703,955	214,754	225,812
FLUE GAS FLOW RATE BY COMPOSITION			
CO2 (SCFH)	84,052	78,390	78,593
H2O (SCFH)	126,899	115,755	116,153
N2 (SCFH)	472,888	16,228	21,458
O2 (SCFH)	19,916	4,180	4,180
Ar (SCFH)	200	200	5,427
TOTAL (SCFH)	703,955	214,754	225,812
FLUE GAS COMPOSITION			
CO2 (% WET)	11.9	36.5	34.8
H2O (% WET)	18.0	53.9	51.4
N2 (% WET)	67.2	7.6	9.5
O2 (% WET)	2.8	1.9	1.9
Ar (% WET)	0.0	0.1	2.4
TOTAL (%)	100	100	100
CO2 (% DRY)	14.6	79.2	71.7
N2 (% DRY)	81.9	16.4	19.6
O2 (% DRY)	3.5	4.2	3.8
Ar (% DRY)	0.0	0.2	4.9
TOTAL (%)	100	100	100
MELTER AVG CROWN TEMPERATURE (F)	2,890	2,800	2,800
MELTER GAS EXIT TEMPERATURE (F)	2,800	2,650	2,650
GLASS TEMPERATURE AT THROAT (F)	2,400	2,400	2,400
REGEN TOP TEMPERATURE (F)	2,300		
FLUE PORT RADIATION TEMP (F)		1,500	1,500
REGEN PORT AREA (FT^2)	86.7		
FLUE PORT AREA (FT^2)		16.0	16.0

TABLE VII. GLASS FURNACE ENERGY BALANCE
MELTER #1 - GALLO GLASS CO., MODESTO, CA

	AIR BASE CASE	OXY-FUEL (LIQUID SUPPLY)	OXY-FUEL (VPSA SUPPLY)
MELTER ENERGY BALANCE			
ENERGY INPUT (MMBTU/HR)(hhv)			
FUEL	53.16	47.48	47.68
ELECTRIC POWER (@3410 BTU/KWH)	7.37	6.09	6.09
OXIDANT PREHEAT	26.26	0.00	0.00
BATCH PREHEAT	0.00	0.00	0.00
CULLET PREHEAT	0.00	0.00	0.00
TOTAL INPUT	86.79	53.57	53.77
ENERGY OUTPUT (MMBTU/HR)(hhv)			
ENERGY TO GLASS	25.55	25.55	25.55
FLUE LOSS			
WATER FROM BATCH	1.91	1.84	1.84
WATER FROM CULLET	0.85	0.82	0.82
CO2 FROM BATCH	2.75	2.60	2.60
COMB. FLUE GAS & INFIL. AIR	46.29	16.79	17.13
FLUE LOSSES (TOTAL)	50.95	21.23	21.57
WALL HEAT LOSSES			
RADIATION TO REGEN PORTS	4.58	0.00	0.00
RADIATION TO FLUE PORT	0.00	1.22	1.22
WALL HEAT CONDUCTION	4.00	4.00	4.00
RADIATION TO WALL OPENINGS	1.63	1.46	1.46
WALL & RAD. LOSSES (TOTAL)	10.22	6.69	6.69
TOTAL OUTPUT	86.72	53.47	53.81
MELTER ENERGY BALANCE - SUMMARY			
ENERGY INPUT (MMBTU/TON)(hhv)			
FUEL	3.75	3.35	3.37
ELECTRIC POWER (@3410 BTU/KWH)	0.52	0.43	0.43
OXIDANT PREHEAT	1.85	0.00	0.00
BATCH PREHEAT	0.00	0.00	0.00
CULLET PREHEAT	0.00	0.00	0.00
TOTAL INPUT	6.13	3.78	3.80
ENERGY OUTPUT (MMBTU/TON)(hhv)			
ENERGY TO GLASS	1.80	1.80	1.80
FLUE LOSSES (TOTAL)	3.60	1.50	1.52
WALL HEAT LOSSES (TOTAL)	0.72	0.47	0.47
TOTAL OUTPUT	6.12	3.77	3.80

By the time the VPSA plants at Gallo became operational, a second melter had been converted to 100% OEC operation. The combined oxygen demand of the two melters exceeded the capacity of the VPSA plants, and piping arrangements did not allow the VPSA oxygen to be dedicated to melter #1. Consequently, the 100% OEC melters received an oxidant mixture supplied 60% by the VPSA plant oxygen, and 40% by the liquid storage tanks. The composition of this mixture was approximately 94% oxygen, 3% nitrogen, and 3% argon.

No change in the energy consumption of melter #1 was detectable following VPSA oxygen plant start up. This was as expected based on analysis of the predicted change in overall heat load caused by nitrogen and argon impurities in the VPSA oxygen. VPSA oxygen typically contains 3 to 5 percent nitrogen by volume, and about 5% argon by volume. As indicated by the third column in Table VII, even with all oxygen to the melter supplied by a VPSA plant supplying 90% purity oxygen, these impurities cause a less than 1 percent increase in melter heating load and firing rate relative to operation with pure oxygen. As was the case at Gallo, this impact is too small to detect within the normal variability of energy performance data.

5.3.2 Stack Emissions

Gaseous and particulate emissions from Gallo's melter #1 were measured by Monarch Analytical Laboratories, Inc. several months before the end of the baseline melting campaign, and about 2 months after the start of the oxy-fuel melting campaign. Gaseous emissions were measured a third time in February 1993, when the majority of the oxygen requirement of melter #1 was supplied by the on-site VPSA plant.

5.3.2.1 NO_x Emissions

Table VIII summarizes NO_x emissions data collected during stack tests at Gallo. As indicated, with all of the melter's oxygen requirement supplied by the liquid storage tanks,

NOx EMISSIONS - GALLO GLASS MELTER #1

	BASELINE	100% OEC	
		LIQUID O2	LIQ/VPSA MIXTURE
GLASS PULL (TPD)	335	342	339
COMBUSTION SPACE ATMOSPHERE			
NITROGEN	72%	3%	4-5%
WATER VAPOR	17%	51%	51%
CARBON DIOXIDE	9%	45%	44%
OXYGEN	2%	1%	0.5-1%
NOx EMISSION (LB/TON)	5.0	0.81	0.94

Table VIII

NO_x emissions were reduced to 0.8 lbs per ton of glass, from a baseline level of 5.0 pounds per ton. Based on measured CO_2, and O_2 concentrations, air infiltration into the combustion space was very low during the first 100% OEC stack test, and resulted in a calculated nitrogen concentration of only 3 percent. The large reduction in NO_x emissions from baseline levels is primarily attributable to this more than 20-fold reduction in furnace nitrogen concentration relative to baseline concentration.

The CO_2 and O_2 concentrations listed are averages of measurements made at several locations along the length of the melter near the oxy-fuel burners. Oxygen and nitrogen concentrations in the exhaust ports were significantly higher than the typical values in the combustion space, due to air infiltration through the batch charger and backwall. This air tended to "short circuit" to the exhaust ports, and therefore had little influence on nitrogen and oxygen concentrations or NO_x formation in the melter combustion zone.

The importance of limiting air infiltration into the combustion space for achieving minimum NO_x emissions was made clear by measurements taken in the very first days of glass production with 100% OEC, before the melter had been sealed and fully insulated. During this period, calculated (wet basis) combustion space nitrogen concentration based on CO_2 and O_2 measurements was as high as 12%, and NO_x emissions as high as 2.3 pounds per ton were measured. A careful job of melter sealing by Gallo allowed the very low nitrogen concentration and NO_x emissions level indicated in Table VIII to be achieved when stack emissions tests were conducted during the second month of the melting campaign. Careful control of excess oxygen concentrations in the combustion space also contributed to the low NO_x emissions achieved during both 100% OEC stack emissions tests at Gallo.

Following start up of the VPSA oxygen plants, melter #1 was supplied with a mix of VPSA and liquid oxygen containing about 3% nitrogen and 3% argon by volume. NO_x emissions measured under this condition were 0.94 lbs per ton of glass, more than 80% below the baseline emissions level, and about 18 percent higher than the level measured with liquid oxygen supply. CO_2 and oxygen concentration measurements indicated a combustion space nitrogen concentration during these tests ranging from 4 to 5 percent. This increase

in combustion space nitrogen concentration relative to the 3% concentration determined during the initial 100% OEC stack test was consistent with the calculated expectation of about a 1.5 percentage point increase due to the 3% nitrogen concentration of the VPSA oxygen. This suggests that there was little change in air infiltration rates between the two 100% OEC stack tests. The impact of the nitrogen impurity in VPSA oxygen on the overall level of NO_x emissions was small, especially relative to the variability in NO_x emissions measured at different points in the melter sealing process.

5.3.2.2 Particulate Emissions

Baseline and 100% OEC particulate emissions results from Gallo are summarized in Table IX. Three one-hour sample runs were conducted late in the baseline campaign, and again during the second month of oxy-fuel melting, using EPA method 5. Unlike at Carr-Lowrey, the stack tests were conducted at nearly equal pulls, which greatly facilitates comparison of the data. Also facilitating comparison was the absence of a regenerator between the melter and the sample point, which at Carr-Lowrey may have acted as a transient emissions source as checker temperatures increased during 100% OEC operation.

Particulate emissions at Gallo were reduced by about 25 percent from baseline levels, to 0.88 pounds per ton of glass, following conversion to 100% OEC. This reduction occurred despite the lower electric boost usage during 100% OEC operation than during baseline operation discussed earlier. Higher electric boost typically allows a given rate of melting to be achieved at a lower glass surface temperature, which in turn lowers the rate of NaOH volatilization from the glass melt.

TABLE IX

PARTICULATE EMISSIONS - GALLO GLASS MELTER #1

	BASELINE	100% OEC
GLASS PULL (TPD)	335	342
SUMMARY OF THREE 1-HOUR MEASUREMENTS:		
PARTICULATE (LB/HR):		
TEST 1	17.3	15.4
TEST 2	16.9	10.9
TEST 3	15.5	11.5
AVERAGE (LB/HR)	16.6	12.6
(LB/TON)	1.19	0.88

The particulate emissions reduction achieved at Gallo is in general agreement with predictions of the volatilization study referenced in section 4.3.4.2. However, the model suggests the reduction might have been greater if the burners were located further from the glass surface, lowering peak glass temperatures and gas velocities at the glass surface. However, no attempt was made to test this proposition, or to determine what tradeoffs (such as higher peak refractory temperatures) might be required to achieve still lower particulate emissions.

5.3.2.3 Carbon Monoxide and SO_2 Emissions

Carbon monoxide and sulfur dioxide emissions measurements are summarized in Table X. As indicated, CO emissions decreased on average following conversion to 100% OEC.

In contrast to other emissions, SO_2 emissions from Gallo melter #1 increased an average of 10 percent from baseline levels following conversion to 100% OEC. This increase may be related to the observed reduction in particulate emissions. (Particulate and SO_2 emissions were measured on consecutive days). Sodium hydroxide present in the flue gases reacts with a portion of the available SO_2 to form sodium sulphate particulate. The reduction in particulate emissions following 100% OEC conversion indicates less sodium hydroxide was present, which would result in a lower consumption of SO_2 by this reaction. More specifically, particulate emissions were reduced by about 4 pounds per hour following conversion to 100% OEC. Assuming most of this particulate was sodium sulphate, the sulfur content of this reduced emission was likely in the range of 0.7 to 0.8 pounds per hour. This matches well with the 1 to 2 pound per hour SO_2 emissions increase observed, the sulfur portion of which would be 0.5 to 1.0 pounds per hour.

TABLE X

CO AND SO2 EMISSIONS - GALLO GLASS MELTER #1

	BASELINE	100% OEC	
		LIQUID O2	LIQ/VPSA MIXTURE
GLASS PULL (TPD)	335	342	339
CO EMISSION LB/HR	1.0	0.09	<0.2
SO2 EMISSION LB/HR	12.9	13.8	14.7

A reduction in sulfur retention by the glass would also contribute to increased SO_2 emissions, by the necessary data to evaluate whether such a change occurred was not collected as part of this project.

5.4 Burner Performance

The oxy-fuel burners supplied by Corning for melter #1 at Gallo operated the first two years of the oxy-fuel melting campaign without maintenance or any signs of deterioration to the burners or burner blocks. Based on these observations, the burners are expected to last the entire melting campaign without any major maintenance requirement.

5.5 VPSA Oxygen Supply System

A key objective of Phase II was to demonstrate the capabilities of a large scale PSA system, and in particular, to show that the power requirements and costs were as projected in Phase I. Specific goals were:

1. Verify that an advanced PSA system can reliably supply oxygen at a low energy consumption rate of less than 350 kwh/ton of equivalent pure oxygen produced.
2. Demonstrate that large PSA systems will result in significantly lower power draw and product cost as a result of their attractive economies of scale.

The objective was to demonstrate the above on a plant that required a minimum of 20 tons per day of oxygen, and install and run the plant after the furnace had operated on liquid oxygen for a few months test period.

5.5.1 Process Description and Plant Design

The basis of Praxair's advanced PSA technology and what makes it leading state of the art is inherent in two aspects of its design:

1. The adsorbent used is highly efficient with over twice the separating capability of other PSA oxygen adsorbents on the market. It was developed specifically for air separation.

2. The Vacuum/Pressure Swing Adsorption (VPSA) cycle employed makes optimum use of the advanced adsorbent to lower power draw and product cost.

The adsorbent and cycle directly result in low power draw. Additionally, the high efficiency of the adsorbent allows plants that are much smaller with fewer vessels and valves than today's typical PSA/VSA systems. This also allows a high degree of prepackaging which reduces installation time and costs. Overall, the combination allows for highly efficient operation while minimizing installation and operating complexity.

The oxygen enriched air production system demonstrated in Phase I of this project by Praxair was scaled up from 1 ton per day to over 50 tons per day and a pair of units were built and installed at Gallo. The first major task was to design this scaled up system. This included process design, equipment selection, control systems design, computerization, and overall system optimization.

Figure 19 shows a schematic of a VPSA system. The major equipment includes the feed air blower, vacuum pump, vessels with sieve, motors and motor control center, valve skid, and product compressor (when required). During process sequencing, the two adsorption vessels operate 180° out of phase. While one vessel is on a pressure adsorption step to produce high purity oxygen, the remaining vessel undergoes regeneration to remove previously adsorbed materials from the adsorbent.

FIGURE 19

OxyGEN™ VPSA System

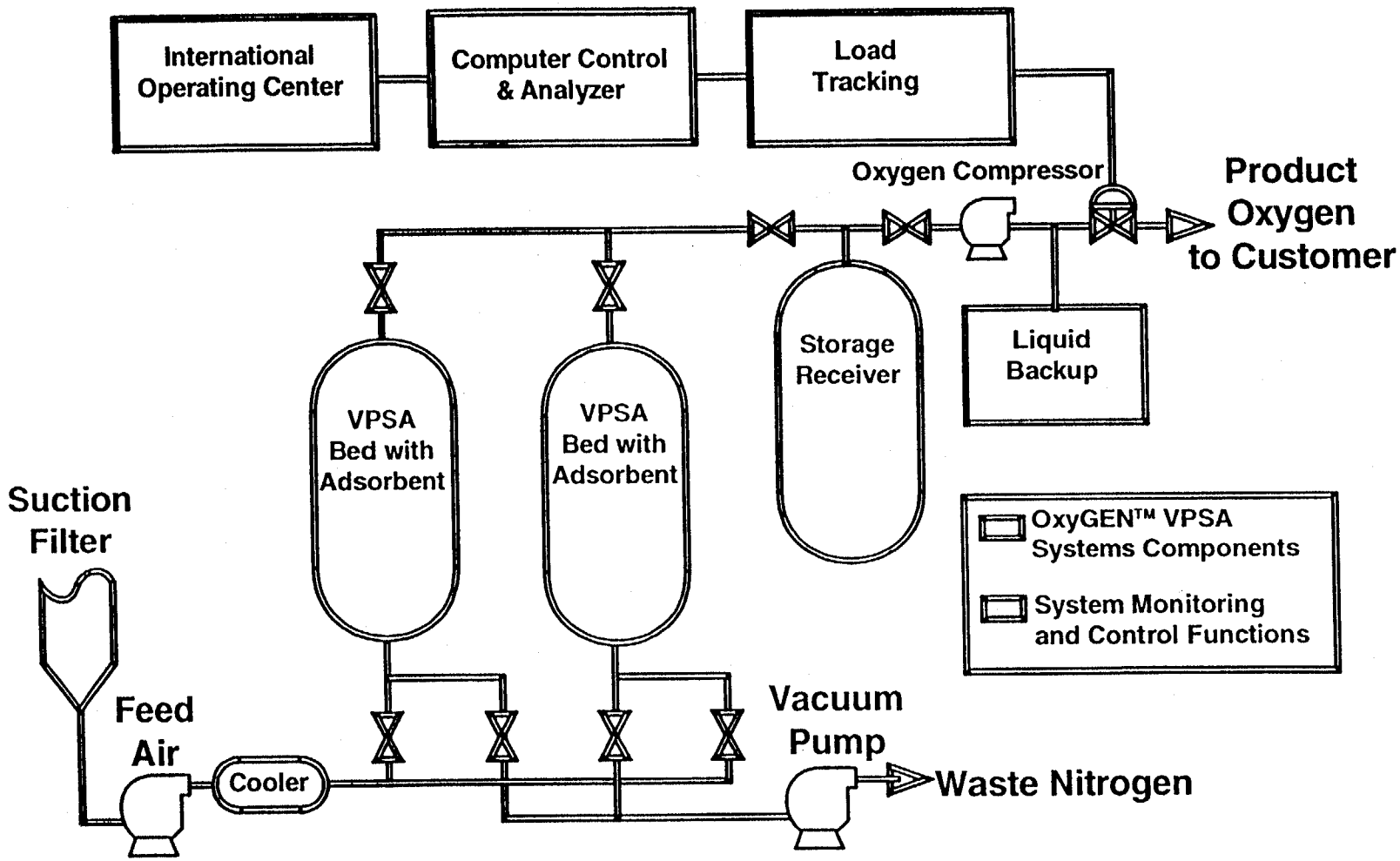

The adsorption step takes place at elevated pressures with feed air supplied by the feed blower. During adsorption nitrogen, water, and carbon dioxide are preferably adsorbed, while the majority of oxygen and argon pass through the vessel along with a small quantity of nitrogen. This oxygen product gas undergoes only a small pressure loss during the step, thereby entering the product surge tank at pressures near the adsorption pressure.

Regeneration occurs at reduced pressures, with this pressure reduction resulting in previously adsorbed nitrogen, water, and carbon dioxide being stripped from the adsorbent material. Utilization of a vacuum pump results in enhanced regeneration and therefore, utilization of the adsorbent, resulting in maximum process performance. Discharge of the vacuum pump is directly to the surroundings.

Duration of the adsorption/regeneration steps is monitored by a process controller, with the desired step time inputted to the controller. Following the termination of a step, the controller adjusts the process valves, such that the vessel previously on adsorption now undergoes regeneration, and the second vessel undergoes adsorption.

The oxygen product is provided automatically on demand to the customer from the product purge tank. It is delivered directly to the customer use point if low pressure is required (< 5 psig) or through a product oxygen compressor if higher pressure is required.*

The design and selection of all plant components must factor in initial costs as well as on-going operating costs, particularly energy costs. The feed blower and vacuum pump, for example, have a number of commercial options to meet the flow and pressure

* The oxygen supplied to the Gallo plant was at a pressure of 20 to 25 psig, so a compressor was required.

requirements of the process. Options include centrifugal and reciprocating type machines as well as Roots type blowers. Considering the dynamic nature of the VPSA cycle, positive displacement machines offer significantly improved efficiency over centrifugal machines. When comparing positive displacement machines, Roots type blowers are lower cost, easier to install, and require less maintenance over the long term. For vacuum service the Roots type blower can be water sealed which results in about 20% lower energy requirement than "dry" operation. The major disadvantage of the blowers is that they require more "noise treatment" than the other options. Overall the optimum choice is the Roots type blowers.

The rest of the equipment must also be designed with consideration for the trade-off between initial cost and power cost. For example, vessels, piping and valves are optimized considering the impact of pressure drop on system efficiency.

The control system is designed for unattended operation with the capability to remotely monitor and control the plant. Another key component for reliable operation is the design of the automatic valves. This dynamic process requires control valves that can withstand high cyclic service (over 1 million cycles per year). Complete valve assemblies - solenoids, actuators, and butterfly valves are selected on that basis.

The overall optimization of the Gallo VPSA system included the final selection of the process, equipment, and controls to ensure the lowest cost product considering the customer's availability of utilities and the final product requirements (i.e. pressure). This optimization included consideration for operating costs (i.e. power) as well as initial cost of the equipment and installation.

5.5.2 Installation and Start Up

The installation phase of the project included plant packaging and detail construction design as well as the actual installation. Each 55 ton per day VPSA plant was prepackaged in five skids to minimize the field construction time and cost. As shown in Figure 20 the packages were broken down as follows: feed blower skid, process skid, vacuum blower skid, auxiliary skid, and the electrical skid. The packages were designed with detailed piping, tubing and wiring done to minimize those activities in the field.

Other detail design activity was completed in the control systems area such as wiring schematics, panel designs, and process and instrumentation drawings. The construction package then was completed including civil, mechanical, and electrical drawings and specifications. At the end of the detail design stage "Design Safety Checklists" are completed to ensure that the design met all applicable safety standards.

The construction package was released for bidding purposes and a qualified contractor was selected to assemble and install the VPSA System at Gallo. Praxair provided on-site construction assistance throughout the mechanical and electrical installation. During this time, a number of quality assurance and safety checks were made as the plant was being built per Praxair's quality work process. At the completion of the construction phase the plant was functionally checked out to ensure all systems would perform as intended. Because the plant was highly prepackaged, the time to install the two plants was reduced significantly from plants that were not prepackaged.

FIGURE 20

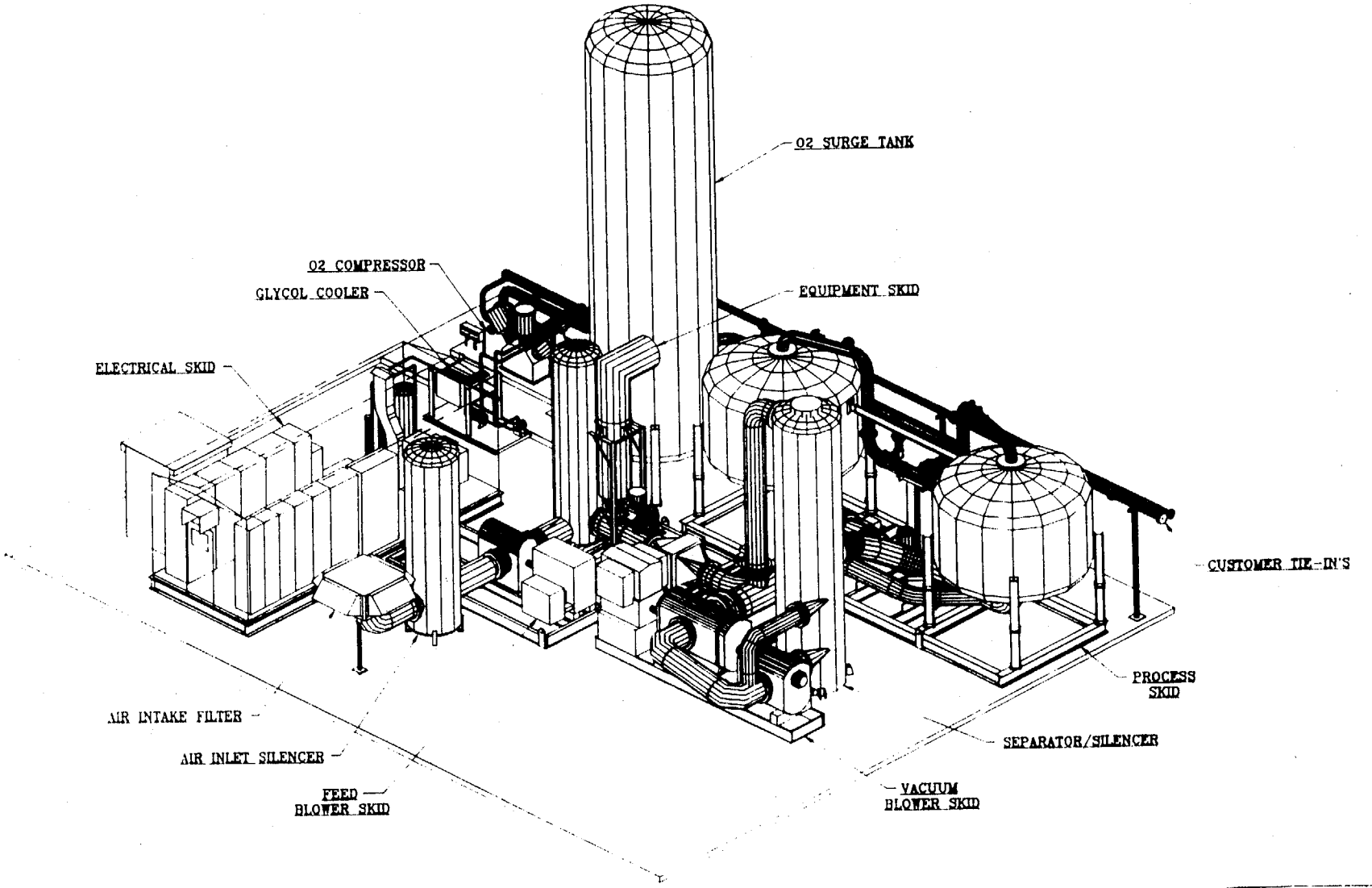

CONFIDENTIAL

VPSA PORTABLE OXYGEN

PRAXAIR

OVERALL PLANT ISOMETRIC VIEW

After completion of the functional systems checks, including run-in of the feed blower and vacuum pump, the VPSA process skid was started and cycle adjustments made to optimize performance. Mechanically and VPSA process wise, the plant start-up went smoothly, however, a problem encountered at this time was the noise from the plant. Although it was anticipated that the plant would be "noisy",it is an unattended facility, and given its location within the Gallo plant boundaries, it was not expected to be a problem for people at the plant, in the community or for Praxair personnel. The noise characteristics were, however, a problem for some members of the Modesto community. Praxair worked with Gallo to develop and agree upon noise treatment required to satisfy the neighboring community. After the noise treatment was completed, the plant was put on-stream around the clock to provide oxygen for the Gallo furnaces.

The plants operate automatically with the capability to remotely monitor performance. The plant computer can provide instantaneous information on flows, purity, temperatures, pressures, etc., or historical information such as hourly or daily averages. This information is also very valuable for troubleshooting to pinpoint problems after they happen (i.e. the historical data) or for anticipating potential problems (i.e. instantaneous information).

5.5.3 VPSA Plant Performance.

After the VPSA plant had been operated for a few weeks, a detailed performance test was conducted to measure product oxygen flow, purity, and total system power draw for one of the 55 ton per day plants. Table XI lists of the instrumentation used to collect the data. Two test runs were made and are summarized in Table XII. The single plant

TABLE XI

VPSA PERFORMANCE TEST INSTRUMENTATION

	COMPONENT	DESCRIPTION	EXPECTED ACCURACY	CALIBRATION
1.	Servomex Oxygen Analyzer	Model: OA 272 Range: 0-100% O_2	0.5%	By Praxair Technology Center
2.	Orifice Plates	Daniel Flow Tube/ Orifice	2%	" " " "
3.	Rosemount Pressure Transmitter	Model: 1151 & Model: 2044	0.5%	" " " "
4.	Rosemount Differential Pressure Transmitter	Model: 1151 & Model: 2088	0.5%	" " "
5.	Omega Thermocouples	Models: CASS-18	1%	" " " "
6.	Dranatz Power Demand Analyzer	Model: 808 with Isolated CT Terminations	2%	At Factory
7.	Potential Transformer	GE-643X92	.3%	At Factory
8.	Current Transformer	GE-750410G353	.6%	At Factory
9.	Plant Control Computer	Analog Devices-input cards Octagon Systems Corp. - Basic Programming • Flow Computer • Data Recorder	.5%	By Praxair Technology Center

TABLE XII. VPSA PERFORMANCE TEST SUMMARY

	TEST #1	TEST #2
TOTAL GAS FLOW (NCFH)	64160	61370
PRODUCT PURITY (% O2)	90.24	90.32
TOTAL OXY FLOW (TPD)	57.55	55.1
TOTAL POWER DRAW (kW)	776	739
ENERGY (kWh/TON O2)	323	322

produced 55 to 58 tons per day of contained oxygen at 90 to 91% purity and at an electrical power demand of 320 to 325 kwh/ton of oxygen. It is important to note that the addition of silencers on the plant to solve the noise problem added 10 to 15 kwh/ton. The silencers add pressure drop in the system which equates to more work by the feed blower and vacuum pump to overcome this added drop. Without the silencers the power draw would be approximately 310 kwh/ton. Subsequent plants have been designed to minimize the effect of noise attenuation on power draw based on the knowledge gained on this project.

Due to the success of the use of oxygen in combustion, the market for VPSA systems for this application has grown rapidly. Since the DOE/Gallo project was started, a number of other VPSA/combustion projects have been successfully completed, allowing the impact of various operating variable of power consumption to be assessed. Electrical power draw for these plants has varied from 250 kwh/ton to 320 kwh/ton depending on the oxygen supply pressure and the noise attenuation required. The higher the oxygen pressure requirement, the higher the power draw, and resultant oxygen cost (see Figure 21). The oxygen pressure requirement at the inlet to Gallo's distribution is 20 to 25 psig. If lower pressure can be used (i.e. 5 psig), then the power draw would be 30 to 40 kwh/ton lower. The lowest power requirement achieved (i.e. 250 kwh/ton) reflects a 5 psig system with the latest technology advances. The number is continuing to fall as new adsorbents and cycles are developed.

In the Phase I report, the economics of larger scale VPSA system was projected to be as depicted in Figure 22. It was recognized that the cost of oxygen ($/ton) would decrease significantly as the plant size was increased above 1 ton per day. Specifically, it was projected that costs would go from about $100/ton to less than $50/ton. At the low specific

FIGURE 21

Effect Of Product Pressure On Product Cost

VPSA Systems

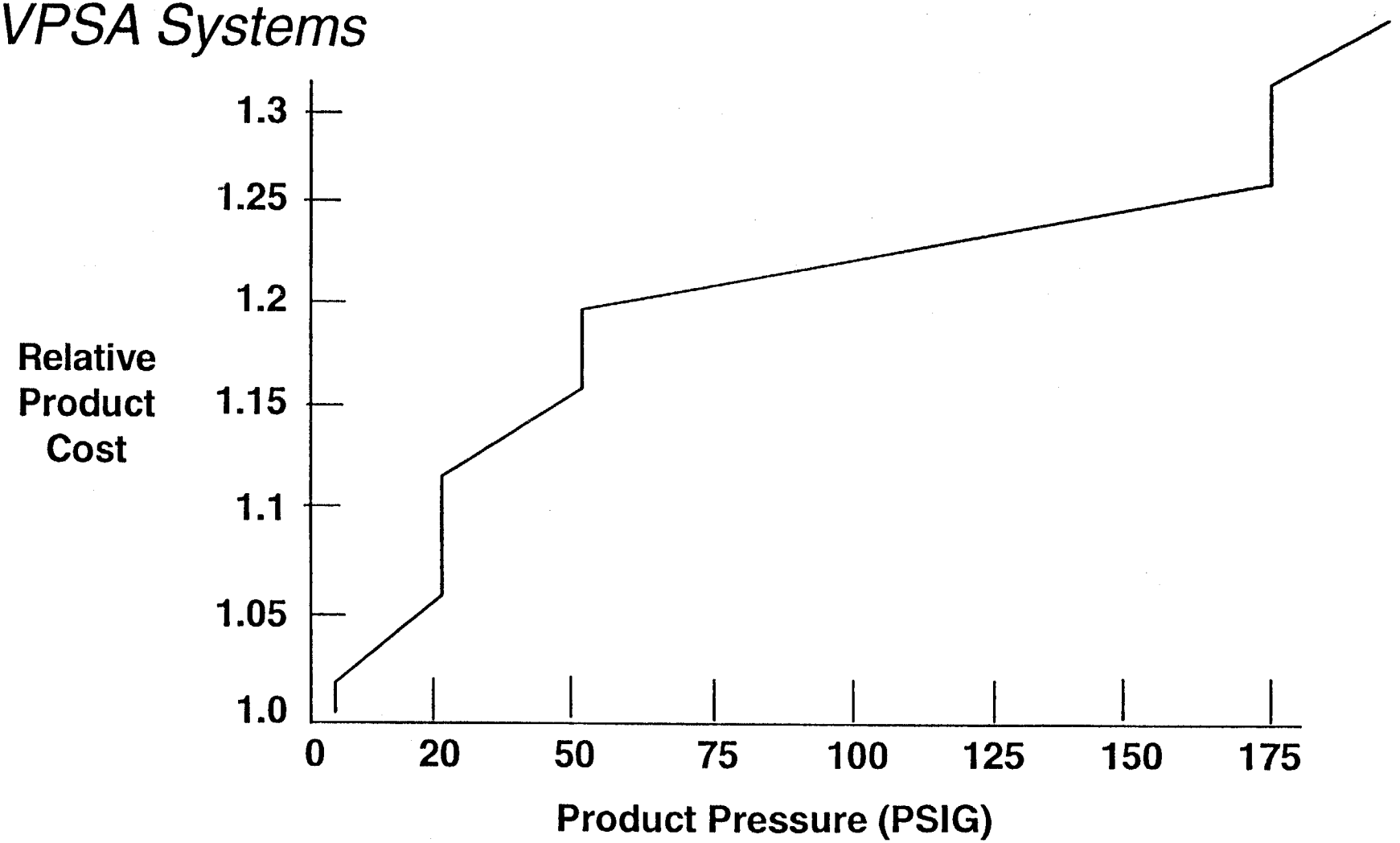

OXYGEN COST VERSUS PRODUCTION
100% UTILIZATION

FIGURE 22

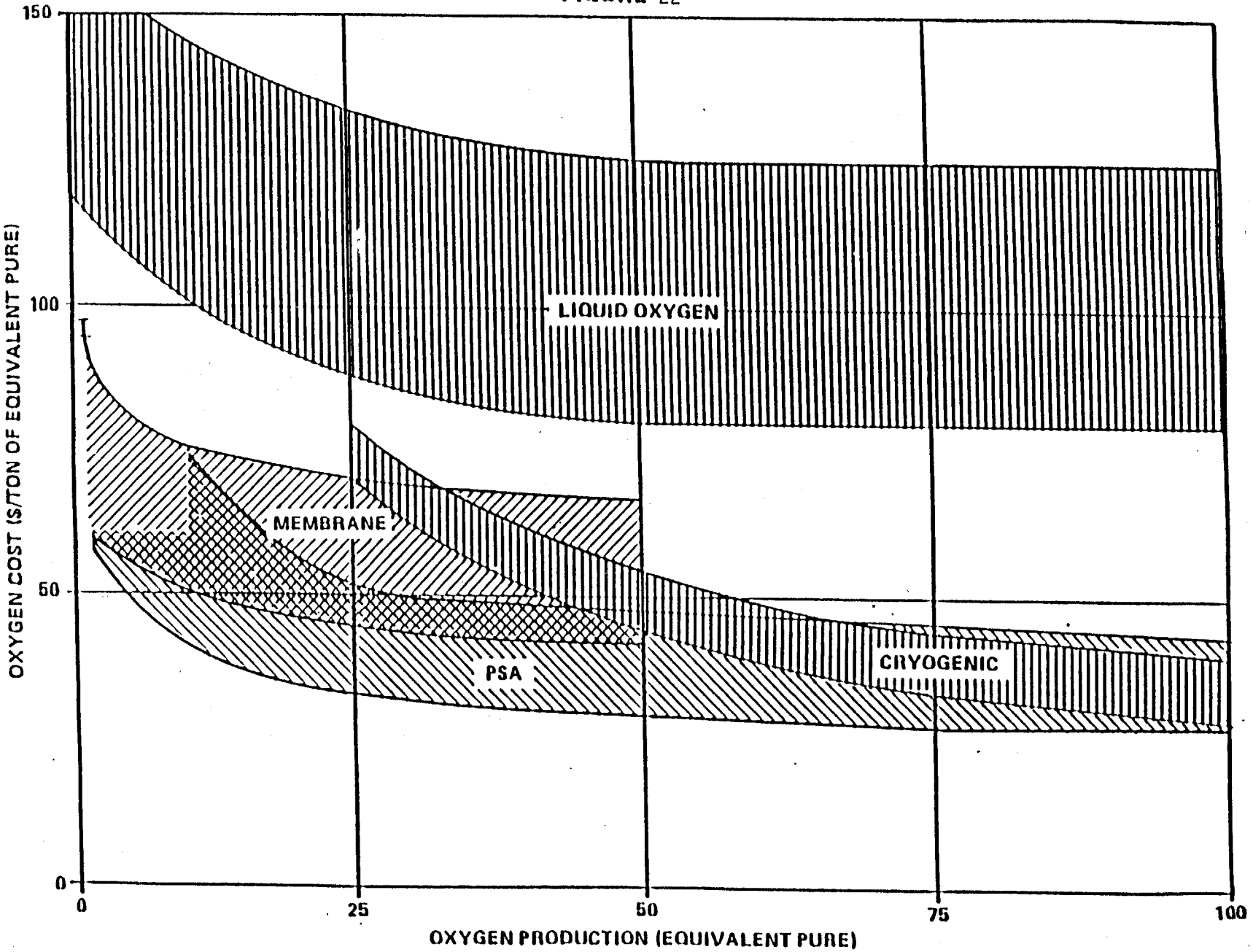

power requirements described above, VPSA oxygen can typically be supplied today at a cost of $30 to $35/ton, which is at the bottom edge of the original projections per Figure 22. Typically, about 40% of the cost is for power. As seen from the results, scale-up of the VPSA oxygen system has resulted in a low cost method to produce oxygen at the customer's site.

6.0 ENERGY IMPLICATIONS AND ECONOMICS OF REGENERATIVE MELTER CONVERSION TO 100% O.E.C.

6.1 Energy Implications

The energy performance comparisons conducted at Carr-Lowrey and Gallo indicate that the energy consumption of a regenerative glass melter can be reduced by conversion from regenerative firing to 100% OEC. However, the production of oxygen for 100% OEC melting requires electrical input, which in turn requires consumption of fuel at an electric power plant. Therefore, a broader, "back to the power plant" analysis must be performed to determine the overall energy impact of regenerative melter conversions to 100% OEC.

Whether or not overall energy consumption is reduced by a particular glass melter conversion will depend on numerous factors. First of all, the energy requirements for baseline regenerative operation can vary greatly depending on factors such as the heat recovery effectiveness of the regenerators, glass pull per unit hearth area, oxidant:fuel ratio settings and accuracy of ratio control, and the amount of electric boost utilized. Some of these factors, as well as others such as oxygen plant energy efficiency and oxygen supply pressure, will also affect the overall energy requirement for oxy-fuel melting.

Conversion to 100% OEC potentially allows different melting strategies to be

employed that can affect overall energy consumption. For example, electric boost is used in regenerative melters to achieve increased pull without increasing refractory temperature, or to maintain a given pull at lower firing rate and glass surface temperature in order to comply with air emissions regulations. Auxiliary oxy-fuel burners have been used in regenerative glass melting to achieve significant pull increases without increasing electric boost or crown temperatures (13). This was done by taking advantage of increased flexibility in locating and orienting oxy-fuel burners to optimize heat release patterns and accelerate batch melting. Although not demonstrated in this project, it should be possible to incorporate these same firing strategies into 100% OEC operation, lessening the need for electric boost. Additionally, the reduced NO_x and particulate emissions rates achieved with 100% OEC operation lessen the need for electric boost to achieve compliance with environmental regulations.

With these considerations in mind, Table XIII presents an analysis of the overall energy requirements of a generic 300 TPD container glass melting operation, comparing several cases of regenerative and oxy-fuel operation. Two base cases are presented: a regenerative melter operating with electric boost of 0.5 MMbtu/ton, and fuel input of 3.7 MMbtu/ton (case 1), and an unboosted regenerative melter with a specific fuel consumption of 4.45 MMbtu/ton (case 2). Contrasted to these are 2 oxy-fuel melting cases: a melter with electric boost of 0.4 MMbtu/ton, and fuel input of 3.35 MMbtu/ton (case 3), and an unboosted melter operating at 3.95 MMbtu/ton (case 4). The percentage melter energy savings achieved with 100% OEC reflected in these various cases is in line with the savings observed at Gallo and Carr-Lowrey.

TABLE XIII. GLOBAL ENERGY ANALYSIS

300 TPD CONTAINER GLASS OPERATION

	CASE 1	CASE 2	CASE 3	CASE 4	CASE 5
OXIDANT:	AIR	AIR	OXYGEN	OXYGEN	OXYGEN (WITH BATCH/ CULLET PREHT
ELECTRIC BOOST?	YES	NO	YES	NO	NO
GLASS PULL (TPD):	300	300	300	300	300
NOX EMISSIONS (LB/TON GLASS)	3-6	4-6	0.6-1	0.6-1	0.5-0.8
MELTER ENERGY: (MMBTU/TON)					
FUEL	3.70	4.45	3.35	3.95	3.20
ELECTRIC	0.50	0.00	0.40	0.00	0.00
OXYGEN (TPD)	0	0	83.8	98.8	80.0
"GLOBAL" ENERGY ANALYSIS					
ELECTRICITY (kWh/DAY)					
MELTER	43950	0	35160	0	0
OXYGEN PROD'N	0	0	22194	26169	21200
TOTAL ELEC.	43950	0	57353	26169	21200
FUEL FOR ELECTICITY PRODUCTION (*) (MMBTU/D)	448	0	585	267	216
MELTER FUEL (MMBTU/D)	1110	1335	1005	1185	960
TOTAL FUEL CONSUMPTION (MMBTU/DAY)	1558	1335	1590	1452	1176
RELATIVE FUEL REQUIREMENT:	BASE	86%	102%	93%	75%

* Assumes 10,200 Btu power plant fuel input per kWh of electric output.

It is important to note that cases 1 through 4 in Table XIII compare air-fuel cases in which a large portion of exhaust gas energy is recovered to preheat combustion air, to oxy-fuel cases with no heat recovery from the melter exhaust gases. Over 1/3 of the fuel energy input to an oxy-fuel melter is carried away by exhaust gases. About three-fourths of this is sensible heat that typically leaves the melter at a temperature of 2650 to 2750°F. Case 5 in Table XIII represents a hypothetical oxy-fuel firing case where a portion of this exhaust gas energy is used to preheat batch and cullet to 700°F before charging them to the melter. While batch/cullet preheating can also be applied to regenerative melters, it is not as economically attractive, since fuel savings alone are achieved. Batch/cullet preheating applied to an oxy-fuel fired melting results in oxygen savings roughly equal in dollar value to the value of the fuel savings.

Comparison of cases 1 through 4 in Table XIII shows that, if electric boost usage is unchanged following conversion to oxy-fuel operation, the fuel savings in the melter will typically be insufficient to balance increased power plant fuel input for oxygen production. However, an electric boost reduction of about 0.1 MMbtu per ton of glass results in a roughly "break even" energy comparison between regenerative and 100% OEC operation, and deeper boost reductions result in a clear overall energy advantage for 100% OEC. Batch and cullet preheating combined with oxy-fuel firing results in a 12 to 25 percent reduction in overall energy requirement relative to air-fuel firing.

6.2 Economics of Melter Conversion

The comparative economics of converting to 100% OEC versus other options varies with the specific circumstances and timing of a proposed conversion, and must be evaluated

on a case by case basis. Still, a generic analysis sheds light on the relative importance of various factors affecting the economics of 100% OEC.

An economic analysis of regenerative air-fuel fired glass furnaces and oxy-fuel fired furnaces was conducted for a generic 300 TPD container melter. The analysis takes as a starting point an existing melter approaching the end of its campaign, and evaluates various rebuild, retrofit, and replacement options. The following cases were analyzed, using specific energy consumption values from the previous section where applicable:

1. Rebuild melter for regenerative air-fuel firing, without stack gas treatment for emissions abatement, and with electric boost. Minimum achievable NO_x emissions is 3 to 4 pounds per ton, and emissions are typically higher. This could result in noncompliance with regulations in some jurisdictions before the end of the melting campaign.
2. Rebuild melter for 100% OEC operation, without NO_x emissions abatement, and with 20 percent electric boost reduction. NO_x emissions of 0.6 to 1 lb per ton achievable, depending on burner design and application.
3. Rebuild melter for 100% OEC operation, with electric boost eliminated. NO_x emissions of 1 pound or less per ton of glass are achievable.
4. Rebuild melter for regenerative air-fuel firing, with added investment for Selective Catalytic $DENO_x$. This option is analyzed, even though there are serious technical obstacles to SCR's applicability to glass furnaces. Various reports have indicated that, at a minimum, an electrostatic precipitator is required upstream of the $deNO_x$ system, and that even with this precaution the SCR catalyst is gradually "poisoned" by volatiles in the melter exhaust

gases, reducing its effectiveness (14). If this problem can be solved, NO_x emissions below 1 lb per ton should be achievable.

5. Replace the existing melter with a new electric melter. This would essentially eliminate NO_x emissions.

Table XIV shows the capital outlays required for each case, for the initial and subsequent rebuilds respectively. These costs are based on estimates provided to Praxair by glass furnace engineering companies for the glass tank itself, and on Praxair's own estimates of oxy-fuel equipment costs. The cost of an initial conversion to 100% OEC operation is about $1.3 MM less than rebuilding for conventional firing due to elimination of regenerators. This cost difference increases to $5.5 MM if investment if a deNO_x system is required to meet NO_x emissions requirements with air-fuel firing.

The cycle times for furnace and regenerator rebuilds are also listed in Table XIV. For the regenerative melter, the melter and regenerator rebuild cycles are assumed to be 7 and 14 years, respectively. The rebuilding cycle of the oxy-fuel furnace is assumed to be the same as the air furnace. A 3 year rebuild cycle is assumed for the electric melter.

Since capital and operating costs vary substantially over time for the different cases evaluated, Net Present Value (NPV) analyses were conducted from year 0 to year 20 to compare relative economics. Details of the NPV calculations at a discount rate of 15% are presented in Table XV.

At year 0 the initial rebuild or furnace replacement cost is charged. A rebuild period of 30 days is assumed, and entered in year 1. Annual utility costs' are calculated based on 365 days minus the rebuild period. Annual maintenance and insurance costs are included, and assumed to equal 3% of the initial capital investment. The amount of the initial capital

TABLE XIV. REBUILD COSTS - 300 TPD CONTAINER GLASS FURNACES

	AIR	OXY	AIR WITH SCR DENOX	ELECTRIC (NEW)
INITIAL REBUILD				
SUSPENDED CROWN				140
MELTER / REFINER	735	770	735	2,000
PORTS	350		350	
REGENERATOR	1,350		1,350	
STRUCTURAL STEEL	50	50	50	300
CHARGER/INJECTOR	30	30	30	60
BURNER/COMBUSTOR	30	250	30	80
FLUE / STACK	40	40	40	40
ELEC & CONTROL	45	150	45	900
COOLING	20	20	20	180
ENGINEERING	120	150	120	300
WATER & AIR	5	5	5	50
E.P. & SCRUBBER			2250	
DE-NOx SYSTEM			1750	
CATALYST			200	
TOTAL ($1,000)	2,775	1,465	6,975	4,050
SUBSEQUENT REBUILDS				
SUS. CROWN				14
MELTER / REFINER	735	770	735	1,600
PORTS	350		350	
REGEN (EVERY OTHER REBUILD)	1,350		1,350	
STRUCTURAL STEEL	50	30	50	30
CHARGER/INJECTOR	30	30	30	10
BURNER/COMBUSTOR	30	30	30	10
FLUE / STACK	40	10	40	
ELEC & CONTROL	45	30	45	180
COOLING	20	20	20	20
ENGINEERING	120	80	120	120
WATER & AIR	5	5	5	10
E.P. & SCRUBBER			225	
DE-NOx SYSTEM			500	
CATALYST				
TOTAL ($1,000)	2,775	1,005	3,500	1,994
FURNACE REBUILD CYCLE (YR)	7	7	7	3
REGEN REBUILD CYCLE (YR)	14		14	

TABLE XV.

NPV COST ANALYSIS 300 TPD CONTAINER GLASS MELTERS

1. AIR FURNACE REBUILD YR	0	1	2	3	4	5	6	7	8	9	10	11	12	13	14	15	16	17	18	19	20
MAINT/CONSTR. PERIOD(DAY)		30						30							30						
REBUILD COST	2775						1425							2775							1425
MAINT./INS.		164	164	164	164	164	164	164	164	164	164	164	164	164	164	164	164	164	164	164	164
CATALYST			0		0		0		0		0		0		0		0		0		0
	2775	164	164	164	164	164	1589	164	164	164	164	164	164	2939	164	164	164	164	164	164	1589
FUEL		1116	1215	1215	1215	1215	1215	1116	1215	1215	1215	1215	1215	1215	1116	1215	1215	1215	1215	1215	1215
ELECTRIC		736	802	802	802	802	802	736	802	802	802	802	802	802	736	802	802	802	802	802	802
OXYGEN		0	0	0	0	0	0	0	0	0	0	0	0	0	0	0	0	0	0	0	0
AMMONIA		0	0	0	0	0	0	0	0	0	0	0	0	0	0	0	0	0	0	0	0
		1852	2018	2018	2018	2018	2018	1852	2018	2018	2018	2018	2018	2018	1852	2018	2018	2018	2018	2018	2018

SUMMARY

TOTAL GLASS PRODUCED	2,163 (IN 1,000 TONS)
NPV - CAPITAL/MAINT.	5502 (IN $1,000)
	2.54 ($/TON)
NPV - UTILITIES	14813 (IN $1,000)
	6.85 ($/TON)
NPV - TOTAL COST	20315 (IN $1,000)
	9.39 ($/TON)

ASSUMPTIONS

AVG PRODUCTION	300 TPD
MELTER ENERGY (MMBTU/TON)	3.7 FUEL, 0.5 ELEC BOOST
DISCOUNT RATE	12 %
COST OF INSTALLED CAPITAL	5.45 MM $$
ANNUAL MAINT./INSURANCE	3 % OF COST OF INSTALLED CAPITAL
UTILITY COSTS - FUEL	3 $/MMBTU
- ELECTRIC	0.05 $/KWH
- OXYGEN	1.5 $/1,000 SCF
- AMMONIA	200 $/TON

2. OXYGEN FURNACE YR	0	1	2	3	4	5	6	7	8	9	10	11	12	13	14	15	16	17	18	19	20
MAINT/CONSTR. PERIOD(DAY)		30						30							30						
REBUILD COST	1465						1005							1005							1005
MAINT./INS.		107	107	107	107	107	107	107	107	107	107	107	107	107	107	107	107	107	107	107	107
CATALYST																					
	1465	107	107	107	107	107	1112	107	107	107	107	107	107	1112	107	107	107	107	107	107	1112
FUEL		1010	1100	1100	1100	1100	1100	1010	1100	1100	1100	1100	1100	1100	1010	1100	1100	1100	1100	1100	1100
ELECTRIC		589	642	642	642	642	642	589	642	642	642	642	642	642	589	642	642	642	642	642	642
OXYGEN		1010	1100	1100	1100	1100	1100	1010	1100	1100	1100	1100	1100	1100	1010	1100	1100	1100	1100	1100	1100
AMMONIA		0	0	0	0	0	0	0	0	0	0	0	0	0	0	0	0	0	0	0	0
		2609	2843	2843	2843	2843	2843	2609	2843	2843	2843	2843	2843	2843	2609	2843	2843	2843	2843	2843	2843

SUMMARY

TOTAL GLASS PRODUCED	2,163 (IN 1,000 TONS)
NPV - CAPITAL/MAINT.	3111 (IN $1,000)
	1.44 ($/TON)
NPV - UTILITIES	20871 (IN $1,000)
	9.65 ($/TON)
NPV - TOTAL COST	23982 (IN $1,000)
	11.09 ($/TON)

ASSUMPTIONS

AVG PRODUCTION	300 TPD
MELTER ENERGY (MMBTU/TON)	3.35 FUEL, 0.4 ELEC BOOST
DISCOUNT RATE	12 %
COST OF INSTALLED CAPITAL	3.58 MM $$
ANNUAL MAINT./INSURANCE	3 % OF COST OF INSTALLED CAPITAL
UTILITY COSTS - FUEL	3 $/MMBTU
- ELECTRIC	0.05 $/KWH
- OXYGEN	1.5 $/1,000 SCF
- AMMONIA	200 $/TON

NPV COST ANALYSIS 300 TPD CONTAINER GLASS MELTERS

3. OXYGEN FURNACE - NO BOOST	0	1	2	3	4	5	6	7	8	9	10	11	12	13	14	15	16	17	18	19	20
MAINT/CONSTR. PERIOD(DAY)		30						30							30						
REBUILD COST	1465						1005							1005							1005
MAINT./INS.		107	107	107	107	107	107	107	107	107	107	107	107	107	107	107	107	107	107	107	107
CATALYST																					
	1465	107	107	107	107	107	1112	107	107	107	107	107	107	1112	107	107	107	107	107	107	1112
FUEL		1191	1298	1298	1298	1298	1298	1191	1298	1298	1298	1298	1298	1298	1191	1298	1298	1298	1298	1298	1298
ELECTRIC		0	0	0	0	0	0	0	0	0	0	0	0	0	0	0	0	0	0	0	0
OXYGEN		1191	1298	1298	1298	1298	1298	1191	1298	1298	1298	1298	1298	1298	1191	1298	1298	1298	1298	1298	1298
AMMONIA		0	0	0	0	0	0	0	0	0	0	0	0	0	0	0	0	0	0	0	0
		2382	2595	2595	2595	2595	2595	2382	2595	2595	2595	2595	2595	2595	2382	2595	2595	2595	2595	2595	2595

SUMMARY

TOTAL GLASS PRODUCED	2,163 (IN 1,000 TONS)
NPV - CAPITAL/MAINT.	3111 (IN $1,000)
	1.44 ($/TON)
NPV - UTILITIES	19054 (IN $1,000)
	8.81 ($/TON)
NPV - TOTAL COST	22165 (IN $1,000)
	10.25 ($/TON)

ASSUMPTIONS

AVG PRODUCTION	300 TPD
MELTER ENERGY (MMBTU/TON)	3.95 FUEL, 0.0 ELEC BOOST
DISCOUNT RATE	12 %
COST OF INSTALLED CAPITAL	3.58 MM $$
ANNUAL MAINT./INSURANCE	3 % OF COST OF INSTALLED CAPITAL
UTILITY COSTS - FUEL	3 $/MMBTU
- ELECTRIC	0.05 $/KWH
- OXYGEN	1.5 $/1,000 SCF
- AMMONIA	200 $/TON

4. AIR FURNACE WITH DENOx	0	1	2	3	4	5	6	7	8	9	10	11	12	13	14	15	16	17	18	19	20
MAINT/CONSTR. PERIOD(DAY)		30						30							30						
REBUILD COST	6975						2150							3500							2150
MAINT./INS.		290	290	290	290	290	290	290	290	290	290	290	290	290	290	290	290	290	290	290	290
CATALYST			200		200		200		200		200		200		200		200		200		200
	6975	290	490	290	490	290	2640	290	490	290	490	290	490	3790	490	290	490	290	490	290	2640
FUEL		1116	1215	1215	1215	1215	1215	1116	1215	1215	1215	1215	1215	1215	1116	1215	1215	1215	1215	1215	1215
ELECTRIC		736	802	802	802	802	802	736	802	802	802	802	802	802	736	802	802	802	802	802	802
OXYGEN		0	0	0	0	0	0	0	0	0	0	0	0	0	0	0	0	0	0	0	0
AMMONIA		54	59	59	59	59	59	54	59	59	59	59	59	59	54	59	59	59	59	59	59
		1906	2077	2077	2077	2077	2077	1906	2077	2077	2077	2077	2077	2077	1906	2077	2077	2077	2077	2077	2077

SUMMARY

TOTAL GLASS PRODUCED	2,163 (IN 1,000 TONS)
NPV - CAPITAL/MAINT.	11956 (IN $1,000)
	5.53 ($/TON)
NPV - UTILITIES	15247 (IN $1,000)
	7.05 ($/TON)
NPV - TOTAL COST	27203 (IN $1,000)
	12.58 ($/TON)

ASSUMPTIONS

AVG PRODUCTION	300 TPD
MELTER ENERGY (MMBTU/TON)	3.7 FUEL, 0.5 ELEC BOOST
DISCOUNT RATE	12 %
COST OF INSTALLED CAPITAL	9.65 MM $$
ANNUAL MAINT./INSURANCE	3 % OF COST OF INSTALLED CAPITAL
UTILITY COSTS - FUEL	3 $/MMBTU
- ELECTRIC	0.05 $/KWH
- OXYGEN	1.5 $/1,000 SCF
- AMMONIA	200 $/TON

NPV COST ANALYSIS 300 TPD CONTAINER GLASS MELTERS

5. ELECTRIC FURNACE	YEAR 0	1	2	3	4	5	6	7	8	9	10	11	12	13	14	15	16	17	18	19	20
MAINT/CONSTR. PERIOD(DAY)		60			30			30			30			30			30			30	
REBUILD COST	4050			1994			1994			1994			1994			1994			1994		1990
MAINT./INS.		122	122	122	122	122	122	122	122	122	122	122	122	122	122	122	122	122	122	122	122
CATALYST																					
	4050	122	122	2116	122	122	2116	122	122	2116	122	122	2116	122	122	2116	122	122	2116	122	2112
FUEL		0	0	0	0	0	0	0	0	0	0	0	0	0	0	0	0	0	0	0	0
ELECTRIC		3660	4380	4380	4020	4380	4380	4020	4380	4380	4020	4380	4380	4020	4380	4380	4020	4380	4380	4020	4380
OXYGEN		0	0	0	0	0	0	0	0	0	0	0	0	0	0	0	0	0	0	0	0
AMMONIA		0	0	0	0	0	0	0	0	0	0	0	0	0	0	0	0	0	0	0	0
		3660	4380	4380	4020	4380	4380	4020	4380	4380	4020	4380	4380	4020	4380	4380	4020	4380	4380	4020	4380

SUMMARY

TOTAL GLASS PRODUCED	2,118	(IN 1,000 TONS)
NPV - CAPITAL/MAINT.	9448	(IN $1,000)
	4.46	($/TON)
NPV - UTILITIES	31383	(IN $1,000)
	14.82	($/TON)
NPV - TOTAL COST	40831	(IN $1,000)
	19.28	($/TON)

ASSUMPTIONS

AVG PRODUCTION	300	TPD
MELTER ENERGY	800	KWH/TON
ANNUAL MAINT./INSURANCE	3	% OF COST OF INSTALLED CAPITAL
DISCOUNT RATE	12	%
UTILITY COSTS - FUEL	3	$/MMBTU
- ELECTRIC	0.05	$/KWH
- OXYGEN	1.5	$/1,000 SCF
- AMMONIA	200	$/TON

investment for each case is listed in the assumptions section of each table, and is based on estimates from furnace engineering companies. These estimates reflect the total costs of installed capital, and exceed the rebuild costs listed in Table XIV.

The furnaces are rebuilt every seven years (three years for the electric melter) and regenerators are rebuilt every fourteen years. Overall cost outlays are projected in this way for 20 years and, assuming a discount rate of 12%, the future costs are discounted and summed. The overall glass production and the costs as net present values are summarized. NPV costs per ton of glass are also calculated.

Results of the analysis are summarized in Figure 23. The following conclusions can be drawn from this economics study:

1. Substantial savings in furnace rebuild and fuel costs are achieved with oxy-fuel firing. However, the overall utility costs of oxy-fuel firing are higher than those of a regenerative furnace due to the additional cost of oxygen.
2. The NPV of the capital and operating costs of converting an existing regenerative melter to oxy-fuel firing is 10 to 20 percent greater than that of rebuilding the regenerative furnace without a deNO_x system. However, the oxy-fuel furnace typically reduces NO_x emissions by 90% relative to regenerative operation.
3. The economics of retrofitting for oxy-fuel firing is about 10 to 20 percent better than that of rebuilding for regenerative firing with a catalytic deNO_x system designed for similar levels of NO_x emissions.
4. Due to high operating cost of electric melting, replacing a regenerative melter with an electric melter is the most expensive option evaluated.

ECONOMICS - 300 TPD CONTAINER MELTER
NPV ANALYSIS; 12% DISCOUNT RATE; 20 YRS

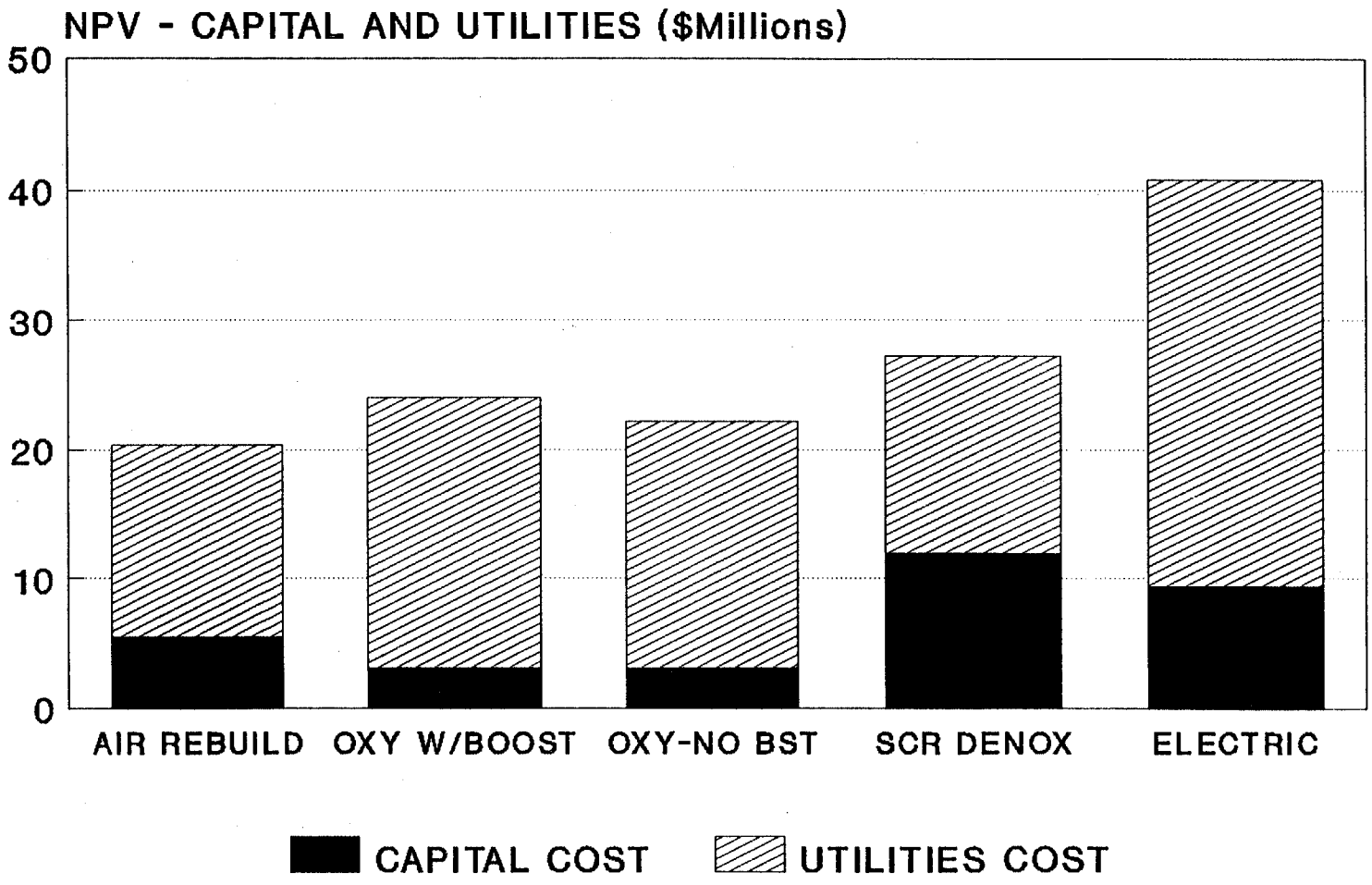

FIGURE 23

7.O COMBUSTION SPACE MODELLING

FURNACE THERMAL ANALYSIS AND VERIFICATION

A furnace heat transfer model was employed during this project, first to model and verify results from pilot scale experimental furnaces, then to analyze flame characteristics and burner placement for glass furnaces, and finally to conduct full glass furnace performance modelling and verification.

The furnace model used was originally developed for boiler applications. In the first study it was modified for glass furnace conditions. In Phase I of this project, model predictions were verified against pilot scale test data taken from experimental furnaces. Good agreements were obtained and the results were reported elsewhere (3,15).

A second study was conducted prior to field tests to analyze the effects of oxy-fuel burner flame characteristics and placement on furnace thermal conditions. A furnace end section which includes the bridge wall and a pair of regenerator ports was modelled in detail for a base air case and several oxy-fuel firing cases. The firing rates of two oxy-fuel burners that matched the heat flux distribution of the base air case were determined. The effects of the height and angle of the oxy-fuel burners on the temperature and heat flux distributions were predicted to evaluate the optimum burner placement of the oxy-fuel burners.

The main conclusions of the simulations were that; (1) in spite of the small flame diameters, the high momentum low flame temperature oxy-fuel burners can create temperature and heat flux distributions equivalent to those of the base air case with a wide flame and (2) both lower burner elevation and angling of the oxy-fuel burners toward the

glass surface tend to increase heat transfer to glass surface and reduce the peak refractory temperatures. A detailed technical paper describing the model assumptions and results was presented previously and attached in Appendix A (16). The results of this study also provided the basis to develop general design considerations for oxy-fuel fired glass furnaces and presented in a glass industry conference (17).

In the third study the model was applied to the furnace at Gallo Glass. Furnace wall temperatures were measured by an optical pyrometer after the conversion to oxy-fuel firing. Model predictions and comparison with measured temperatures will be published in a separate paper.

8.0 REFERENCES

1. H. Kobayashi, "Oxygen Enriched Combustion System Performance Study, Phase I Interim/Final Report, Volume I - Technical and Economic Analysis," U.S. Department of Energy, March, 1987.

2. H. Kobayashi, "Oxygen Enriched Combustion System Performance Study, Phase I Final Report, Volume II - Market Assessment", U.S. Department of Energy, September, 1988.

3. Y. Kwan et. al., "Oxygen Enriched Combustion System Performance Study, Phase I Final Report, Volume III - Burner Tests and Combustion Modeling," U. S. Department of Energy, September, 1988.

4. D. A. LaGree, "Oxygen Enriched Air Production System," U. S. Department of Energy, November, 1988.

5. J. T. Brown, "100% Oxygen-Fuel Combustion for Glass Furnaces", pp.202-217 in the Proceedings of the 51st Conference on Glass Problems, edited by Charles H. Drummond. American Ceramic Society, Westerville, Ohio (1991)

6. D. E. Shamp, D. H. Davis, "Application of 100% Oxygen Firing at Parkersburg, West Virginia", pp.218-239 in the Proceedings of the 51st Conference on Glass Problems, edited by Charles H. Drummond. American Ceramic Society, Westerville, Ohio (1991)

7. D. Moore, J. T. Brown, "Conversion of a Large Container Furnace from Regenerative Firing to Direct Oxy-Fuel Combustion. These Proceedings.

8. M. Cable, C. Rasul, J. Savage, "Laboratory Investigation of Foaming and Reboil in Soda-Lime-Silica Melts", Glass Technology, Vol. 9, No. 2, April 1988.

9. W. Trier, Glass Furnaces, Design Construction and Operation, pp 81-82, Society of Glass 'Technology, Sheffield, England, 1987.

10. R. J. Ryder, E. C. Taylor, K. B. Tanner, "Pollutant Emissions From Glass Container Furnaces", pp. 199-205 Glass Technology, Vol. 21, No.4, August, 1980.

11. H. Kobayashi, R. Beerkens, P. Ercole, R. Barbiero, "Emissions of Particulates and NOx From Oxy-Fuel Fired Glass Furnaces", Proceedings of the Second Conference of the European Society of Glass Science and Technology, June, 1993.

12. R.G.C. Beerkens, TNO, The Netherlands, Proprietary reports to Praxair, Inc. Nov. 1992.

13. G. Tuson, H. Kobayashi, E. Lauwers, "Industrial Experience With Oxy-Fuel Fired Glass Melters", presented at Glassman Europe, April, 1993.

14. G. Moilanen, B. Van Kalsbeek, "NOx Control Options for Glass Furnaces", Proceedings of 51st Conference on Glass Problems, American Ceramic Society, 1991.

15. W. Richter, R. Payne, "Modelling Study of Burner and Furnace Performance For Oxygen Enriched Combustion Systems", AFRC Spring Meeting, May 10-11, 1988.

16. W. Richter, H. Kobayashi, AFRC 1990 Fall International Symposium, San Francisco, CA, October 8-10, 1990.

17. H. Kobayashi, W. Richter, "Design Considerations and Modelling of the Glass Melter Combustion Space for Oxy-Fuel Firing", Proceedings of XVI International Congress on Glass, Sociedad Espanola De Ceramica Y Vidro, 1992.

APPENDIX A

COMBUSTION SPACE MODELLING OF OXY-FUEL FIRED GLASS MELTER

Wolfgang Richter
Consultant
Irvine, California 92714

Hisashi Kobayashi
Union Carbide Industrial Gases Inc., Linde Division
Tarrytown, New York 10561

© 1990 Union Carbide Industrial Gases Technology Corporation

Paper presented at American Flame Reserach Committee
1990 Fall International Symposium on NO_x Control,
Waste Incineration and Oxygen Enriched Combustion,
San Francisco, CA, October 8-10, 1990.

COMBUSTION SPACE MODELLING OF OXY-FUEL FIRED GLASS MELTER

Wolfgang Richter
Consultant
Irvine, California 92714

Hisashi Kobayashi
Union Carbide Industrial Gases, Inc., Linde Division
Tarrytown, New York 10561

ABSTRACT

A three-dimensional heat transfer code based on the zonal method was applied to evaluate the oxygen-fuel firing of a cross-fired regenerative glass melter. A furnace end section which includes the bridge wall and a pair of the regenerator ports was modelled in detail for a base air case and several oxy-fuel firing cases. The firing rates of two oxy-fuel burners that matched the heat flux distribution of the base air case were determined. The effects of the height and angle of the oxy-fuel burners on the temperature and heat flux distributions were predicted to evaluate the optimum burner placement of the oxy-fuel burners. The main conclusions of the simulation are that; (1) in spite of the small flame diameters, the high momentum low flame temperature oxy-fuel burners can create temperature and heat flux distributions equivalent to those of the base air case with a wide flame and (2) both lower burner elevation and angling of the oxy-fuel burners toward the glass surface tend to increase heat transfer to glass surface and reduce the peak refractory temperatures.

INTRODUCTION

Oxygen-fuel firing of glass melters is gaining increasing industry acceptance as a viable way to reduce NOx, particulates and other toxic emissions and to improve energy efficiency. Small specialty glass tanks have been converted to oxygen firing and operating commercially for several years (Ref. 1). A 110 TPD unit melter was converted to oxygen firing about a year ago (Ref. 2). Union Carbide Industrial Gases (UCIG), Inc. has recently conducted successful oxy-fuel firing programs in large tanks for glass bottles and fibers. Since the combustion and heat transfer conditions with oxy-fuel firing can be substantially different from those with the conventional air firing, retrofitting of existing air fired furnaces with oxy-fuel burners requires a careful selection of the type and number of oxy-fuel burners and their proper placement on the glass tank walls. At present these burner decisions are made based on (1) experiences in other industrial furnaces, (2) experimental data on flame characteristics of small scale burners in test furnaces and (3) theoretical heat transfer considerations. Very conservative approaches are generally taken in converting existing furnaces

and designing new furnaces for oxy-fuel firing to avoid costly commercial mistakes.

The optimum furnace design with oxy-fuel firing is likely to be different from the existing furnaces designs for air firing due to a sharp reduction in the flue gas volume and to the heat transfer rate increase possible with oxy-fuel firing. Numerical modelling of the combustion space of glass furnaces offers potential to optimize the furnace design and burner placement for oxy-fuel firing. Although numerical simulation has been used for many years to understand the mechanism of glass melting and for commercial design of glass furnaces, simplified heat transfer models were often used for the combustion space as the focus of modelling was the analysis of glass flow patterns (Ref. 3). In particular, most of these simplified combustion space heat transfer models, do not account for the effects of flame position and characteristics on glass bath heat transfer.

On the other side, advances in numerical methods and computer speed and capacities, have led to the development of complex models, which directly couple comprehensive 3-D finite-difference combustion space analysis, with 3-D melter analysis (Refs. 4,5). However, these latter models, while attractive in the straightforwardness of their approach, require still an enormous effort in time to set up and to validate, and in computational and financial resources to run.

Therefore, the current analysis was based on a approach which is complex enough to allow to study the impact of local flame radiation on heat transfer to the glass, but which avoids the complexity of the comprehensive models by using simplified boundary conditions at the glass surface and by decoupling the combustion space gas flow analysis, as well.

APPROACH

The current approach uses a 3-D heat transfer and combustion zone model, which allows accurate assessment of local radiative heat transfer between gas heat sources, furnace gas volume, refractory walls and heat sinks. Furnace flow and flame heat release pattern are semi-empirically prescribed. However, flame heat release patterns are based on measurements in pilot-scale furnaces and actual flame observations. Thermal boundary conditions at the glass surface are simplified either by assigning effective temperatures and emissivities, or by use of a simple heat conduction model into the glass bath. Use of these simplified boundary conditions is justified by the fact that one of the goals of the current study is to identify O2-Burner configurations which generate similar net heat flux distributions as does conventional air firing.

A further simplification was introduced by considering only a section of a cross-fired glass furnace. In the current project only the end-section of such a furnace was modelled. This allowed to use computational grids small enough that the computer code of the model could be executed on PC's. The model developed for above approach is described in detail in the following sections.

3-D Zone Model

As already mentioned, the present study is based on a 3-D heat transfer and combustion zone model (Ref. 6). This model has successfully been applied in the past for thermal performances studies of a variety of boiler, industrial and pilot-scale furnaces (Ref. 7) including furnaces almost completely insulated by refractory walls like a glass furnace. The model is especially suitable for the latter furnaces, since emphasis is laid on accurate treatment of multi-directional radiative exchange, which is by far the dominant mode of heat transfer in these high temperature furnaces.

In zone-type models such as the current one, the combustion space is sub-divided by a net of well-stirred volume zones, and by a net of corresponding boundary zones. Average zone temperatures are obtained of total energy balances set up for each zone. The heat balance for a volume zone is formulated by Eq. (1) :

$$Q_r + Q_s + Q_d - Q_{ch} = 0 \quad , \qquad (1)$$

where Q_r and Q_s are the net heat fluxes over the zone boundaries by radiation and advection, respectively. Q_d, which is small in high temperature furnaces, represents the convective transport through a wall boundary layer from a near wall volume zone to a adjacent surface zone. Q_{ch}, finally is the net heat release in the volume zone due to flame reactions obtained from species balances solved in addition to the volume zone heat balances.

Contrary to the more expensive finite-difference combustor models, the advective mass flow rates necessary to calculate the terms Q_s in Eq. (1) are not obtained from a simultaneous solution of momentum balances, but are rather input into the zone model, thus allowing to spend available computational resources for a more accurate simulation of radiative exchange.

The multi-directional transport of radiative energy between all wall and surface zones (i.e. term Q_r in Eq. (1)) is calculated with the semistochastic method (Ref. 6). This method which is derived from Monte-Carlo calculation techniques is illustrated in Fig. 1. Q_r is expressed by Eq. (2) :

$$Q_r = 4\ V\ \Sigma^4_{n=1}\ a_n\ K_n\ \sigma T_g^4 - \Sigma^4_{n=1}\ \Sigma_{beam}\ Q_{beam,a} \qquad (2)$$

Eq. (2) implies that the radiative properties of the combustion products are approximated with a so-called 'Weighted-Grey-Gas Approach' (Ref. 8) with n=4 grey ranges. a_n is the weighing factor and K_n is the grey absorption co-efficient assigned to the n th range.

The radiation model works as follows. The emissive power of all grey ranges (1 st term of Eq. (2)) of a volume zone (surface zones are treated in analogy) is distributed among a finite number of beams. The beams are emitted over the whole view angle and traced through the arrangement of volume zones until they impinge on wall. The beam gradually loose energy through absorption. The amount of energy $Q_{beam,a}$ absorbed from a beam by a volume zone is expressed by :

$$Q_{beam,a} = Q_{beam,in}\ [1-\exp(-\ K_n\ ds)] \qquad (3)$$

$Q_{beam,in}$ is the energy flux of a beam incident on the volume zone and ds is the path length of the beam cut out by this zone. The energy amounts $Q_{beam,a}$ absorbed from all beams passing a zone are accumulated. The radiative sub-balance according to Eq. (2) is calculated for each iteration cycle necessary to solve the total energy balance (1).

Since in the current study wall surfaces are treated as grey, diffuse radiators and reflectors, reflected energy amounts from beams incident on a wall are accumulated at the corresponding surface zones, and added to surface emission in the next iteration step. Combined wall emission and reflection is then treated in analogy of volume emission described above, however taking the cosine law into account.

The current semistochastic method is distinguished from pure Monte-Carlo methods by the fact, that some events in the history of a beam are deterministically influenced rather than based solely on random numbers (see Ref. 6).

The zone model considers, besides radiation from wall zones, radiation from gaseous species CO2 and H2O and from soot particles. Zonal concentration of these species are calculated from the combustion model described further below. Weighing factors and specific absorption coefficients of the gaseous species utilized for the 'Weighted-Grey-Gases-Approach' are taken from Ref. 8. The specific absorption coefficients for soot are prescribed according to an approach suggested in Ref. 9.

Furnace Flow Distribution and Heat Release Pattern

Furnace Flow Field

Besides the radiation terms, the total energy balance of each volume zone includes contributions from convective transport and from heat release due the flame reactions. As mentioned above, the advective transport of sensible heat is based on predetermined zonal mass flux distributions. There are several means to obtain such distributions ranging from simple engineering guesses to sophisticated 3-D fluid dynamics calculations. In the present study, suitable furnace flow distributions were determined from a mixed-type approach, combining enclosed jet theory, educated guesses and computer routines for continuity considerations and for direct graphical display of mass flux density vectors.

The jet theory was in particular applied to estimate the flow for the O_2 firing configuration. It was assumed that the forward flows of the high momentum O_2-jets which fired from opposite furnace sides in a staggered manner, were not interacting. The flow fields associated with each burner were constructed as follows.

The multi-jet outlet of an O_2 burner was replaced by an equivalent nozzle diameter taking flame expansion into account. Forward flow profiles and local entrainment rates were calculated with the assumption that the jet entrains fluid halfway the distance between jet origin and impingement of the jet envelope at surrounding walls. The backflow necessary to support the entrainment rates was empirically distributed over the furnace with help of profile factors.

In a final step, the flow fields derived for the individual burners were arithmetically superimposed. Also superimposed are pairs of turbulent mass flux vectors with prescribed strength, in order to simulate large scale turbulent exchange over zone boundaries. The simple approach described above is currently validated by 3-D fluid dynamics modeling. Entrainment rates of the O_2-flames were also validated with results of comprehensive 2-D modeling previously carried out for pilot-scale O_2-burner trials (Ref. 10).

Combustion Model

The calculation of zonal heat release is based on the furnace flow obtained from above model and on an empirical function, which accounts for the mixing controlled progress of burn-out. In this model, the gaseous fuel is represented by fuel lumps, which

follow the turbulent flow. The lumps are tracked within the zone arrangement. The lifetime of individual lumps is statistically calculated with help of weighted random numbers in such a way that the unburnt matter of a large assembly gas fuel lumps of same origin is an exponential function of residence time t :

$$Q_{unb}/Q_{unb,o} = \exp\left[-(1/c_b)\,(t/t_b)^m\right] \qquad (4)$$

$Q_{unb,o}$ is the sum of chemical heat of all gaseous fuel lumps originating from the same burner inlet zone, and Q_{unb} is the corresponding amount after time t. Accumulation of chemical heat from all fuel lumps reacted in a volume zone yields the chemical source term Q_{ch} needed for the total energy balance (Eq. 1). By using the value 0.1448 for the constant c_b, t_b can be identified as the time needed to achieve (at least on average) burn-out down to 99.9%.

In the current study, the heat release distribution in the air flames was calculated using t_b = 0.75 s and m = 2. The value for t_b was chosen so, that 99.9% burn-out was achieved just at the flue gas port. Thus the observed flame length was matched.

The time constant tb for the O_2 flames was chosen so that the length of the O_2 flames observed in pilot scale experiments was matched. Fig. 2 shows measured axial values of unburnt fuel and of O_2-concentration dependent on distance from the O_2 burner normalized with an equivalent nozzle diameter d_{eq}. The distance Z/d_{eq} = 121.2 represents the width of the furnace investigated in the current study. Also plotted into Fig. 2 are burn-out distributions based on Eq. 4 and used in the model. The curves denoted by A5 represent an O_2 flame with a load 3.71 higher than the flame represented by curves A6 (see also below). Both sets of curves were obtained for m = 3. For flame A5, t_b = 0.045 s was utilized and for the lower load flame, t_b = 0.167 s, i.e. the ratio for t_b of both flames was assumed to be proportional to their load ratio.

The heat release model described above is coupled with species transport equations which allow to calculate zonal concentrations of major combustion products and O_2 needed to compute specific heats. The zonal concentrations of CO_2 and H_2O are also used to calculate zonal absorption coefficients K_n as required by Eq. (2). The current radiation model requires additionally estimation of flame soot concentrations. Whereas the O_2 flames are soot free, luminous radiation plays a certain role in air flames. The natural gas/air flames considered in this study were very sooty. In order to calculate soot absorption coefficients in these flames, it was assumed that flame soot is present in a zone in proportion to unburnt fuel calculated with above

combustion model for the same zone. An empirical value was used for the constant of proportionality.

Thermal Boundary Conditions

Prescription of thermal boundary conditions for the combustion space must distinguish between the refractory surfaces above glass melt, the port openings as well as the glass bath itself. All three sections require either calculation or prescription of effective temperatures and effective emissivities of the radiating boundaries.

Heat Losses through Refractory Walls

Local surface temperatures of the refractories exposed to the combustion space were calculated with the zone model and with a 1-D model for heat conduction through the refractory walls using effective values for the ratio k/s of conductance to refractory thickness and estimations for outside refractory temperatures.

Calculation of Port Heat Losses

Net radiation through the port openings constitutes a major heat loss of the combustion space. In case of O_2-combustion, the ports were also considered to be open, since the experimental set-up for O_2-conversion of the furnace considered in this study was planned for all ports to be left open. The analysis of port radiation was separately carried out by applying the zone model for a representative section of a port and the upper regenerator.

The port analysis yielded ultimately port view factors, which differed between the cycles for air combustion and also for O_2-combustion. The view factors $F_{f-->rg}$ are defined by Eq. (5)., which relate the net heat flux Q_p through the combustion space port opening with area A_p to the incident radiation q_p,in from the combustion space and to an effective black regenerator temperature $T_{rg,eff}$:

$$Q_p = F_{f->rg} A_p (q_{p,in} - \sigma T^4_{rg,eff}) \qquad (5)$$

Boundary Conditions at Glass Surface

In prescribing thermal boundary conditions at the melter surface, it was assumed that the glass of the end-section was batch-free. Two different types of thermal boundary conditions were then studied.

In a first set of calculations, a uniform effective temperature T_{gl} = 2600°F (1700 K) and an effective emissivity of ϵ_{gl} = 0.88 were used for the whole glass surface. The value used for ϵ_{gl} corresponds to the greys hemispherical emissivity of a transparent glass sheet with infinite optical thickness and a refractive index of 1.7 (Ref. 11).

The second set of calculations was carried out by calculating effective temperatures of the glass surface with help of a simple heat conduction model into the glass. It is assumed that temperatures of the glass are uniform (2410°F = 1600 K) in a horizontal plane located at a certain vertical distance into the bath. A uniform effective ratio of conductance to thickness of the glass layer was then determined so, that the area-weighted effective glass surface temperature was 1700 K (2600F). The surface emissivity used in this approach was again ϵ_{gl} = 0.88.

It is believed, that use of a uniform value for glass surface temperatures simulates closer conditions for a transparent glass, where as the second way to calculate boundary conditions, is more representative for a darker glass. Both approaches are certainly very approximate. However, it has to be pointed out, that predictions of relative performance changes for the air and O_2-system can still be accurate provided similar incident heat flux distributions at the glass bath can be achieved in the O_2-system by appropriate burner selection, placement and operation.

INPUT DESCRIPTION AND CASE DEFINITIONS

Furnace Description

The glass furnace investigated in this study is designed for a pull rate of 350 TPD. The furnace is cross-fired and is currently operated with natural gas using regeneratively heated air as oxidizer. A horizontal cross-section of the furnace is shown in Fig. 3. The furnace is 27.2 ft (8.28 m) wide and 49.6 ft (15.11 m) long. The distance between glass surface and crown is 8.7 ft (2.64 m). Each of the five ports of each furnace side is equipped with two pipe burners with 2.3" nozzle diameters. The burners point from each port side at an angle of 47 degrees relative to the port axis and produce five long flames which extend over the whole furnace width. The time between a switch of the burners of one side to the opposite side is 30 min.

Oxy-fuel Burner

The Linde "A" Burner, patented by Union Carbide Industrial Gases, Inc., was chosen for the oxy-fuel firing cases. The burner offers high momentum low flame temperature characteristics

suitable for glass furnaces (Ref. 12). The arrangement of the burners are shown in Fig. 4.

Model Geometry for End-Section

For reasons described in an earlier section, it was decided to conduct the 3-D modeling study of the combustion space for only one section of the furnace, namely the end-section. The space covered by the model, which is indicated in Fig. 3, extends from the center-plane between the fourth and the fifth ports to the bridge-wall. Thus, the model assumes that heat transfer in the combustion space is symmetrical with respect to the vertical center-plane. In the graphical display of the results following later, this symmetry feature will be utilized by extending the plots of the furnace variables up to the center-plane of the fourth port.

The 3-D zone arrangement used in the heat transfer model of the end-section is displayed in Fig. 4. The zone arrangement utilized basically consists of a 9*6*7 rectangular volume zones with some of the near roof zones distorted or omitted in order to simulate the curvature of the furnace roof.

Thermal Boundary Conditions for End-Section

The thermal boundary conditions considered for the end-section are summarized in Table 1.

A uniform value of 0.5 was assumed for the emissivity of all refractory surfaces. The effective ratios of conductance to wall thickness $(k/s)_{eff}$ as well as the outside surface temperatures for various furnace wall sections were deducted from an heat loss analysis carried out for air operation by a furnace manufacturer. In particular, the ratios $(k/s)_{eff}$ were determined so that the current zone model will predict the same overall heat losses, if the flame side surface temperatures coincide with those used in the heat loss analysis mentioned above.

Table 1 also lists the view factors and effective regenerator temperatures used in Eq. (5) to calculate the port losses for air and O_2 combustion, respectively. The mean values for $T_{rg,eff}$ used in the air case are also supported by measurements of gas and refractory temperatures in the upper regenerator carried out over the whole firing cycle.

The boundary conditions at the glass surface were prescribed as discussed in the general description of the approach. In particular, two sets of calculations were carried out. The first set of calculations was carried out assuming a uniform effective

glass surface temperature of 2600°F (1700 K). In the second set of calculations, a constant temperature of 2420°F (1600 K) was assumed to occur someway into the glass bath. A uniform effective ratio of conductance to thickness of k/s = 0.612 kW / m^2 K was used in order to calculate heat transfer through the upper glass bath layer. This value was determined so, that the area weighted glass surface temperatures averaged 2600°F (1700 K) for the baseline O_2 firing configuration. In both set of calculations, an effective glass surface emissivity of 0.88 was utilized.

Major Operating Conditions and Case Definitions

Major operating conditions of the end-section considered for air and O_2-Firing are listed in Table 2. The gross fuel heat input of 12.16 MMBtU/hr (3563 kW) utilized for air firing is related to the gas burners of one port. The fuel heat input cited for O_2 firing relates to half of the fuel input for O_2 burner A5 plus the heat input for O_2 burner A6 (see Fig. 4). The air preheat of 2330°F (1550 K) utilized for conventional air firing corresponds to average measured values for the burner load considered. Similarly, the O_2 concentrations of 2.2 Vol. %, dry corresponds to average O_2 concentrations measured during the flue gas cycle in the upper regenerator.

All cases studied in this paper are defined in Table 3. The 3-D modeling effort comprises five major cases. However, four of these cases are also presented for a variation, in which the glass surface temperatures are calculated from a simple model rather than prescribed to be constant. The cases with constant glass surface temperatures are numbered 1.0 through 5.0, and the cases with variable surface temperatures 1.1 through 5.1.

Case 1 is the case conducted for conventional air combustion and serves, in the context of this study, as bench mark for performance comparisons with predictions of Cases 2 through 5 for the O_2-firing system. The firing arrangement for Case 1 is shown in Fig. 4.

Case 2 through 5 were performed for a latitudinal arrangement of two oxygen burners as shown in Fig. 4. The burners are numbered A5 and A6. A5 fires along the centerline between the two last ports of the glass furnace (Ports 4 and 5). A6 fires in opposite direction with burner axis located in the plane which divides the breast wall section between last port and the bridge wall in half.

Case 2 with equal burner load A5/A6 was performed to optimize the O_2 configuration. All other oxygen cases were performed for burner load ratio A5/A6 of 3.71. Case 3 is defined

as baseline with burner directed horizontally and mounted 2 ft (0.610 m) above the glass bath. Case 4 with horizontal burners 1.3 ft (0.396 m) above glass surface was conducted to study the impact of burner elevation. In Case 5 finally, the O_2 burners mounted at 2 ft were angled downwards towards the center-line of the furnace.

RESULTS AND DISCUSSION

Air Case and Model Verification

Results obtained for conventional air firing (Case 1) of the end-section are displayed in Figs. 5 through 8. Fig. 5 shows the relative mass flux distribution utilized in horizontal and vertical cross-sections of the furnace. The flow is characterized by a weak outer recirculation field surrounding the forward flow emerging from the firing port. The recirculation eddy extends over the whole furnace depth. Its strength was prescribed to be 1.0 times the inlet mass flow. However, previous experience with the zone model has shown that, in weak recirculating flows like in the current air case, the actual recirculation strength has only a weak effect on thermal performance provided bulk flow features are approximately simulated.

Fig. 6 shows the distributions of gas temperatures (F) predicted for air firing in a horizontal and in a vertical furnace cross-section through the flame as well as in a vertical cross-section located halfway between Port 5 and the bridge wall. The predicted flame extends over the whole furnace depth up to the flue gas port. This agrees with observations made in the actual furnace. It was observed that sooty flame tips extended intermittently into the opposite port. The mean gas exit temperature predicted is 2851°F (1840 K). This is in good agreement with optical pyrometer measurements, which yielded averaged gas temperatures near the flue gas port of ca. 2857°F (1843 K) as seen from the regenerator observation ports.

Fig. 7 shows the distribution of refractory temperatures (F) predicted for all walls of the furnace end-section for air firing. In this graph, as well as in all following graphs for air combustion, the display of the variables (i.e. the refractory temperatures in this case) is symmetrized with respect to the furnace axis. This approximately accounts for the complete firing cycle. Maximum refractory temperatures of 2684°F predicted for the furnace roof fall into the range of measured mean crown temperatures, which varied from 2650°F for the section of Port 1 to 2850°F for the end-section (Port 5). The maximum roof refractory temperature of the non-symmetric prediction was 2694°F (1752 K). In comparing the model predictions with the

behavior of the actual furnace, one has to consider that the actual fuel distribution between the port burners was not uniform. Furthermore, the actual furnace volume is larger than that the virtual volume of twice the end-section considered in the current model set-up.

Some gradients of predicted refractory temperatures are due to the fact that the refractory material and outer insulation differed from section to section. This effect is especially obvious for the uninsulated tuckstones located just over the glass surface. Relatively low surface temperatures are predicted for these stones.

Fig. 8a shows the symmetrized net heat flux distribution predicted at the glass surface for air combustion and assuming uniform effective temperatures of the glass surface of 2600°F (1700 K). The shape and the inhomogeneity of these heat flux profiles indicate a considerable influence of direct flame radiation on overall heat transfer to the glass. The heat fluxes to the glass vary from maximal 98 kW/m^2 below the flame to less than 40 kW/m^2 adjacent to the bridge wall.

O_2-Burner Load Optimization and O_2 Base Case

In the first step carried out to optimize the O_2-firing configuration, the thermal load of the A5 and A6 O_2 burners of the end-section (see Fig. 4) was considered to be equal (Case 2). The resulting net heat flux distribution to the glass surface is shown in Fig. 8b. Like in the air case, the O_2-flames generate a radiation image on the glass surface. Maximum heat fluxes of 114 kW/m^2 predicted for flame A5 was slightly higher than those predicted for air combustion.

However, by comparing Fig. 8b with Fig. 8a, it is obvious, that the glass surface section near the bridgewall receives too much heat in the O_2 case. If two glass surface sections are defined so that Section 1 is the glass area between the center-lines of Ports 4 and 5 and Section 2 is the remaining area up to the bridge wall, then the heat flux ratio between Sections 1 and 2 is 1.54 for air Case 1 compared to only 1.03 for O_2 Case 2. Furthermore in the O_2 case, maximum refractory temperatures of the bridge wall exceeded the ones predicted for air Case 1 by 67°F (37 K).

In order to lower the bridge wall temperatures and in order to achieve a heat flux ratio between Sections 1 and 2 which is more similar to that predicted for air combustion, the load ratio A5/A6 was increased from 1 in Case 2 to 3.71 in Case 3. This resulted in an increase of the heat flux ratio between Sections 1 and Sections 2 from 1.03 to 1.31. It also led to a local heat

flux distribution at the glass surface, which is more similar to that predicted for air Case 1 (Compare Fig. 9b with Fig. 9a), and lowered maximum bridgewall temperatures from 2725°F (1769 K) to 2696°F (1753 K). The O_2 case with load ratio A5/A6 = 3.71 was consequently defined as baseline O_2 Case 3.

Further results for the baseline O_2 Case 3 are depicted in Figs. 10 through 12. Fig. 10 shows the relative mass flux distribution of the baseline O_2 case determined for the horizontal and two vertical cross-sections through the axes of Burners A5 and A6. Note, that the mass flux density vectors shown in this figure were plotted in a scale ten times smaller than in corresponding Fig. 5 for the air case.

Derivation of the flow patterns displayed in Fig. 10 is based on enclosed jet theory and flow superposition as described earlier. In particular, a recirculation strength of 15 times the inlet jet mass was utilized for both O_2 jets. Fig. 10 shows that the jets do not significantly influence each other, however, due to its much higher absolute mass flow, jet A5 determines the flow direction in recirculation regions. These features were confirmed in 3-D fluid dynamics calculations carried out independently for the burner configuration of Case 3.

Gas temperature distributions (F) predicted for the O_2 baseline Case 3 in horizontal and vertical burner planes are depicted in Fig. 11. Due to the high recirculation rates, maximum flame temperatures of 3432°F (2162 K) are only slightly higher than those predicted for air combustion (3364°F = 2124 K). These gas temperature maxima are found in Flame A5 which is hotter than Flame A6 due to its much higher load.

Fig. 12 shows the refractory temperatures predicted for O_2 Case 3 at all walls of the furnace end-section. Maximum refractory temperatures of the roof are with 2732°F (1773 K) ca. 48 R (27 K) higher than those predicted for air combustion (Fig. 6). There is a clear correlation between the location of the maximum refractory temperatures and the adjacent gas flow. Maximum refractory temperatures are encountered there, where the gas flow vectors, especially in the flame tail, are directed towards the walls. In O_2 Case 3, these areas are the breastwall region opposite to the A5 burner and the roof section adjacent to this breastwall area. This behavior is less noticeable for Burner A6 due to the shorter high temperature flame zone.

A similar correlation can be found between near wall flow direction and maximum heat fluxes, although the heat flux peaks are influenced as well by bulk radiation effects. Fig. 8b shows, that, compared to O_2 Case 2 with burner load ratio A5/A6 = 1 (Fig.7b), maximum heat fluxes to the glass shifted nearer to the

opposite breastwall of Burner A5 and are found in the region, where the flame envelope touches the glass surface. The weaker relative heat flux maximum associated with Flame A6 is located more towards the center of the furnace due to the shortness of the high temperature zone of this flame.

Impact of O_2-Burner Elevation and Burner Angling

It is clear from the previous statements, that burner positioning and angling must have some influence on maximum refractory temperatures, on net heat flux distribution to the glass and on overall heat transfer efficiency. In order to investigate these influences, O_2 Cases 4 and 5 were conducted.

In Case 4, both the A5 and the A6 burners remained horizontally directed, but were lowered from 2 ft above glass surface to only 1.3 ft over glass surface. The impact of burner elevation on net heat flux distribution is shown in Fig. 12, which compares the results obtained for Case 4 with the heat fluxes predicted for the baseline O_2 Case 3. By lowering the burners from 2 ft to 1.3 ft, peak heat fluxes at the glass increased from 115 kW/m^2 to 122 kW/m^2. This increase is accompanied by a decrease of peak roof refractory temperatures by 15 R (8 K).

A still more dramatic effect on heat flux distribution to the glass is obtained when the O_2-burners are angled towards the glass surface in direction of the furnace center-line (Case 5). The relative mass flux distribution utilized in this case is shown in Fig. 13. Fig. 14 shows the gas temperature distributions predicted for the angled O_2 flames. Compared to the horizontal O_2 flames of the baseline case (Fig. 10), maximum flame temperatures decreased by ca. 150 (F). This is an indication for an improved heat transfer to glass surface. The net heat flux distribution at the glass surface produced by the angled flames is depicted in Fig. 15b. Compared to the baseline Case 3 (Fig. 15a), maximum heat flux densities increased from 115 kW/m^2 to 131 kW/m^2 and, as can be expected, the location of the heat flux maximum of each flame shifted more towards its corresponding burner wall. The increase of peak heat fluxes is accompanied by an overall increase of heat transfer efficiencies (see section on overall performance).

The angling of the O_2-burners also causes a considerable redistribution of refractory temperatures as shown in Fig. 16. Compared to the distribution for the baseline O_2 Case 3 (Fig. 11), maximum roof refractory temperatures are lowered by 20 R (11 K) and the location of roof peak fluxes has shifted towards Burner A5. However, the stronger flow along the glass after

impingement of jet A5 on the glass surface causes an increase of maximum breast wall temperatures by 40 R (22 K) compared to the baseline O_2 case.

Effect of Variable Glass Surface Temperatures

The preceding results, which were obtained using a uniform effective surface temperature of the glass, showed relative large in homegenities in the distribution of net heat fluxes at the glass surface. Largest and smallest net heat fluxes of 95 kW/m^2 and 35 kW/m^2, respectively, were for instance predicted for air combustion (Case 1), and of 110 kW/m^2 and 40 kW/m^2 for the baseline O_2 case (Case 3). For the O_2-cases in particular, the local heat flux distributions at the glass surfaces were to a certain extent mirror images of the gas temperature distribution within the O_2-flames.

Considerably flatter net heat flux distributions are predicted, when the glass near the surface responds to the imprint of the net heat flux distributions through change of its temperature. This effect is modelled by the simple model for variable glass surface temperatures . Results obtained from this model are shown in Fig. 18a for air combustion and in Fig. 18b for the baseline O_2 burner configuration. In case of air combustion and variable glass temperatures (Case 1.1), largest and lowest heat fluxes are only 83 kW/m^2 and 47 kW/m^2, respectively. Similarly, for the baseline O_2 Case with variable glass surface temperatures (Case 3.1), highest and lowest heat fluxes amount to 80 kW/m^2 and 50 kW/m^2, respectively.

Resulting distributions of calculated effective surface temperatures for air Case 1.1 and baseline O_2 Case 3.1 are compared in Figs. 19a and 19b., respectively. Peak glass temperatures $T_{s,gl,max}$ for air combustion reach 2663°F (1735 K) and the differences between this peak and the lowest temperatures predicted is $dT_{s,gl}$ = 105 R (59 K). For O_2 combustion, these numbers are $T_{s,gl,max}$ = 2656°F (1731 K) and $dT_{s,gl}$ = 90 R (50 K), respectively.

As it can be expected, in all cases investigated with variable glass surface temperatures, maximum refractory temperatures increased by about 10 K (20F) compared to corresponding cases assuming a uniform effective glass surface temperature. The higher peak refractory temperatures are offset by lower refractory temperatures in furnace corners, especially in the O_2 cases which exhibit a somewhat more inhomogeneous refractory temperature distribution. This can be seen in Figs. 20 and 21 which display the refractory temperature distribution predicted for the air Case 1.1 and for the O_2 Case 3.1, respectively.

OVERALL PERFORMANCE COMPARISON AND CONCLUSIONS

Overall heat transfer performance data predicted for all cases is listed in Table 4. Note, that the fuel heat input cited in this table, is calculated with the lower calorific value. Table 1 confirms the known fact, that overall heat transfer efficiency of the O_2-firing system is improved compared to conventional air combustion. For the O_2-firing systems studied, this increase is achieved without significant increase in maximum flame temperatures and maximum refractory temperatures. Although the air flames are wider than the O_2 jet flames, the discrepancy in size of the O_2 flames is offset by much higher mixing and recirculation rates induced by the O_2-burners.

It is also obvious from Table 4, that positioning and angling of the O_2-burners can influence overall performance to a certain degree. Lowering the burners (Case 3) slightly increases heat transfer efficiency to the glass surface. A somewhat stronger improvement is achieved when the burners are angled towards the glass surface. In this case, heat transfer efficiency is increased by 0.5 percentage points compared to the baseline O_2 case with horizontal burner orientation.

The study also showed, that there is certainly an impact of the glass surface thermal properties on heat transfer in the combustion space itself. A darker glass will likely tend to smooth out local inhomogenties of net heat fluxes to the glass by increase of glass surface or near surface temperatures, thus reducing the effect of the firing system or of the burner placement on heat flux distribution.

Although some of the absolute predictions made in the present study may be inaccurate due to simplifications of the current approach, there is little doubt that the general trends concluded from this study are realistic. This is due to the dominance of radiation on overall heat transfer in the high temperature glass furnace, and radiative exchange is treated very accurately by the current model.

ACKNOWLEDGEMENT

This work was jointly funded by the U. S. Department of Energy and Union Carbide Industrial Gases, Inc. under Contract No. DE-FC07-88ID12833. The authors would like to express appreciation to Mr. J. Keller of EG&G and Mr. R. N. Chappell of the U. S. Department of Energy for their support and advice.

REFERENCES

[1] J. Brown, et. al., "Oxygen-Fuel Fired Glass Furnace," Amer. Ceramic Society, Glass Division, Pacific Coast Regional Meeting, Nov. 1-3, 1987.

[2] Shamp, D.E. and Davis, D. "Application of 100% Oxygen Firing at Parkersberg, W.V." H.A. Nelson Memorial Glass Seminar, Louisville, KY, April 11, 1990.

[3] Nolet, D. A., and R. A. Murnane. Development of Modeling Techniques for Glass Furnaces. 1st International Conference on Advances in the Fusion of Glass. Alfred University, New York, June 14-17, 1988, pp. 13.1 - 13.21

[4] Ungan, A. and Viskanta, R., "State-of-the-Art Numerical Simulation of Glass Melting Furnaces," Ceramic Eng. Sci. ProC., 9 [3-4], pp. 203-220 (1988).

[5] Carvavalho, M. G., P Oliveira and V. Semiao. A Three-Dimensional Modelling of an Industrial Glass Furnace. J. Inst. Energy, 1988, 448, pp. 143-156.

[6] Richter, W., and M. P. Heap. A Semistochstic Method for the Prediction of Radiative Heat Transfer in Combustion Chambers. Western States Section, The Combustion Institute, 1981 Spring Meeting, Paper 81-17, 1981.

[7] Richter, W., Scale-Up and Advanced Performance Analysis of Boiler Combustion Chambers. 1985 ASME Winter Annual Meeting, Paper 85-WA/HT-80, 1985.

[8] Smith, T. F., and Z. F. Shen. Evaluation of Coefficients for the Weighted Sum of Gray Gases Model. 20th Joint ASME/AICHE National Heat Transfer Conference, Paper 81-ht-55, 1981.

[9] Johnson, T. R., and J. M. Beer. The Zone Method Analysis of Radiant Heat Transfer: A Model for Luminous Radiation. J. Inst. Fuel, Vol 46, 1973, p 388.

[10] Richter, W., and R. Payne. Modeling Study of Burner and Furnace Performance for Oxygen Enriched Combustion Systems. AFRC 1988 Spring Meeting, May 10-11, 1988, Toronto, Canada.

[11] Gardon, R. A review of Radiant Heat Transfer in Glass. J. of the American Ceramic Society. Vol. 44., No. 7, July 1961

[12] Anderson, J.E., "A Low NO_x Low Temperature Oxygen Fuel Burner," 1986 Symposium on Industrial Combustion Technologies, Chicago, IL, Apr. 29-30, 1986.

List of Tables

Table 1: Input Parameters for Boundary Conditions at Refractory Walls, Ports and Glass Surface

Table 2: Major Operating Conditions Considered for Air and O_2-Firing

Table 3: Case Definitions

Table 4: Overall Performance Comparisons

List of Figures

Figure 1: Beam Tracking in Semistochastic Radiation Model

Figure 2: Modeling of Heat Release Distribution in 'A' Burner O_2-Flames

Figure 3: Cross-section of 350 tons/day Glass Furnace, Location of Oxygen Burners and Definition of End-Section Considered in Model

Figure 4: Zone Arrangement Used in 3-D Heat Transfer Model of End-Section

Figure 5: Relative Distribution of Mass Flux Density Vectors Used in Heat Transfer Model for Conventional Air Operation (Case 1)

Figure 6: Distribution of Gas Temperatures (F) Predicted for Conventional Air Operation (Case 1)

Figure 7: Distribution of Refractory Surface Temperatures (F) for Conventional Air Operation and Uniform Glass Surface Temperatures (Case 1)

Figure 8: Net Heat Flux Densities (kW/m^2) at Glass Surface for Conventional Air Operation (Case 1) and Comparison with O_2-Firing Configuration for Burner Load Ratio A5/A6 = 1 (Case 2)

Figure 9: Net Heat Flux Densities (kW/m^2) at Glass Surface for Conventional Air Operation (Case 1) and Comparison with O_2-Firing Configuration for Burner Load Ratio A5/A6 = 3.71 (Case 3)

Figure 10: Relative Distribution of Mass Flux Density Vectors Used in Heat Transfer Model for Baseline O_2-Burner Configuration (Case 3)

Figure 11: Distribution of Gas Temperatures (F) Predicted for Baseline O_2-Burner Configuration (Case 3)

Figure 12: Distribution of Refractory Surface Temperatures (F) for Baseline O_2-Burner Configuration and Uniform Glass Surface Temperatures (Case 3)

Figure 13: Impact of Burner Elevation on Net Heat Flux Densities (kW/m^2) at Glass Surface for O_2-Firing (Case 3 vs. Case 4)

Figure 14: Relative Distribution of Mass Flux Density Vectors Used in Heat Transfer Model for Study of Impact of O_2-Burner Inclination (Case 5)

Figure 15: Distribution of Gas Temperatures (F) Predicted for Configuration with Inclined O_2-Burners (Case 5)

Figure 16: Impact of O_2-Burner Inclination on Net Heat Flux Densities (kW/m^2) at Glass Surface for Uniform Glass Surface Temperatures (Case 3 vs. Case 5)

Figure 17: Distribution of Refractory Surface Temperatures (F) Predicted for Configuration with Inclined O_2-Burners (Case 5)

Figure 18: Comparison of Net Heat Flux Densities (kW/m^2) at Glass Surface between Air and O_2 Firing Predicted Non-uniform Glass Surface Temperatures (Case 1.1 vs. Case 3.1)

Figure 19: Effective Glass Surface Temperatures (F) Calculated from Simple Model for Non-uniform Glass Temperatures and Comparison between Air and O_2 Firing (Case 1.1 vs. Case 3.1)

Figure 20: Distribution of Refractory Surface Temperatures (F) Predicted for Conventional Air Firing and Non-uniform Glass Surface Temperatures (Case 1.1)

Figure 21: Distribution of Refractory Surface Temperatures (F) Predicted for Baseline O_2-Burner Configuration and Non-uniform Glass surface Temperatures (Case 3.1)

TABLE 1 : INPUT PARAMETERS FOR BOUNDARY CONDITIONS AT REFRACTORY WALLS, PORTS AND GLASS SURFACE

PARAMETER	DIMENSION		POSITION / COMMENT
REFRACTORY WALLS :			
EMISSIVITY	-	0.5	ALL SECTIONS
EFF. RATIO COND./THICKNESS	W/M**2 K	2.496	BRIDGE W. (NOT J=1 ZONES)
		0.701	MELTER CROWN (EXEPT SKEWS OVER PORT I= 3,4 ZONES)
		2.329	SKEWS OVER PORTS (I=3,4)
		0.615	BREAST WALLS (EXCEPT J=1)
		6.997	TUCKSTONES (J=1 ZONES, BUT NOT BELOW PORTS)
		13.333	TUCKSTONES BELOW PORTS (J=1)
EFF. OUTER SKIN TEMP.	F	341	BRIDGE W. (NOT J=1 ZONES)
		212	MELTER CROWN (EXEPT SKEWS OVER PORT, I= 3,4 ZONES)
		294	SKEWS OVER PORTS (I=3,4)
		255	BREAST WALLS (EXCEPT J=1)
		511	TUCKSTONES (J=1 ZONES, BUT NOT BELOW PORTS)
		742	TUCKSTONES BELOW PORTS (J=1)
PORTS :			
VIEW FACTORS :			
AIR FLUE CYC.		0.30	
AIR AIR CYC.		0.57	
O2 - FIRING		0.33	
REG. TEMP. T RG			
AIR FLUE CYC.	F	2510	
AIR AIR CYC.	F	2420	
O2 - FIRING	F	2366	CASES 2.0, 3.1, 3.2, 3.3
O2 - FIRING	F	2465	ALL OTHER O2 CASES
GLASS SURFACE :			
EMISSIVITY	-	0.88	ALL CASES
EFF. SURFACE TEMPERATURE	F	2600	CASES 1.0 THROUGH 5.0,
EFF. RATIO COND./THICKN. OF UPPER GLASS LAYER	W/M**2 K	612	CASES 1.1 THROUGH 5.1 (SURFACE TEMPERATURES CALCULATED ASSUMING 2420 F IN GLASS BATH)

TABLE 2 : MAJOR OPERATING CONDITIONS FOR SECTION CONSIDERED FOR AIR AND O2-FIRING

PARAMETER	DIMENSION	AIR COMBUSTION	O2 - COMBUSTION
FUEL TYPE	-	NATURAL GAS	NATURAL GAS
UP. CAL. VALUE	BTU/SCF BTU/LB KJ/KG	1010 21674 50414	1013 21674 50414
LOW. CAL. VALUE	BTU/LB KJ/KG	19535 45439	19535 45439
GROSS FIRING RATE	MMBTU/HR MMBTU/HR KW KW	60/5 = 12.5 3519	CASE 2 : 12.5 ALL OTH. : 12.0 CASE 2 : 3519 ALL OTH. : 3388
NET FIRING RATE	MMBTU/HR MMBTU/HR KW KW	10.8 3172	CASE 2 : 10.8 ALL OTH. : 10.4 CASE 2 : 3172 ALL OTH. : 3053
OXIDISER TEMP.	F K	2330 1550	77 298
FUEL TEMP.	F K	77 298	77 298
FLUE GAS O2	VOL.%,DRY	2.2	2.2

TABLE 3 : CASE DEFINITIONS

CASE NR.	TYPE OF OXIDISER	BURNER LOAD RATIO A5/A6	BURNER EL. ABOVE GLASS	BURNER DIRECTION	EFF. GLASS TEMPERATURE
			FT		F
1	AIR	-	1.85	HORIZONTAL	2600
2	O2	1.00	2.00	HORIZONTAL	2600
3	O2	3.71	2.00	HORIZONTAL	2600
4	O2	3.71	1.30	HORIZONTAL	2600
5	O2	3.71	2.00	ANGLED	2600
1.1	AIR	-	1.85	HORIZONTAL	VARIABLE
3.1	O2	3.71	2.00	HORIZONTAL	VARIABLE
4.1	O2	3.71	1.30	HORIZONTAL	VARIABLE
5.1	O2	3.71	2.00	ANGLED	VARIABLE

TABLE 4 : OVERALL PERFORMANCE COMPARISONS FOR END SECTION

Case Nr.	Description	T gas, max	Tcrown, max	T s, glass, max	T s, glass mean	q glass, max	Q fuel+ Q sens, in *)	Q sens, out	Q refr	Q port	Q glass	(Qglass /Qfuel) *100	Q Sec.1 / Q Sec.2
		F	F	F	F	kW/m**2	kW	kW	kW	kW	kW	%	-
1	Air, Base	3331	2684	2600	2600	120.5	3172+ 1790	2701	138	117	2006	63.24	1.54
2	O2, 2ft A5/A6=1.0	3650 **)	2697	2600	2600	130.0 **)	3172	822	139	111 ***)	2100	66.20	1.03
3	O2, Base, 2ft A5/A6=3.7	3432	2709	2600	2600	115.1	3053	817	138	84	2014	65.97	1.31
4	O2, 1.3 ft A5/A6=3.7	3459	2693	2600	2600	121.8	3053	812	138	89	2015	66.00	1.26
5	Case 3, but Burn. Angled	3277	2697	2600	2600	131.2	3053	808	138	80	2027	66.39	1.32
1.1	Air Case 1, Ts,glass Var.	3337	2718	2678	2607	82.6	3172+ 1790	2714	138	127	1983	62.52	1.24
3.1	O2 Case 3, Ts,glass Var.	3437	2719	2656	2606	76.1	3053	820	139	121 ***)	1973	64.63	1.15
8	O2 Case 4, Ts,glass Var.	3464	2712	2674	2605	86.2	3053	815	138	114 ***)	1986	65.05	1.14
9	O2 Case 5, Ts,glass Var.	3277	2705	2708	2606	97.7	3053	808	138	115 ***)	1992	65.25	1.15

*) Heat fluxes calculated until symmetry plane through axis of Burner A5, but heat flux section ratio calculated as defined in text.

**) This calculation was conducted for different flow field with lower recirculation rates leading to somewhat higher gas temperatures and maximum heat fluxes.

***) Calculation conducted for effective regenerator temperatures of 2366 F instead of 2465 F in the other O2 cases

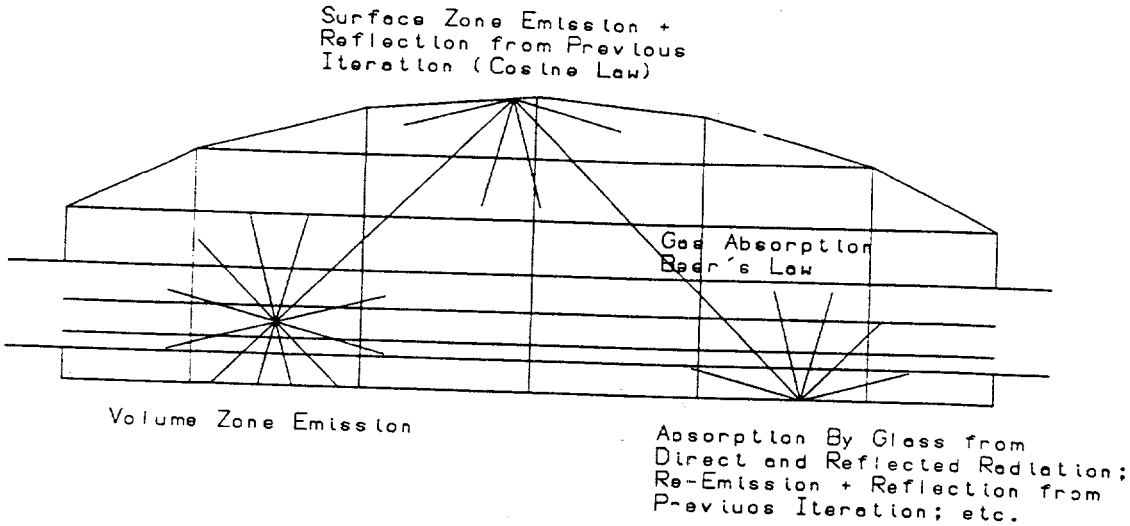

Figure 1 : Beam Tracking in Semistochastic Radiation Model

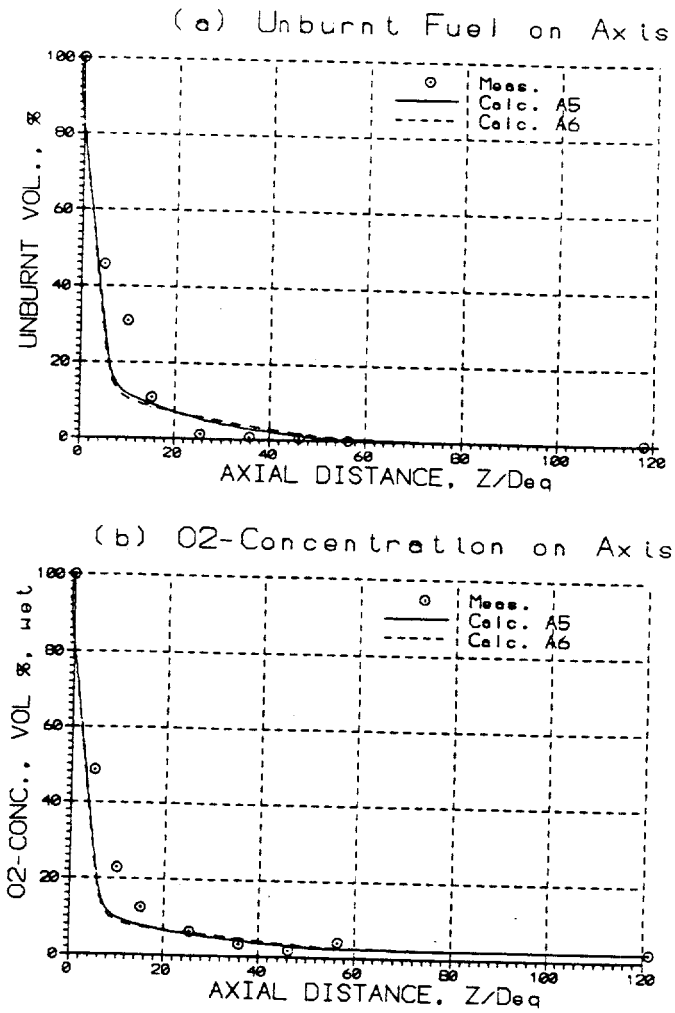

Figure 2 : Modelling of Heat Release Distribution in 'A' Burner O2-Flames

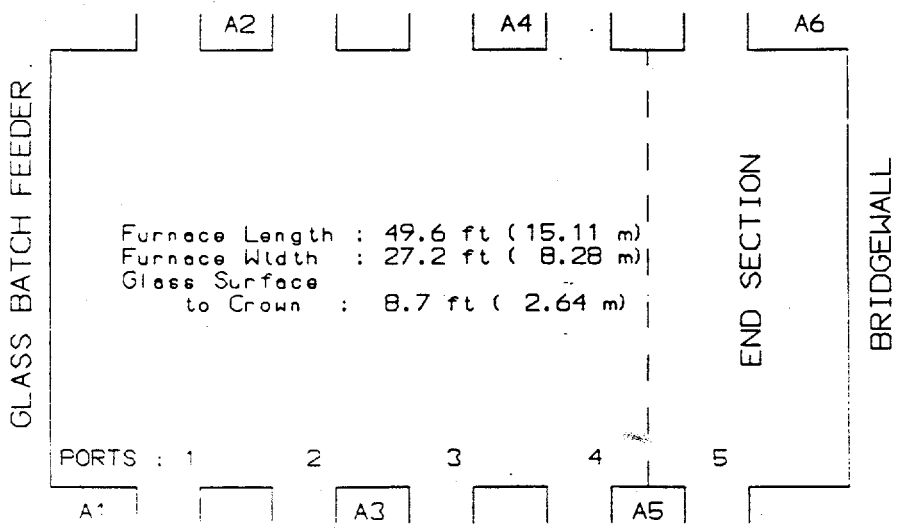

Figure 3 : Cross-Section of 350 tons/day Glass Furnace, Location of Oxygen Burners and Definition of End-Section Considered in Model

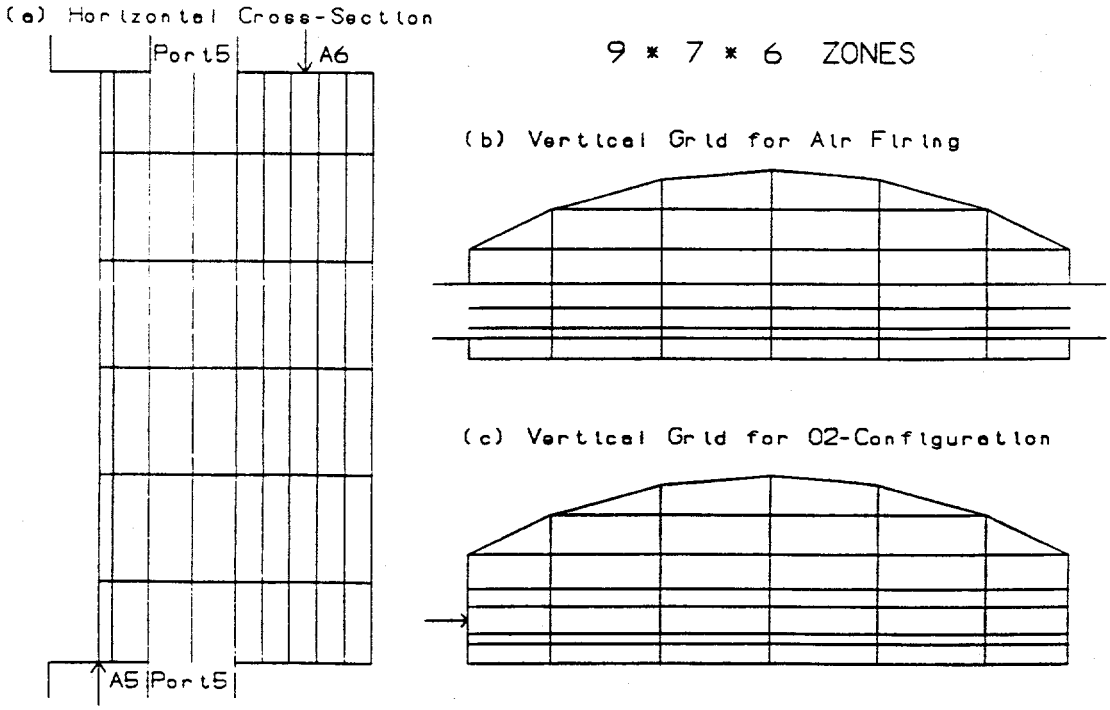

Figure 4 : Zone Arrangement Used in 3-D Heat Transfer Model of End Section

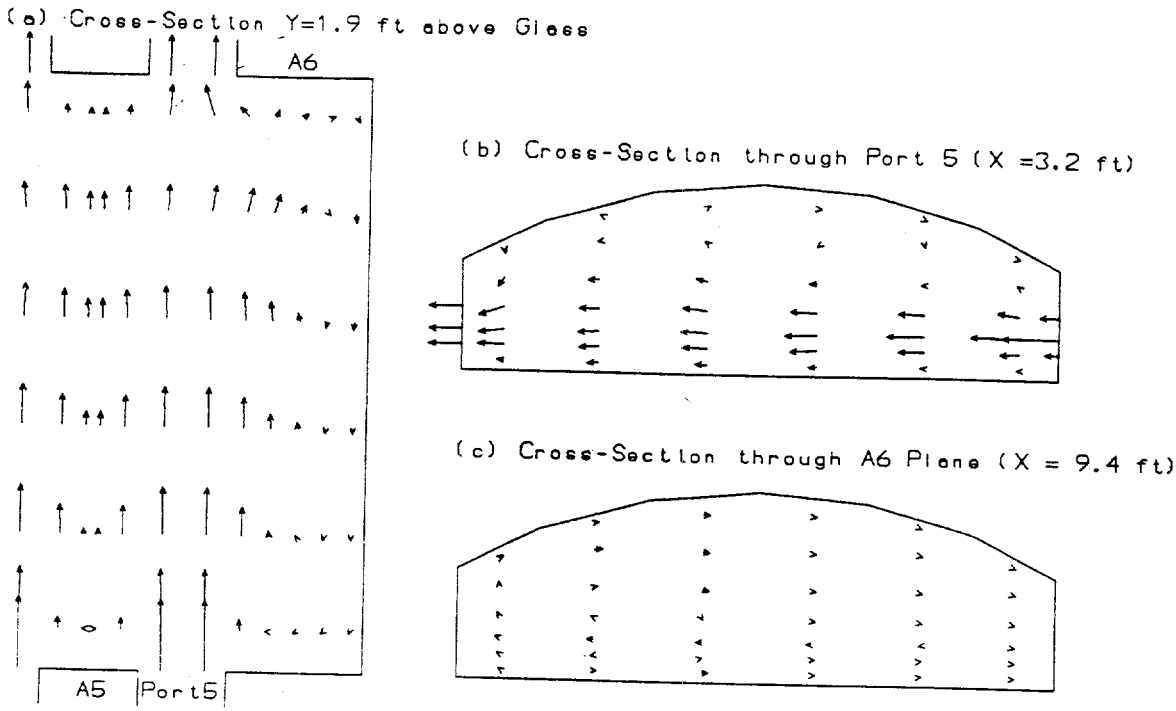

Figure 5 : Relative Distribution of Mass Flux Density Vectors Used in Heat Transfer Model for Air Operation (Case 1)

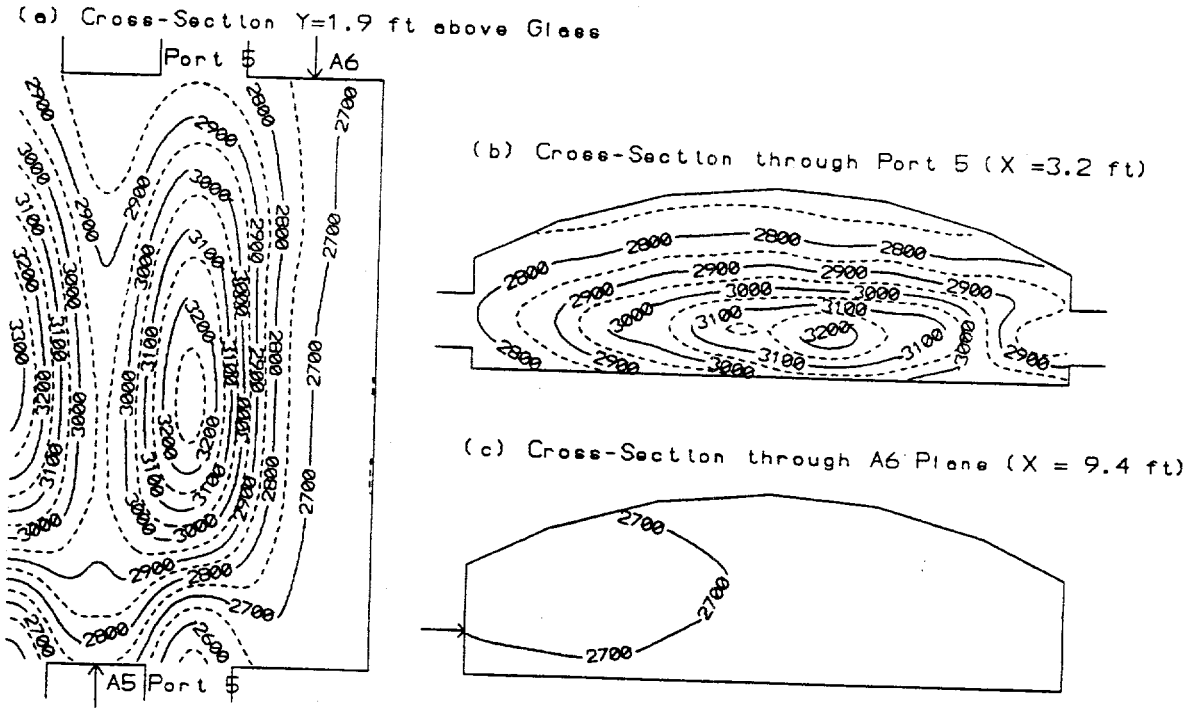

Figure 6 : Distribution of Gas Temperatures (F) Predicted for Conventional Air Operation (Case 1)

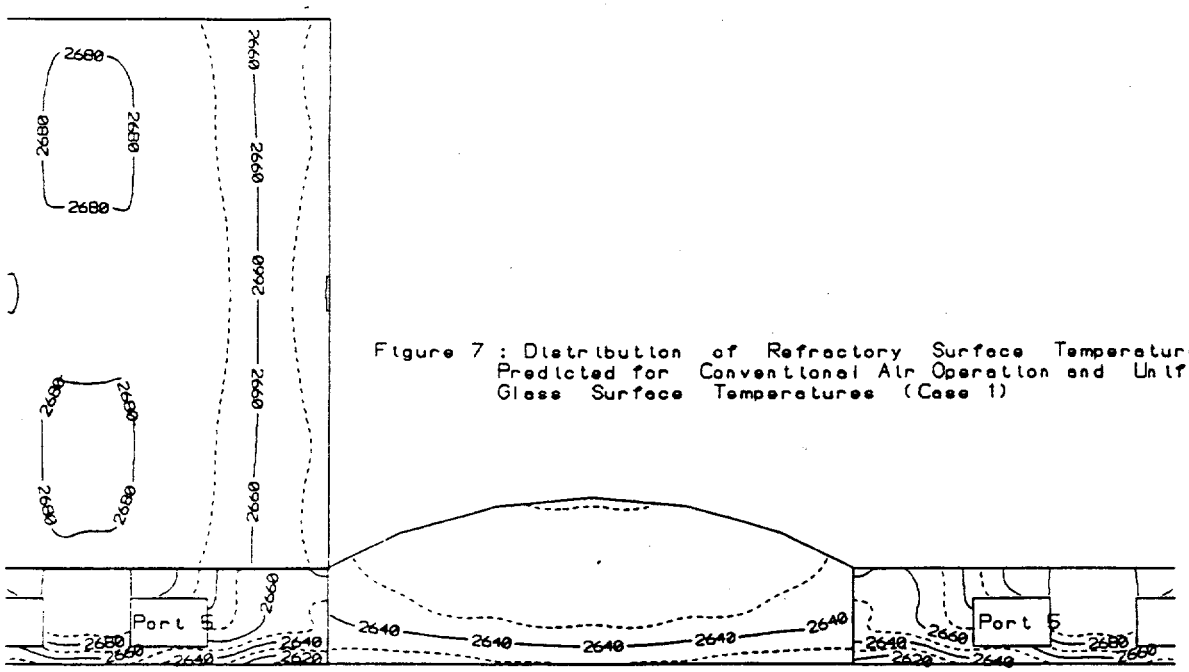

Figure 7 : Distribution of Refractory Surface Temperatures (F) Predicted for Conventional Air Operation and Uniform Glass Surface Temperatures (Case 1)

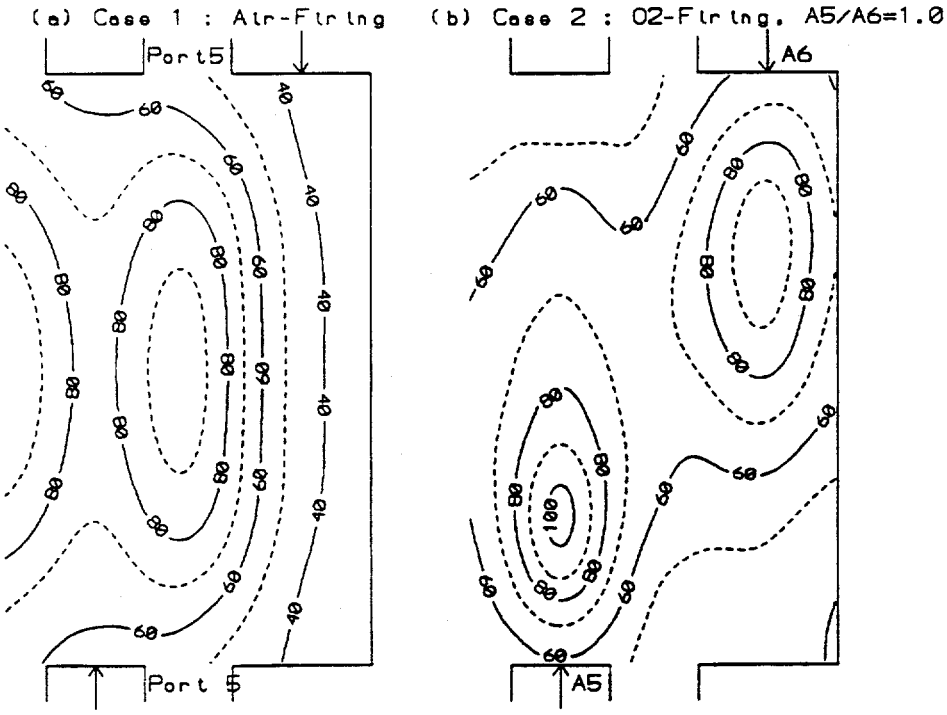

Figure 8 : Net Heat Flux Densities (kW/m**2) at Glass Surface for Conventional Air Operation (Case 1) and Comparison with O2-Firing Configuration for Burner Load Ratio A5/A6 = 1 (Case 2)

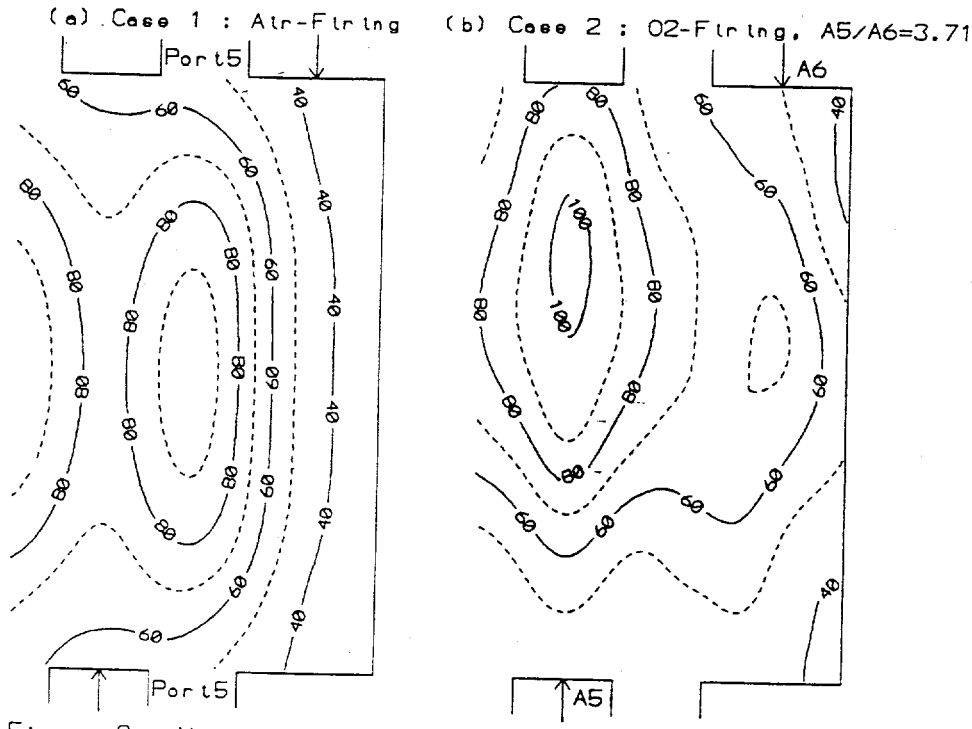

Figure 9 : Net Heat Flux Densities (kW/m**2) at Glass Surface for Conventional Air Operation (Case 1) and for O2-Firing Configuration with Burner Load Ratio A5/A6 = 3.71 (Case 2)

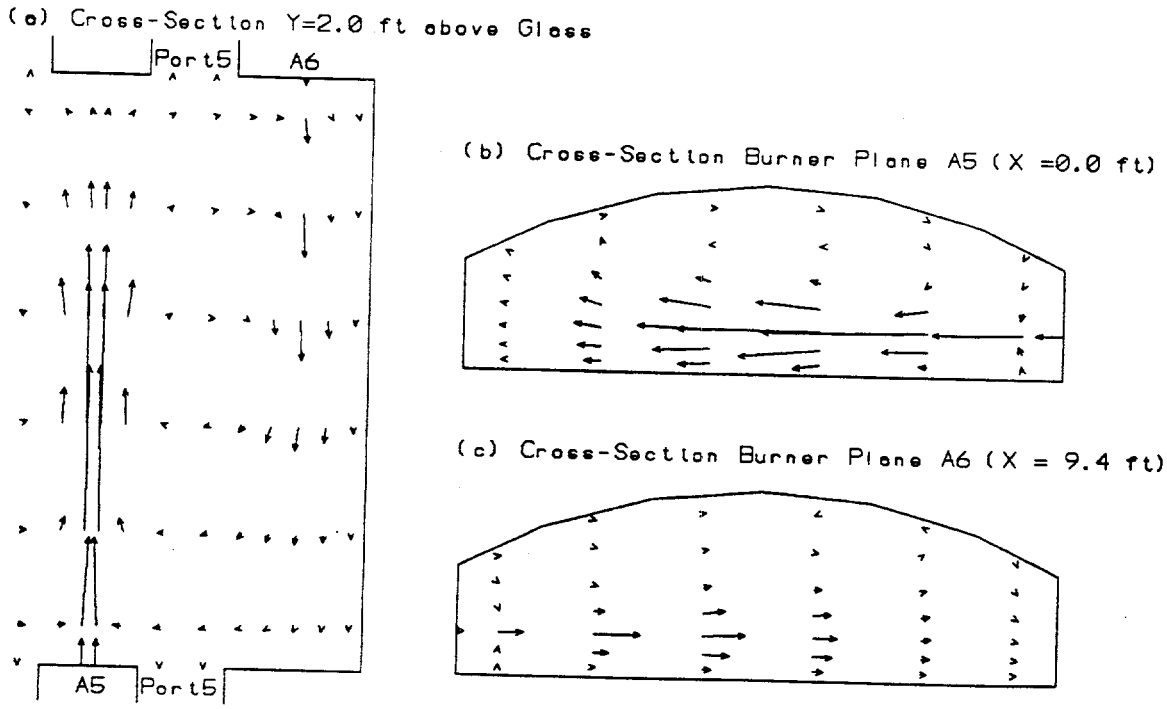

Figure 10 : Relative Distribution of Mass Flux Density Vectors Used in Model for Baseline O2-Burner Configuration (Case 3)

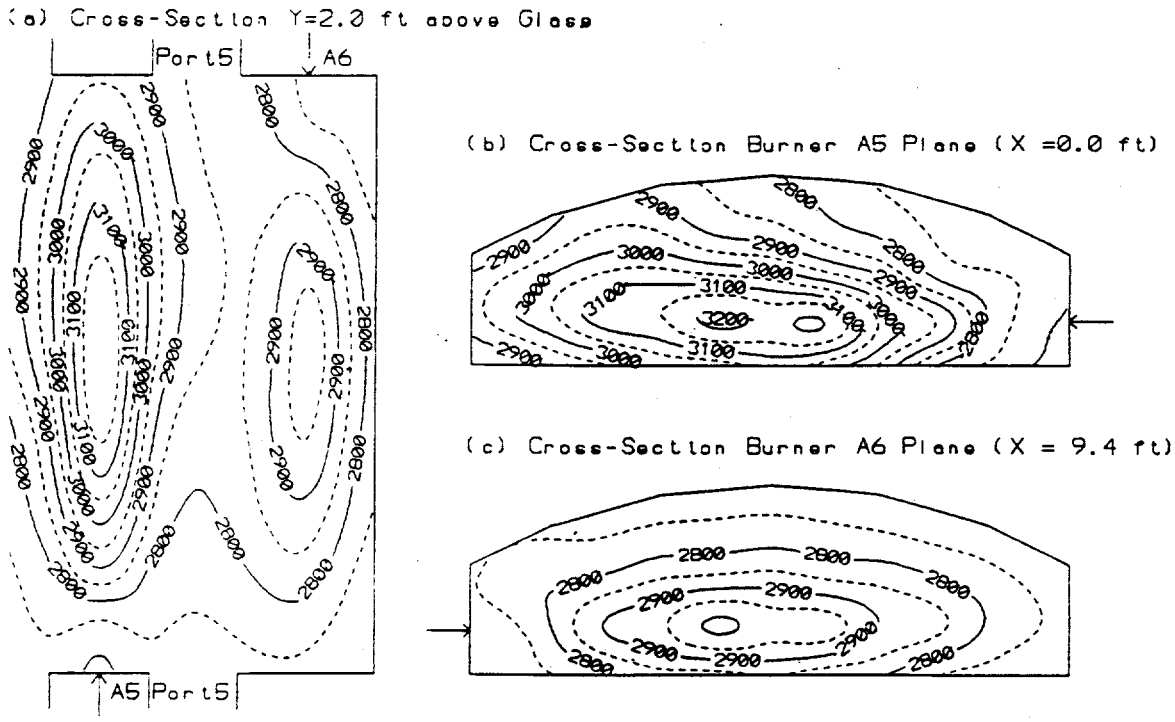

Figure 11 : Distribution of Gas Temperatures (F) Predicted for Baseline O2-Burner Configuration (Case 3)

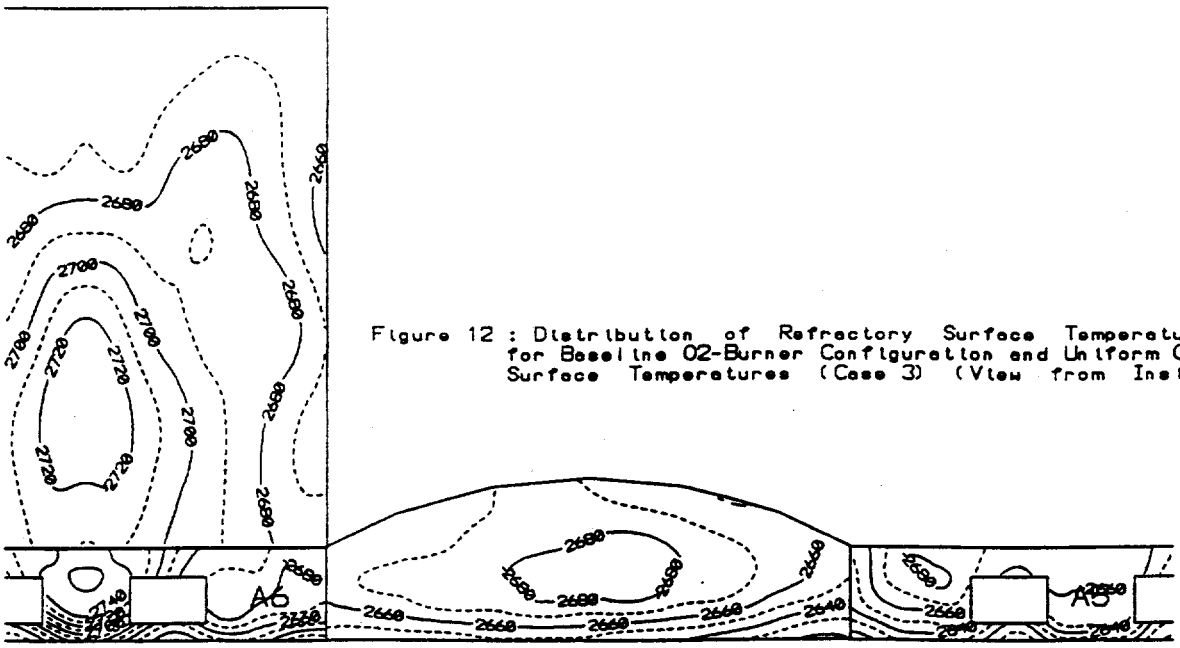

Figure 12 : Distribution of Refractory Surface Temperatures (F) for Baseline O2-Burner Configuration and Uniform Glass Surface Temperatures (Case 3) (View from Inside)

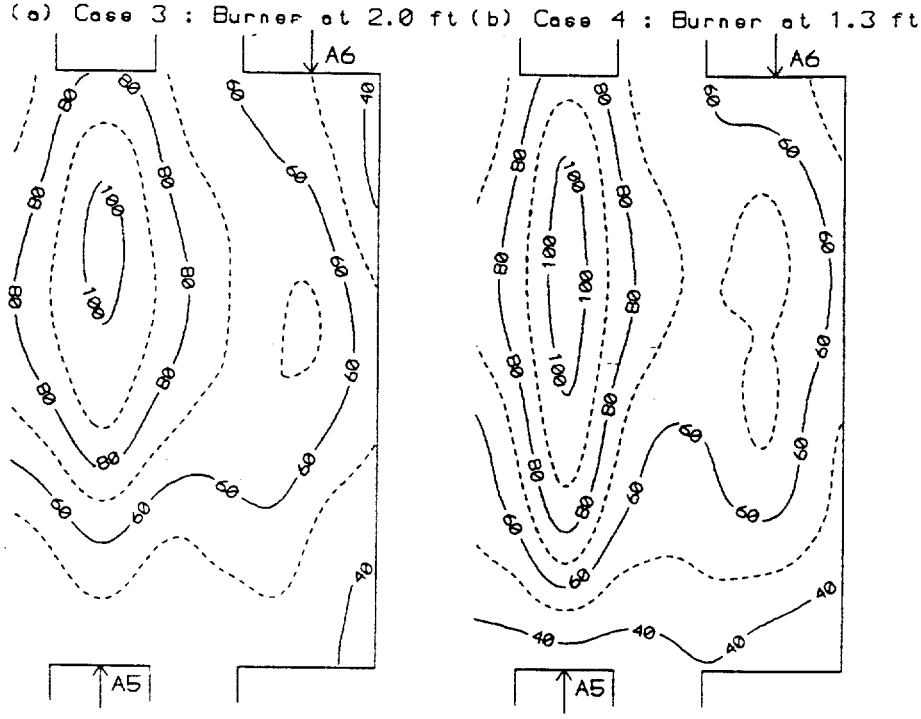

Figure 13 : Impact of Burner Elevation on Net Heat Flux Densities (kW/m**2) at Glass Surface for O2-Firing (Case 3 vs. Case 4)

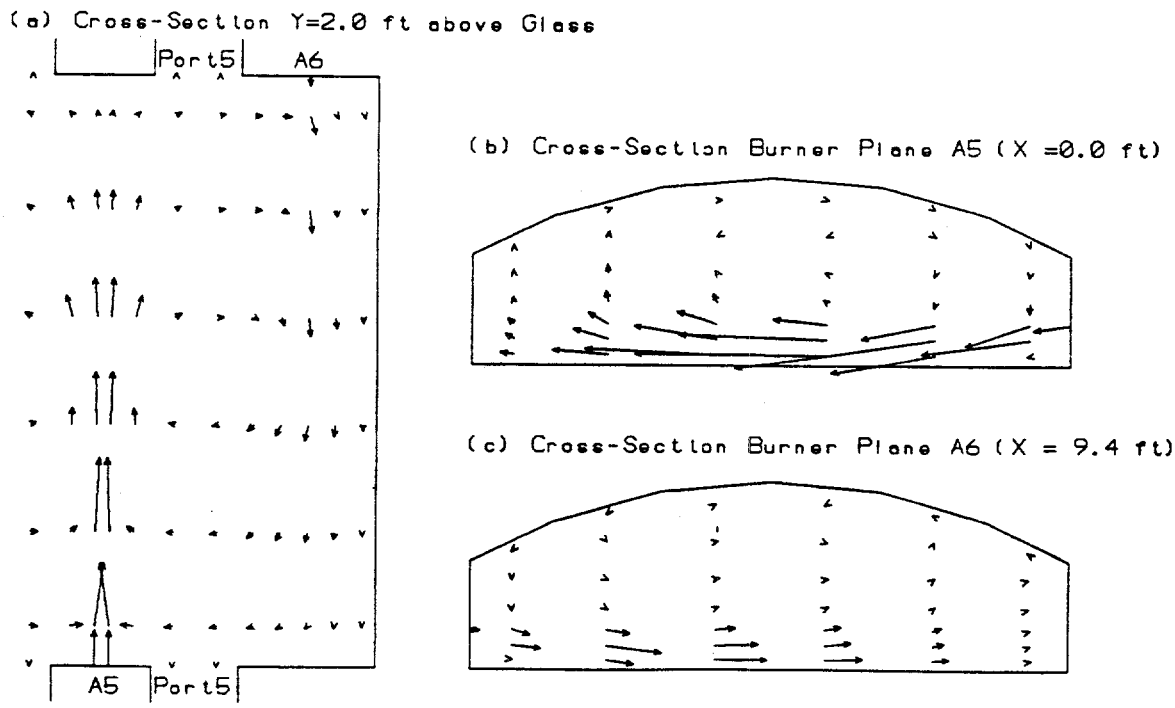

Figure 14 : Relative Distribution of Mass Flux Density Vectors Used in Study of Impact of O2-Burner Inclination (Case 5)

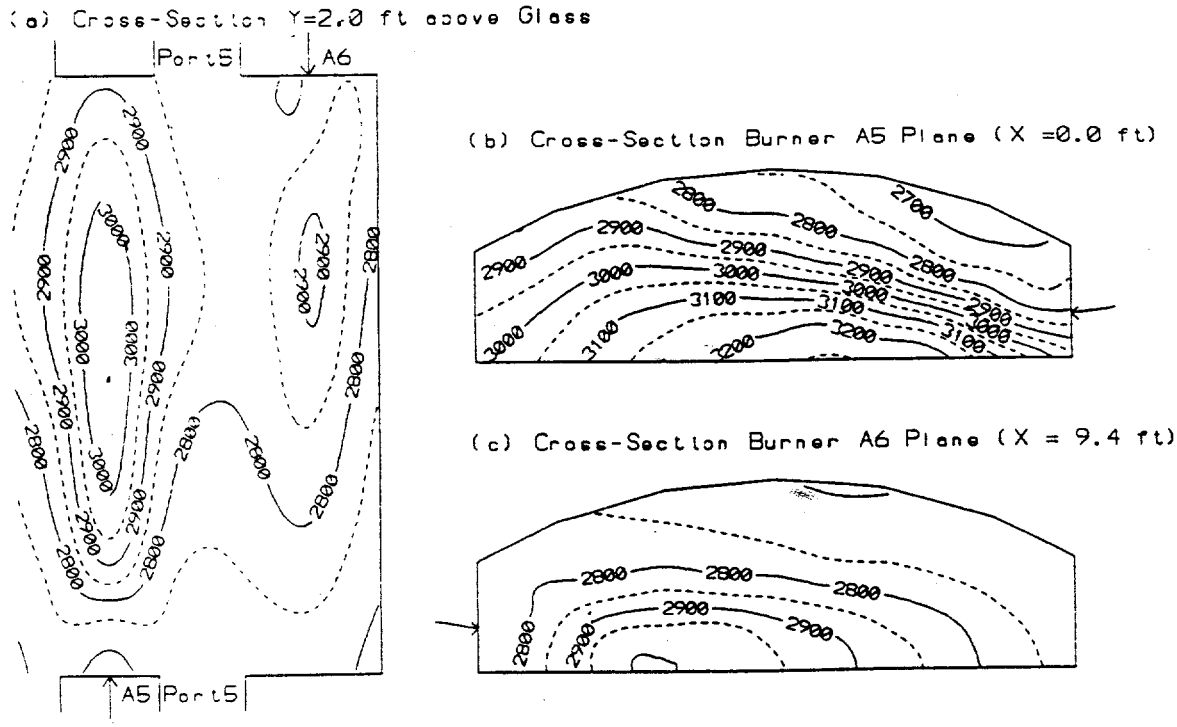

Figure 15 : Distribution of Gas Temperatures (F) Predicted for Configuration with Inclined O2-Burners (Case 5)

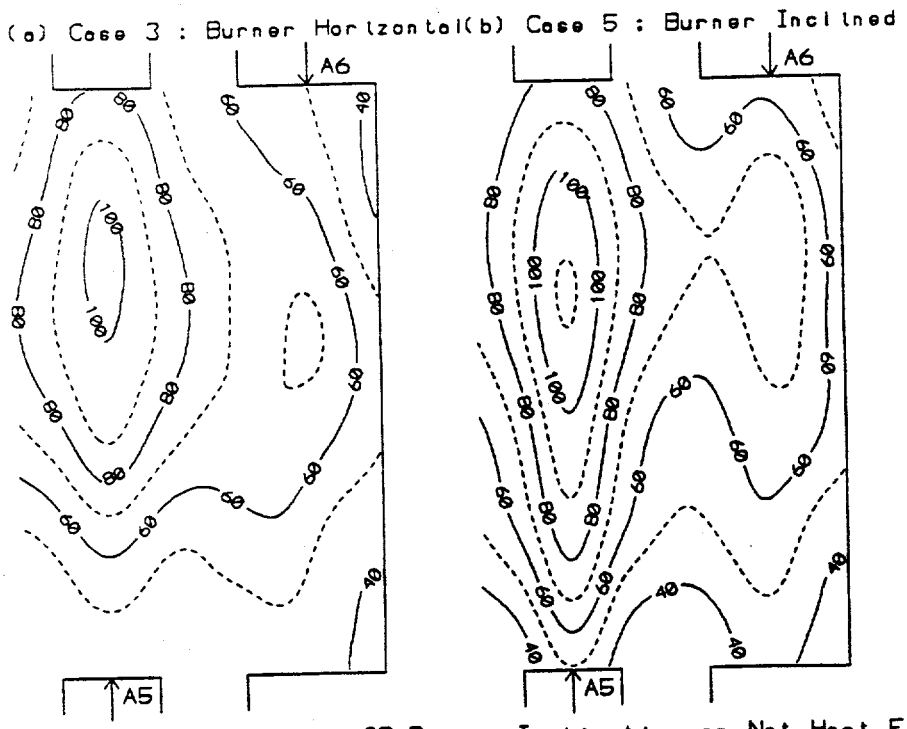

Figure 16 : Impact of O2-Burner Inclination on Net Heat Flux Densities (kW/m**2) at Glass Surface for Uniform Glass Surface Temperatures (Case 3 vs. Case 5)

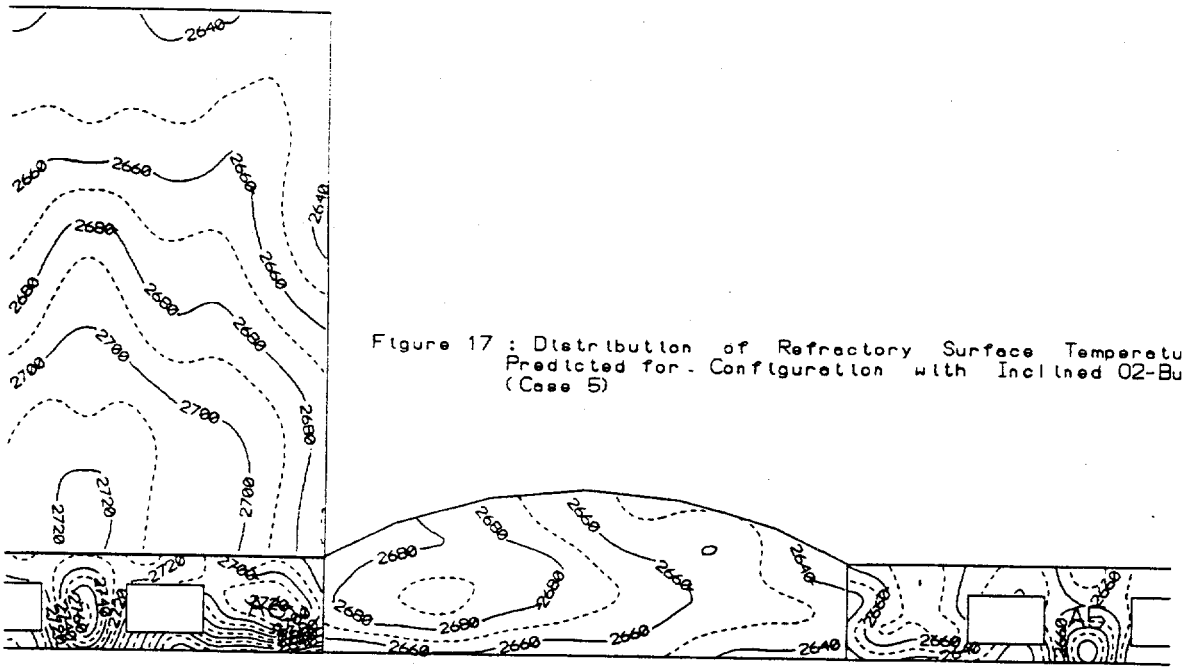

Figure 17 : Distribution of Refractory Surface Temperatures (F) Predicted for Configuration with Inclined O2-Burners (Case 5)

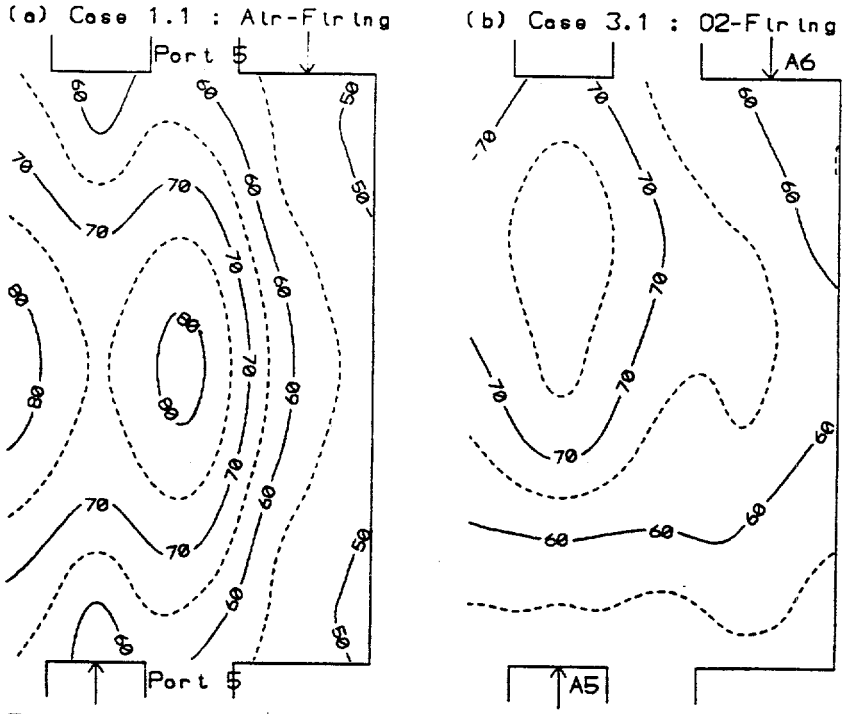

Figure 18 : Comparison of Net Heat Flux Densities (kW/m**2) at Glass Surface between Air and O2-Firing Predicted for Non-Uniform Glass Surface Temperatures (Case 1.1 vs. Case 3.1)

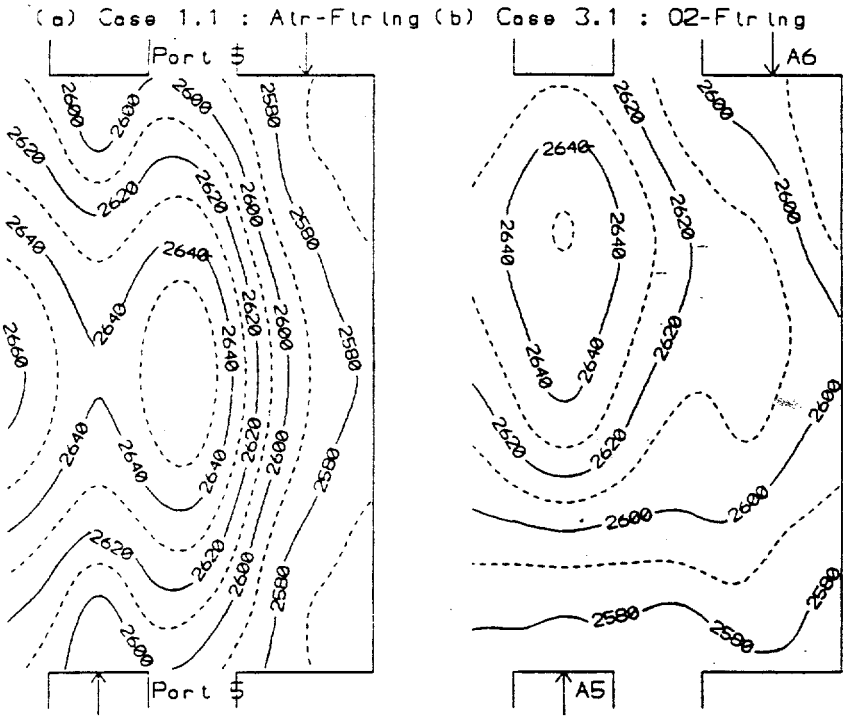

Figure 19 : Effective Glass Surface Temperatures (F) Calculated from Simple Model for Non-Uniform Glass Temperatures and Comparison of Air- and O2-Firing (Case 1.1 vs. Case 3.1)

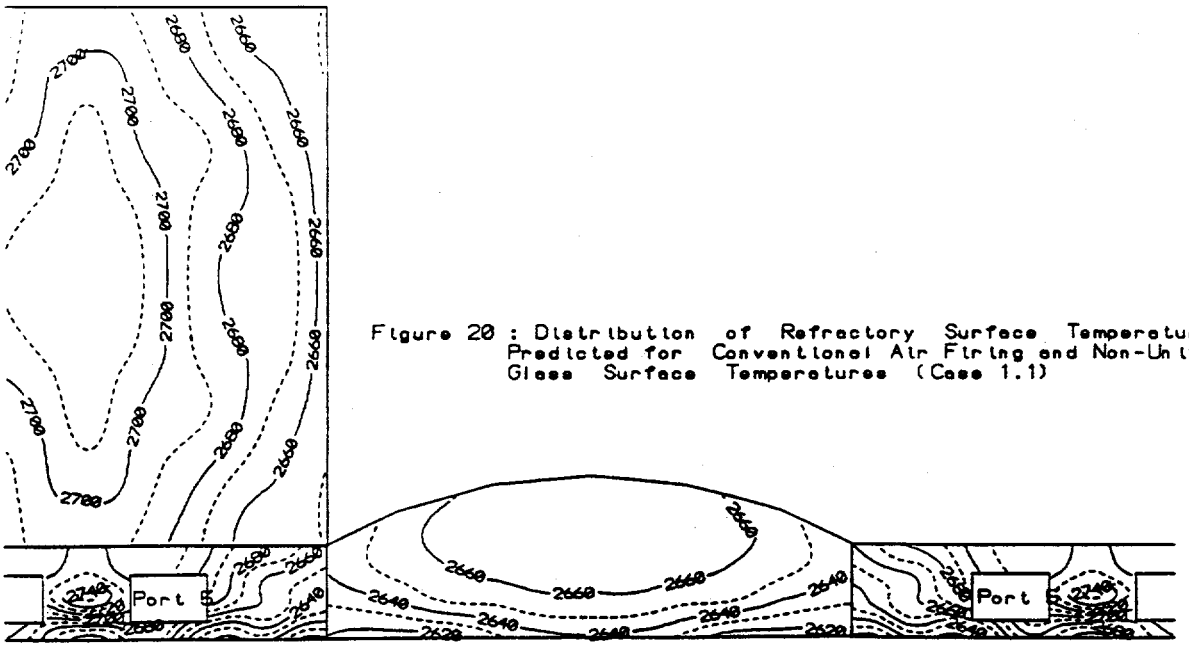

Figure 20 : Distribution of Refractory Surface Temperatures (F) Predicted for Conventional Air Firing and Non-Uniform Glass Surface Temperatures (Case 1.1)

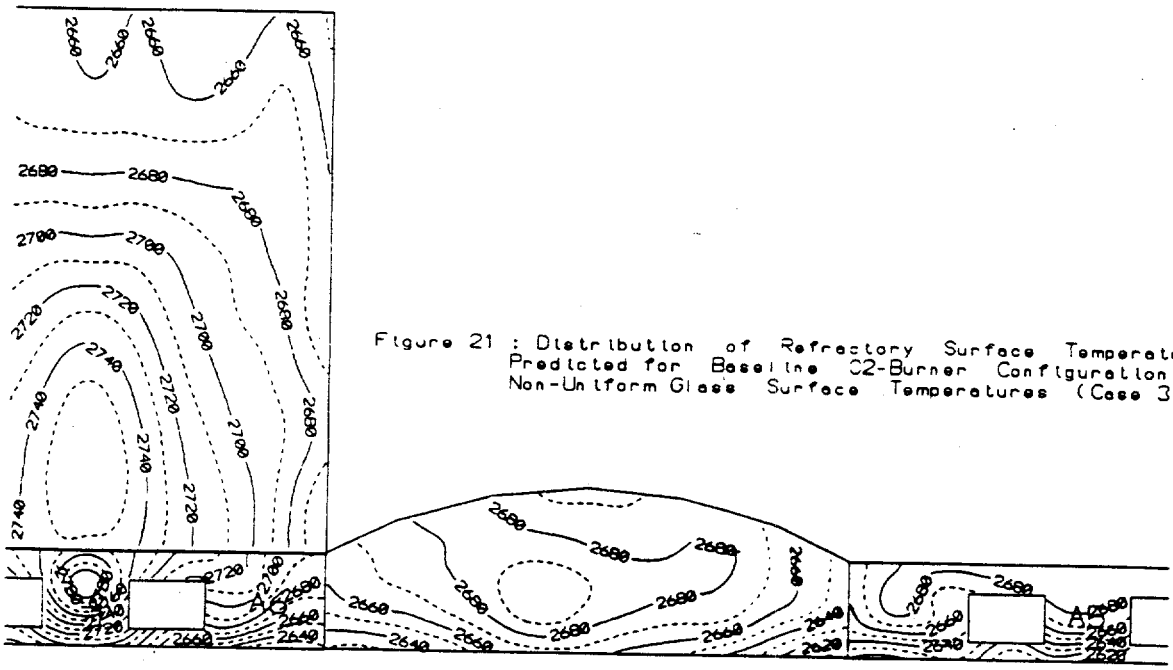

Figure 21 : Distribution of Refractory Surface Temperatures (F) Predicted for Baseline C2-Burner Configuration and Non-Uniform Glass Surface Temperatures (Case 3.1)